NANOPARTICLE-FACILITATED TRANSPORT OF URANIUM AND NICKEL IN CONTAMINATED SEDIMENTS NEAR A NUCLEAR WEAPONS PROCESSING FACILITY

by

SHEA WESTIN BUETTNER

(Under the Direction of Aaron Thompson and John Seaman)

ABSTRACT

The Department of Energy's Savannah River Site (SRS) has released a total of over 44,000 kg of depleted uranium (U) and a similar amount of nickel (Ni) into the Tims Branch-Steed Pond (TBSP) system. Failure of the Steed Pond dam in the 1980s exposed sediments that facilitated significant transfer of U to downstream ecosystems largely in association with particulates suspended during rainfall events. In order to evaluate the effects of TBSP re-vegetation, we assessed U mass flux during rain events, and spiked TBSP soils with several different amendments after oxic, anoxic, and pH adjusted laboratory incubations. Current storm event U mass flux has diminished since re-vegetation. Soil incubations indicated anoxic conditions in seasonally saturated sediments were potentially a major source of generating mobile U, while phosphate amendments can generate colloids. Understanding conditions responsible for U dispersion in contaminated systems and the forms of this U may lead to controlling future mobilization.

INDEX WORDS: uranium, nickel, runoff, colloids, anoxic, apatite, humic, phytate

NANOPARTICLE-FACILITATED TRANSPORT OF URANIUM AND NICKEL IN CONTAMINATED SEDIMENTS NEAR A NUCLEAR WEAPONS PROCESSING FACILITY

by

SHEA WESTIN BUETTNER

B.S.E.S., The University of Georgia, 2010

A Thesis Submitted to the Graduate Faculty of The University of Georgia in Partial Fulfillment of the Requirements for the Degree

MASTER OF SCIENCE

ATHENS, GEORGIA

2012

NANOPARTICLE-FACILITATED TRANSPORT OF URANIUM AND NICKEL IN CONTAMINATED SEDIMENTS NEAR A NUCLEAR WEAPONS PROCESSING FACILITY

by

SHEA WESTIN BUETTNER

Major Professor:	Aaron Thompson John C. Seaman
Committee:	Todd C. Rasmussen Louise Wicker

Electronic Version Approved:

Maureen Grasso
Dean of the Graduate School
The University of Georgia
December 2012

DEDICATION

This thesis is dedicated to my mother, who always encouraged me to work hard and pursue scientific study.

ACKNOWLEDGEMENTS

I would like to thank my wonderful committee: Dr. Aaron Thompson, Dr. John C. Seaman, Dr. Todd Rasmussen and Dr. Louise Wicker. Special thanks is given to Dr. Thompson and Dr. Seaman for their encouragement, and for their great editing that improved my writing approach. Special thanks is also given to Nehru Mantripragada and Russell Henderson for their help in laboratory equipment operation and anoxic chamber experimental methods. Other people that have assisted and loaned equipment are Julian Singer, Dr. Hyun-Shik Chang, Larry Bryan, Dr. Dien Li, Seth Brown, and Thomas Tuten. Their help are greatly appreciated. This material is based upon work supported by the Department of Energy under Award Number DE-FC09-07SR22506 to the University of Georgia Research Foundation as well as the United States Department of Agriculture (USDA), AFRI (Grant # 2009-65107-05830) and the National Science Foundation (NSF) Geobiology and Low-temperature Geochemistry (Award # EAR-1053470).

TABLE OF CONTENTS

Page

LIST OF TABLES

Page

LIST OF FIGURES

Page

CHAPTER 1

INTRODUCTION

Incidental contamination from production of special nuclear materials has occurred at many of the sites operated by the U.S. Department of Energy (DOE). One such site is the DOE's Savannah River Site (SRS), located on the SE Coastal Plain area of South Carolina. SRS lies to the northeast of the Savannah River and Georgia and is close to several major cities, including Augusta, GA and Aiken, SC. The SRS is an 803 km^2 nuclear materials production facility. It was constructed during the early 1950s to produce nuclear materials, primarily tritium (^{3}H) and plutonium-239 (^{239}Pu), used in the fabrication of nuclear devices for the nation's defense programs (Reed et al., 2002).

An important step in the nuclear weapons materials production cycle at the SRS was the manufacture of fuel and target assemblies for nuclear reactors in the site's M-Area (manufacturing area) (Figure 1.1). The site began manufacture of aluminum-clad nuclear fuel and target elements in 1954. The discharge of metal filing wastewater from these facilities led to extensive uranium (U) (~43 metric tons) and nickel (Ni) contamination of the nearby Tims Branch-Steeds Pond (TBSP) riparian ecosystem. At the time of discharge, Steeds Pond served as a natural settling basin where much of the contaminants were deposited (Pickett, 1990).

This increasing contamination develops a need for better understanding of how this stream and wetland can cope with such substantial U and Ni loading. Prior work at Tims Branch (TB) focused on the level of contamination, bioavailability, and fate of

metals/radionuclides occurring while the exposed Steeds Pond sediments were unvegetated and vulnerable to erosion during episodic rain events (Batson, 1994; Batson et al., 1996). In this study we attempt to evaluate metal transport currently occurring since re-vegetation through stream sampling during rain events. We also performed lab batch experiments probing the effects of anoxia, phosphate amendments, and humic substances on U and Ni partitioning, more specifically the dispersion of nanoparticles (< 100 nm) and colloids (< 1 μm) with co-associated U and Ni.

Traditionally, U mobilization is thought to occur most under oxidizing, carbonate-bearing conditions, where U is most soluble (Amonette et al., 1994). However, particles < 1 μm present some of the most abundant and reactive surfaces in soil and environmental systems due to their high surface area, electrical charge, and the high binding efficiency of metal-oxide or organic surface functional groups which are typically present (Albarran et al., 2008; Hochella et al., 2008; Kretzschmar et al., 1999). They can be potent carriers of metals and carbon, facilitating longer transport distances than would be predicted for dissolved ions. Indeed, U strongly binds to high-surface area Fe and Mn-bearing nanoparticles and organic matter, all of which have been implicated in enhanced U transport in surface and ground water systems (Harmsen and Haan, 1980; Hoekstra and Katz, 1954; Langmuir, 1978).

Redox processes, as brought on by reducing conditions from lack of molecular oxygen (O_2), have the potential to dissolve solid phases to which U is bound. Reduction can solubilize U bound to Fe^{III} and Mn^{IV} as well as produce hydroxide ions, thereby increasing solution pH (Eq. 1) (Thompson et al., 2006a).

$$Fe^{III}(OH)_3(s) + e^- \leftrightarrow Fe^{2+}(aq) + 3\ OH^-(aq) \quad (1)$$

The Tims Branch-Steeds Pond site is an area prone to seasonal flooding, in part due to beaver dam activity, and therefore may be influenced by periodic times of anoxia. Following a rupture and repair of the wooden dam during the 1960s, Steeds Pond surface area was reduced from 5.7 ha to 4.5 ha exposing the banks of the pond. Furthermore, in 1984 the dam permanently ruptured leaving the U contaminated sediments exposed. These conditions have allowed for the accumulation and mobilization of U and other metals in the former Steed Pond sediments over time (Looney et al., 2003).

Solid phase speciation of U in Steeds Pond sediments is to a great extent a function of redox conditions. Generally, hexavalent U dominates in oxidized soils and exposed sediments in the form of schoepite, uranyl (UO_2^{2+}) complexes with organic ligands, or Fe/Mn (oxyhydr)oxides (Bertsch et al., 1994; Langmuir, 1978). Under reducing conditions, U speciation shifts toward the tetravalent uranous forms (Tokunaga et al., 2008). Therefore, U solubility in oxidized soils can be altered by manipulating redox conditions (i.e., inundation) with support of anaerobic microbes or by ligand addition (e.g., orthophosphate) to lower U solubility through formation of autunite-like solid phases (Arey et al., 1999; Seaman et al., 2001a).

Our study objectives are: (i) To determine the current extent of U remobilization from contaminated sediments of Steed Pond to Tims Branch as a function of flow during episodic rain events, (ii) to establish the relative influence of Fe reduction and pH increases on the dispersion of particulate-bound U, (iii) to investigate the effects of humic substances and phosphate minerals on U speciation and solubility under reducing conditions, and (iv) to characterize nanoparticle size and composition. We hypothesized: (ia) There would be a decrease of U-bound suspended particles in Tims Branch during rain events relative to prior studies conducted before substantial re-vegetation of the

exposed Steeds Pond sediments, (ib) U is associated preferentially with organic ligands, (iia) particulate bound U would increase following Fe-(oxyhydr)oxide reduction and (iib) is partly explained by the associated increase in pH, (iii) anoxic conditions increases U partitioning to phosphate and soil humic material.

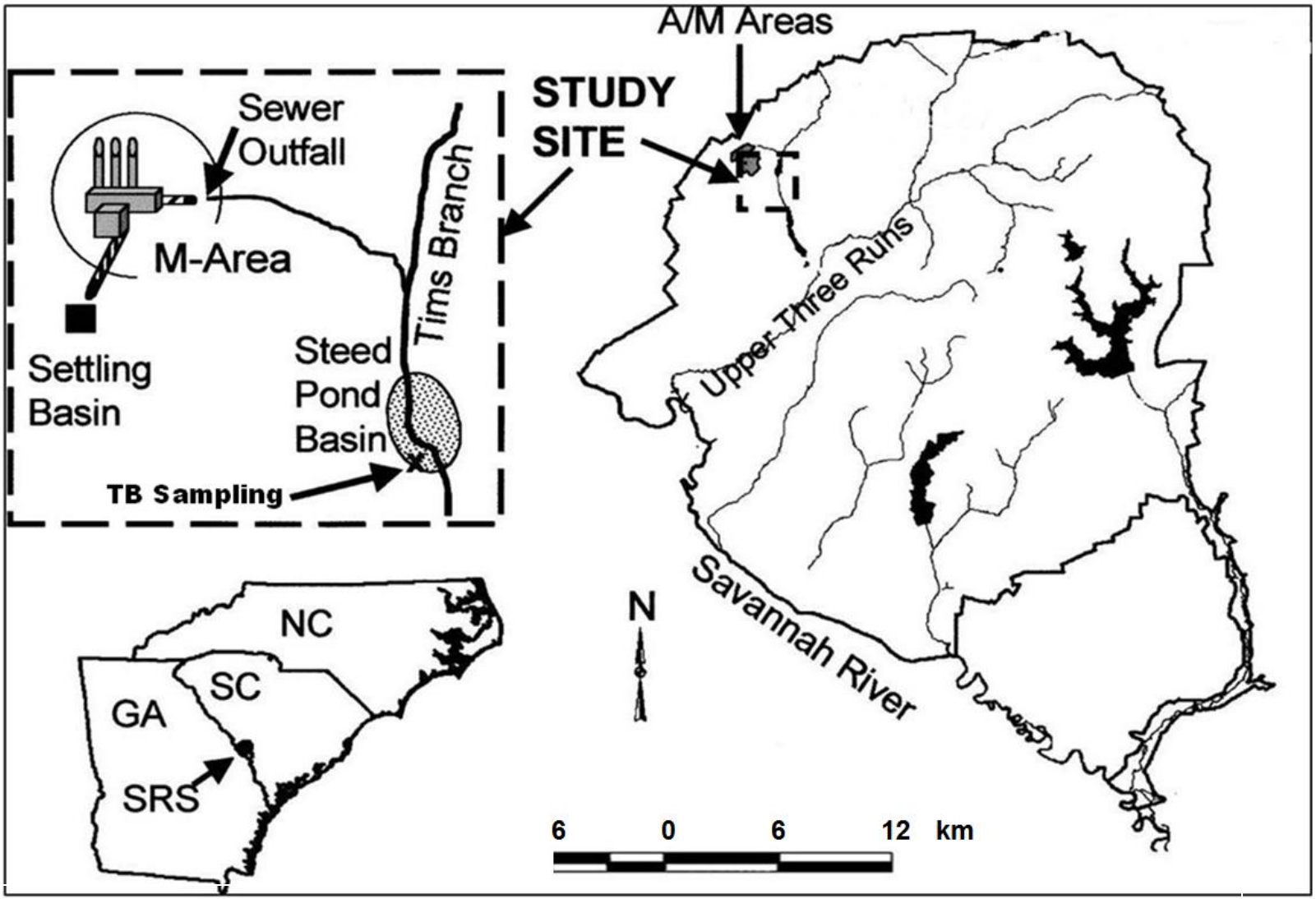

Figure 1.1: Regional location of the Savannah River Site, Manufacturing Area, and Tims Branch/Steed Pond (adapted from (Sowder et al., 2003)).

CHAPTER 2

LITERATURE REVIEW

Tims Branch Steeds Pond System

Tims Branch is a second-order stream which lies in the A/M-area of the northwestern section of SRS (Figure 2.1). Tims Branch drains a sixteen square kilometer basin which flows into Upper Three Runs Creek (UTRC), a tributary of the Savannah River. Tims Branch receives water from rainfall, groundwater, and effluent from the A/M-area of the SRS. The A/M-area effluent flows through an outfall ditch down a steep gradient of ~3% for ~1.5 km, where it enters a flatter stream slope of ~0.4% at Tims Branch (Figure 2.2). As the gradient decreased, initial deposition of suspended particulates occurred in a few small beaver ponds upstream from Steeds Pond. However, the bulk of the deposition occurred in Steeds Pond area due to the longer residence time for water compared to the beaver ponds (Evans et al., 1992). Estimates suggest that Steeds Pond retained up to 70% of the radionuclides released into Tims Branch (Bertsch et al., 1994; Evans et al., 1992; Pickett, 1990). The next ~3 km of Tims Branch consists of a series of depositional areas comprised of natural and man-made impoundments, i.e., beaver ponds, wetlands, and farm ponds, which functioned as settling basins for contaminated sediments. The shallow gradient continues for approximately 3.2 km to the confluence with Upper Three Runs Creek (UTRC).

Substantial contaminant laden discharge to Tims Branch waters finally ended in 1979 with the diversion of the primary U discharge to an engineered settling basin. All

discharge of untreated process waste water was diverted to an engineered settling basin in May 1982 (Evans et al., 1992). The measured M-Area discharge to surface streams from 1955-1988 are shown in Figure 2.3. The peak release years occurred in the late 1960s and early 1970s with discharge declining since that time. Relatively equivalent large quantities of depleted and natural U, Ni, and aluminum (Al) were discharged into TB, as well as lesser amounts of copper (Cu), zinc (Zn), lead (Pb), and chromium (Cr). Associated wastes such as nitric, phosphoric, and sulfuric acids and sodium hydroxide were also discharged. Uranium deposition is one of the main concerns in the TBSP system, with total U released at 23.7 curies estimated to ~43 metric tons (Evans et al., 1992; Pickett, 1990). While this is a considerable amount of depleted U, previous studies have shown that the U is generally associated with immobile stream sediments under baseflow conditions.

Steeds Pond originally had an area of about 5.7 ha as a farm pond, which decreased to 4.5 ha when the wooden dam gave way in the early 1960's (Figure 2.4) (Evans et al., 1992). The wooden dam was repaired ten years later and the pond returned to a surface area of 5.7 ha (Evans et al., 1992). The wooden dam collapsed again in 1984 and the pond was emptied (Evans et al., 1992). Steeds Pond existed as an unvegetated wetland before plant cover could be established. During this initially exposed state, Steeds Pond sediments were prone to remobilization and transport during storms and periods of flooding (Batson et al., 1996). Steeds Pond is currently a vegetated wetland with erosion generally restricted to braided streams within the wetland. Tims Branch is currently a small braided stream flowing through the former Steed Pond area that is prone to infrequent flooding through beaver activity.

Past studies on TBSP and mobilization of U

Past studies have indicated that amounts of suspended sediments in the streams are influenced by episodic rainstorm event erosion resulting in up to 2800% increase in U compared to baseflow (Batson et al., 1996). It has also been demonstrated that organic matter (Sowder et al., 2003) and Fe redox (Arey et al., 1999) play a critical role in controlling U solubility and distribution within Steeds Pond sediments.

Batson's study indicated that what initially served as depositional area within the Tims Branch watershed was subject to extensive erosion sending massive amounts of suspended soil particles downstream. As little as 16 mm of rainfall was needed to cause a measureable increase in stream turbidity and associated U concentration flux (Batson et al., 1996). Additionally, Batson et al. (1996) reported that mobilized U was largely associated with filterable (> 220 nm) colloids and particulates (Figure 2.5). This indicates that most of the U was bound to soil particles and not dissolved in solution.

Other studies have focused on lab experiments using Steeds Pond sediments. Sowder et al. (2003) found that dissolved U concentrations were highly correlated to dissolved organic carbon (DOC) with a correlation value of $r^2 > 0.96$. Sowder et al. (2003) also established that using a non-sequential selective extraction method in contaminated sediments resulted in up to 60% of the total Fe was present in the non-crystalline form, i.e., ammonium oxalate extractable. This likely results from seasonal variations in redox leading to dissolution and reprecipitation of Fe (oxyhydr)oxides with significant substitution by other metals such as Al.

The toxicity of U can be diminished through alteration of its' chemical speciation. In oxic waters and soils, U is present as a linear, hexavalent oxo-cation, UO_2^{2+} (Uranyl).

Uranyl has 4 to 6 free coordination sites around the equator of the linear molecule that form strong complexes with hydroxide or organic ligands (Bertsch et al., 1994; Hudson et al., 1999). Oxygen bearing functional groups on the surface of mineral or organic solids can bind to these equatorial coordination sites and facilitate the removal of U from the aqueous phase. Under reducing conditions, Uranyl is converted to the less toxic and insoluble U^{IV} species (Tokunaga et al., 2008). Indeed, laboratory studies using Steeds Pond sediments have shown that both organic matter and Fe redox chemistry play a strong role in controlling U speciation and solubility, with U solubility largely governed by DOC concentrations (Arey et al., 1999; Sowder et al., 2003).

Despite shifts in redox conditions within Steeds Pond that lead to the formation of poorly crystalline Fe oxides, Bertsch et al. (1994) found that U in the Steeds Pond sediments was present primarily in the oxidized uranyl (U^{VI}) species. In addition, field flow fraction inductively coupled plasma- mass spectroscopy (FFF-ICP-MS) and size exclusion chromatography-inductively coupled plasma- mass spectroscopy (SEC-ICP-MS) analysis on < 220 nm extracted Steeds Pond sediments by Jackson et al. (2005) indicate that a significant amount of U was associated with nanometer-size humic colloids. This suggests that U is largely associated with a specific soil fraction rather than generally distributed within the entire sediment/soil. This is consistent with the results of Sowder et al. (2003), suggesting additional mechanisms of U mobilization due to selective colloid mobilization rather than wholesale erosion of larger particles.

Further, the addition of phosphate minerals (e.g. apatite) immobilize U and other metals (i.e., Pb, Ni, etc.) within contaminated soils and sediments (Arey et al., 1999; Knox et al., 2000; Seaman et al., 2001a). Natural hydroxyapatite [$Ca_5(PO_4)_3OH$] has a

low solubility compared to other forms of phosphate such as phytic acids [$C_6H_{18}O_{24}P_6$] like calcium and sodium phytate (Seaman et al., 2005). Therefore, U solubility can be hindered by redox manipulation or by phosphate additions to lower U solubility through precipitation of autunite-like solids (Arey et al., 1999; Seaman et al., 2001a). This approach of soil remediation is a cost effective and non-destructive alternative to soil excavation and disposal.

Colloids and Nanoparticles in Aquatic Environments

Colloidal particles are size-defined particles having at least one dimension between 1 nm and 1 μm. The smallest colloids are defined as nanoparticles and have diameters < 100 nm. Colloids and nanoparticles exhibit Brownian motion which enables them to resist sedimentation and often have high specific surface areas making them important sorbents for contaminants. In surface freshwaters, they can occur as products of soil weathering, Fe^{III} and $Mn^{III, IV}$ oxides, biological debris, humus colloids, and colloidal Fe(OOH) oxides stabilized by humic or fulvic acids (Kretzschmar et al., 1999). Colloids can be generated by physical fragmentation and erosion of existing solid phases and by the precipitation and nucleation of ions from solution (Cline et al., 1981; McCarthy and Zachara, 1989). Likewise, a host of processes can act on colloids releasing them from solution, including particle aggregation, attachment, and settling (McCarthy and Zachara, 1989). Particle agglomeration can cause large reductions in free energy during electrostatic stabilization and accordingly colloids readily flocculate and form larger aggregates. Consequently, colloid and nanoparticle stability is affected by adsorbates that alter their surface charge and by interparticle attractive and repulsive forces (Stumm, 1977).

Furthermore, the reduction of Fe^{III} oxides and dissolution under anoxic conditions can promote colloid dispersion by dissolving the linkages that hold aggregates together (Goldberg and Glaubig, 1987). However, the reduction of Fe-oxides also results in increases in solution pH through hydroxide production (Gillespie, 1920; Ponnamperuma et al., 1966; Vesparaskas and Faulkner, 2001), which can indirectly influence colloid dispersion through development of greater negative charge on the particles (Bunn et al., 2002; Ryan and Gschwend, 1994). Therefore, Fe reduction can influence colloidal mobilization physically through the dissolution of aggregating particles or changes in pH that increase electrostatic repulsion between particles.

Changes in soil solution chemistry are the most common cause for the release of colloids in soil and groundwater. When the diffusive forces associated with Brownian motion of suspended colloids are greater than the sedimentation rate, colloids may remain stable in suspension over prolonged periods of time. If attractive forces are greater than repulsive forces, colloids can amass, flocculate, and settle out of suspension. If the inverse is true, colloids are repelled from each other and remain dispersed in suspension. The aggregation state of colloids and nanoparticles is important because they are major sorbents for contaminants. When aggregated, colloids and nano-particulates are less likely to be lost to leaching or travel great lengths downstream. However, if colloids are dispersed they may travel vast distances, enhancing the migration of bound contaminants than would otherwise be predicted based on simple solid phase partitioning behavior (McCarthy and Zachara, 1989; McDowell-Boyer, 1992; McDowell-Boyer et al., 1986). Because soil solution chemistry affects the surface chemistry of nanoparticles, understanding the solution chemical processes occurring in a soil-water system will

improve the understanding of the dispersion state of colloids in the soil system (Kretzschmar et al., 1999; McCarthy and Zachara, 1989).

Surface Charge Induced Dispersion of Colloids and Nanoparticles

The charge of particle surfaces greatly influences their flocculation or dispersal. Generally, soil particle surfaces acquire permanent electrical charge from isomorphic substitutions and temporary electrical charge from reactions of surface functional groups. The surface charge in soils explicitly consists of (1) net structural surface charge density (σ_0) due to isomorphic substitution, (2) inner-sphere complex surface charge density (σ_{IS}) from inner-sphere surface complexes of ions, (3) outer-sphere complex surface charge density (σ_{OS}) from outer-sphere complexes of ions, (4) net proton surface charge density (σ_H) from H^+/OH^- surface complexation, and (5) diffuse layer surface charge density (σ_D) from ion adsorption (Sposito, 1992; Sposito, 2000).

The intrinsic surface charge (σ_{in}) of a soil is defined as:

$$\sigma_{in} = \sigma_0 + \sigma_H \qquad (2)$$

Net proton surface charge density is equivalent to the difference between the moles of protons and the moles of hydroxide ions bound by surface functional groups:

$$\sigma_H = q_H - q_{OH} \qquad (3)$$

where q_H is moles of H^+ and q_{OH} is moles of OH^-. This pertains to surface groups and does not include diffuse layer protons or hydroxyls. The value of σ_H can be positive, zero, or negative based on pH and ionic strength (Sposito, 2000).

Weathering of the minerals and organic matter of a soil determines the contribution of σ_0 and σ_H to intrinsic particle charge. Soils at early and intermediate stages of weathering are commonly 2:1 layer silicates that primarily obtain charge from

interstitial siloxane surfaces (in the interlayer region) and are considered permanently charged soils since σ_H affects particle charge modestly. Variable-charge soils in which σ_H primarily affects particle charge are found in increasingly weathered soils where there are numerous minerals bearing reactive hydroxyl groups which can be (de)protonated to become charged. Therefore, pH changes in variable-charge soils are a significant factor in the development of particle surface charge.

The total net particle charge (σ_P) consists of all charges except the diffuse layer surface charge and defined as:

$$\sigma_P = \sigma_0 + \sigma_H + \sigma_{IS} + \sigma_{OS} \qquad (4)$$

Soil particles maintain neutral (zero) charge by absorbing or releasing ions in the diffuse layer to balance the total net particle charge (σ_P). The diffuse layer consists of ions not bound into surface complexes, but adsorbed and held within a few nanometers (the Stern Layer) of the solid-solution interface. This cloud of diffuse ions, known as the electric double layer, generally results in repulsions between particles.

At a given pH, the average surface charge will be equal to zero; this is known as the point of zero charge (PZC). At the point of zero charge (PZC), no σ_P exists for σ_D to balance, therefore, all adsorbed ions are immobilized in surface complexes. When pH is equal to the pH at the PZC (pH_{pzc}):

$$\sigma_H = -(\sigma_0 + \sigma_{IS} + \sigma_{OS}) \qquad (5)$$

The mineral surface will have a net positive charge when the solution pH is below the pH_{pzc}. Likewise, the mineral will have a net negative charge when solution pH is greater than the pH_{pzc}. One method to measure PZC is by determining the pH corresponding with the isoelectric point where soil particles are unresponsive to an

applied electrical field and electrophoretic mobility disappears. The PZC signifies a lack of freely moving adsorbed ions and a reduction of the electric double layer, which increases interparticle forces that cause aggregation. Particle aggregation is highest in variable-charge soil solutions when pH equals pH_{pzc}, due to this reduction in electric double layer, and therefore is important in reducing particle dispersion/mobility.

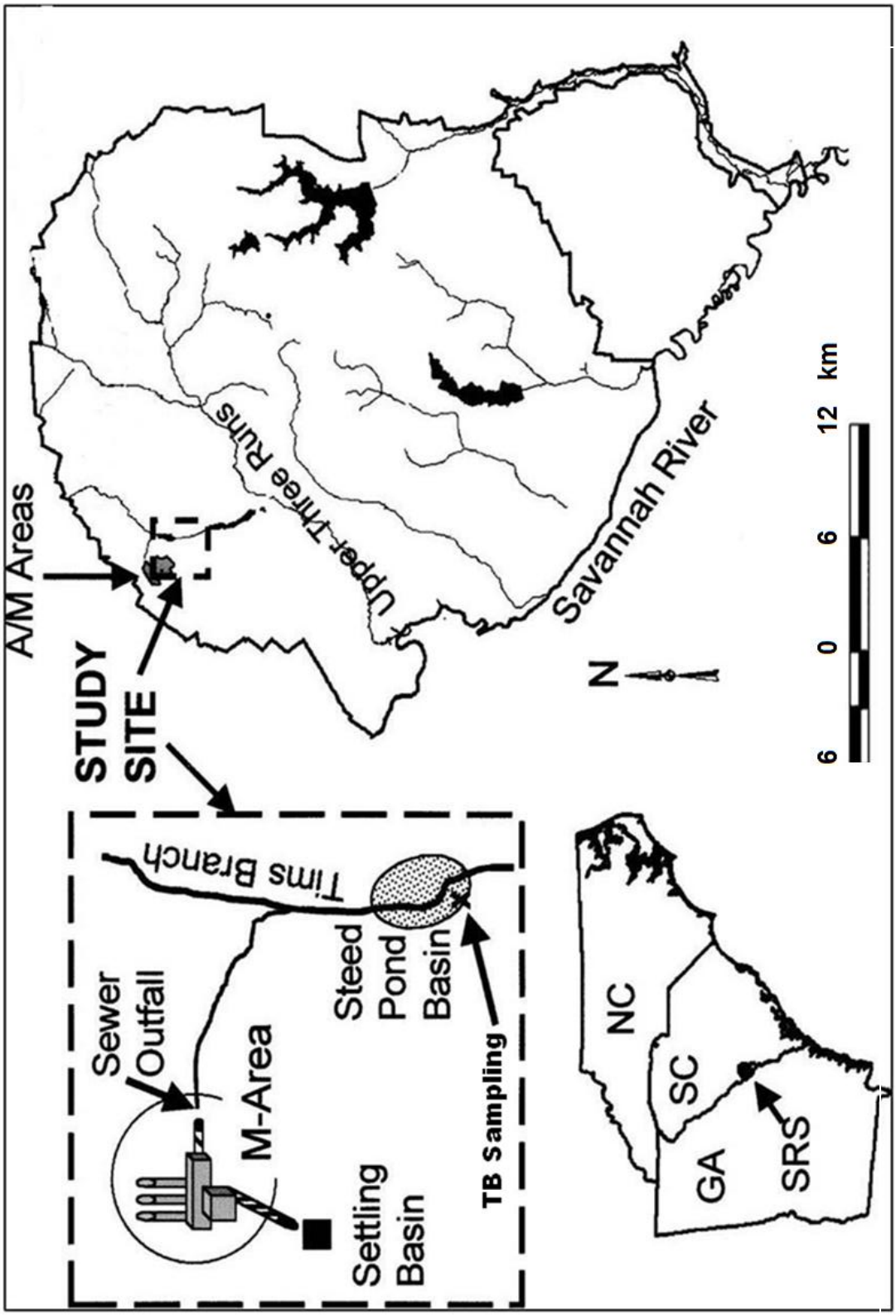

Figure 2.1: Regional location of the Savannah River Site, Manufacturing Area, and Tims Branch/Steed Pond (adapted from (Sowder et al., 2003)).

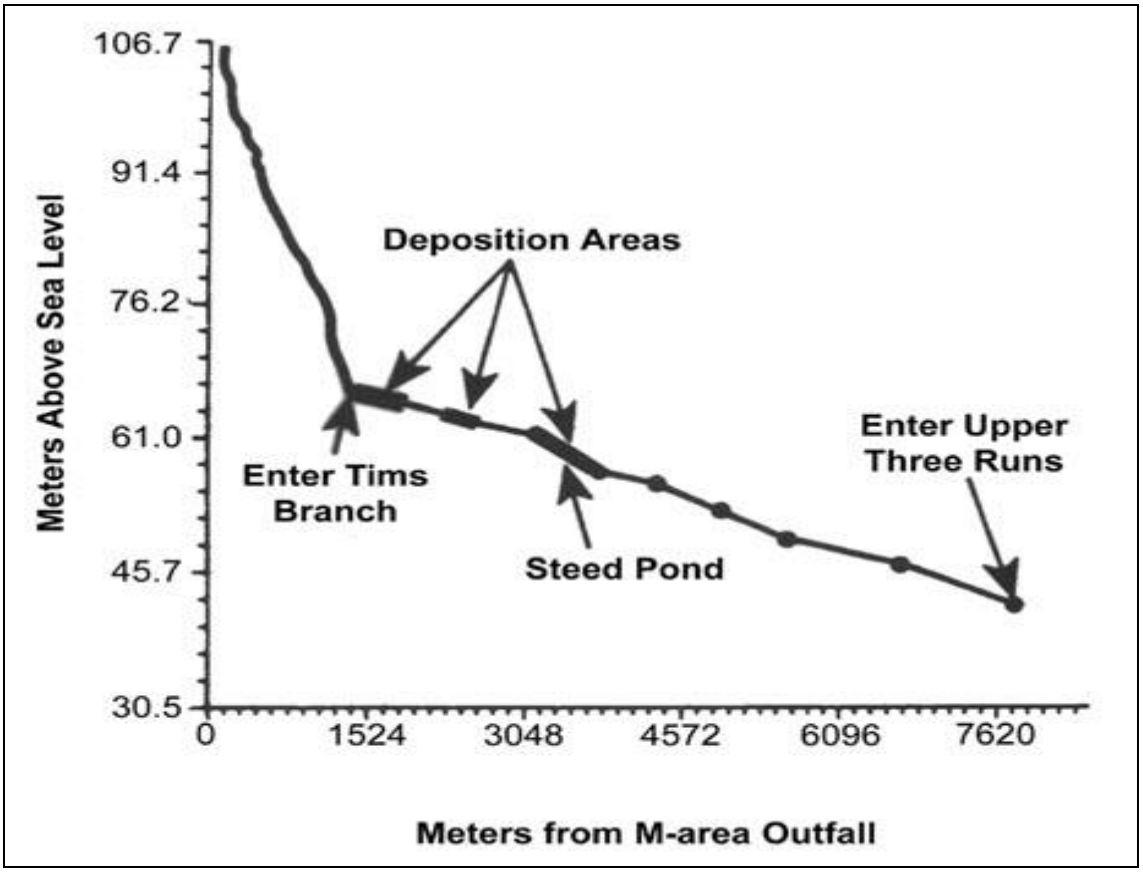

Figure 2.2: Elevation of Tims Branch System from the M-Area outfall to Upper Three Runs Creek (Evans et al., 1992).

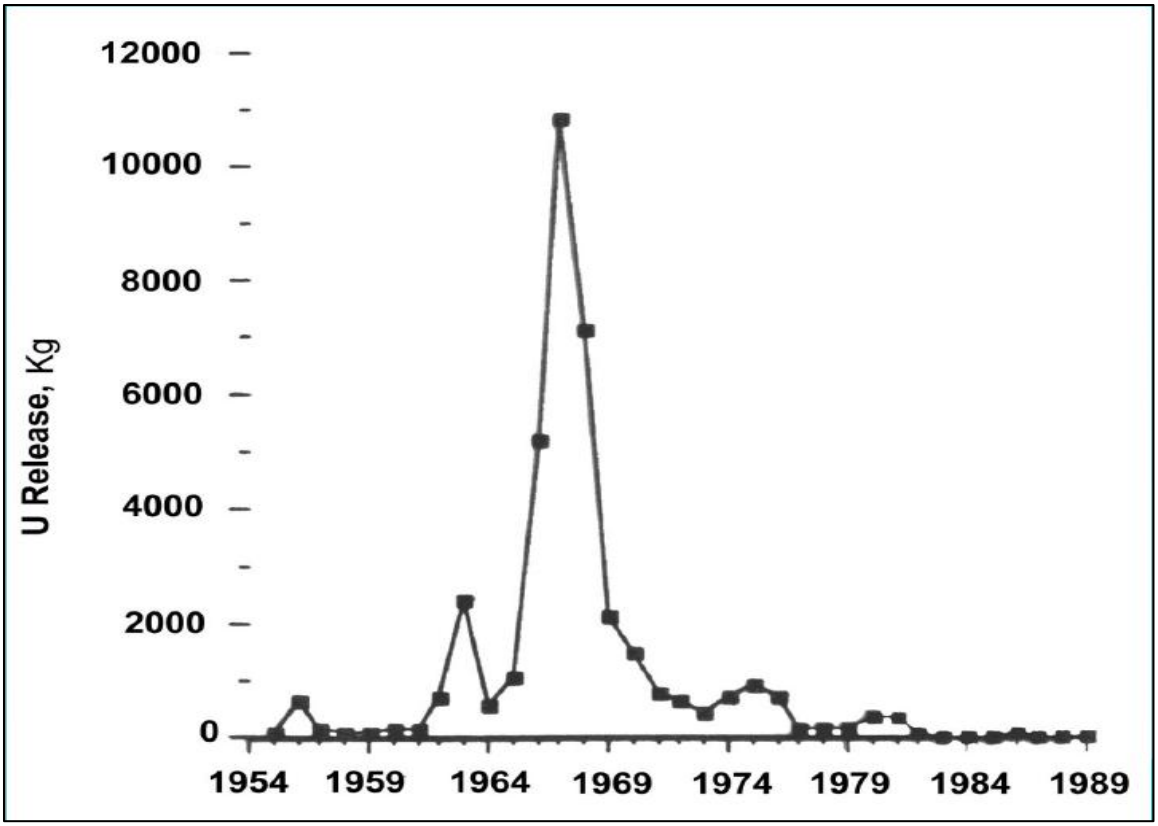

Figure 2.3: Past discharge into Tims Branch. Adapted from Pickett et al., (1990).

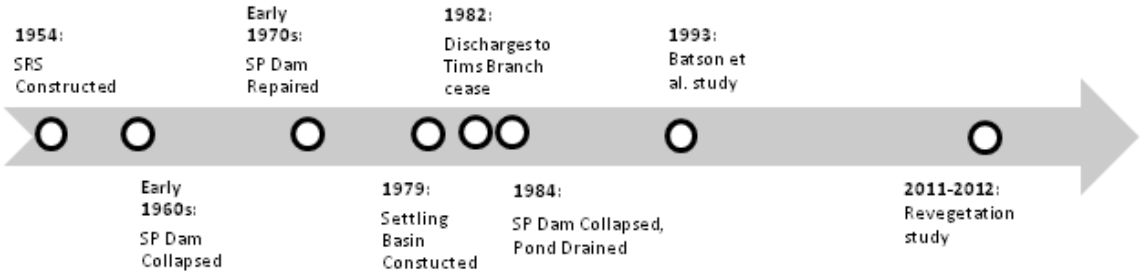

Figure 2.4: Timeline of Events at Steed Pond (SP)

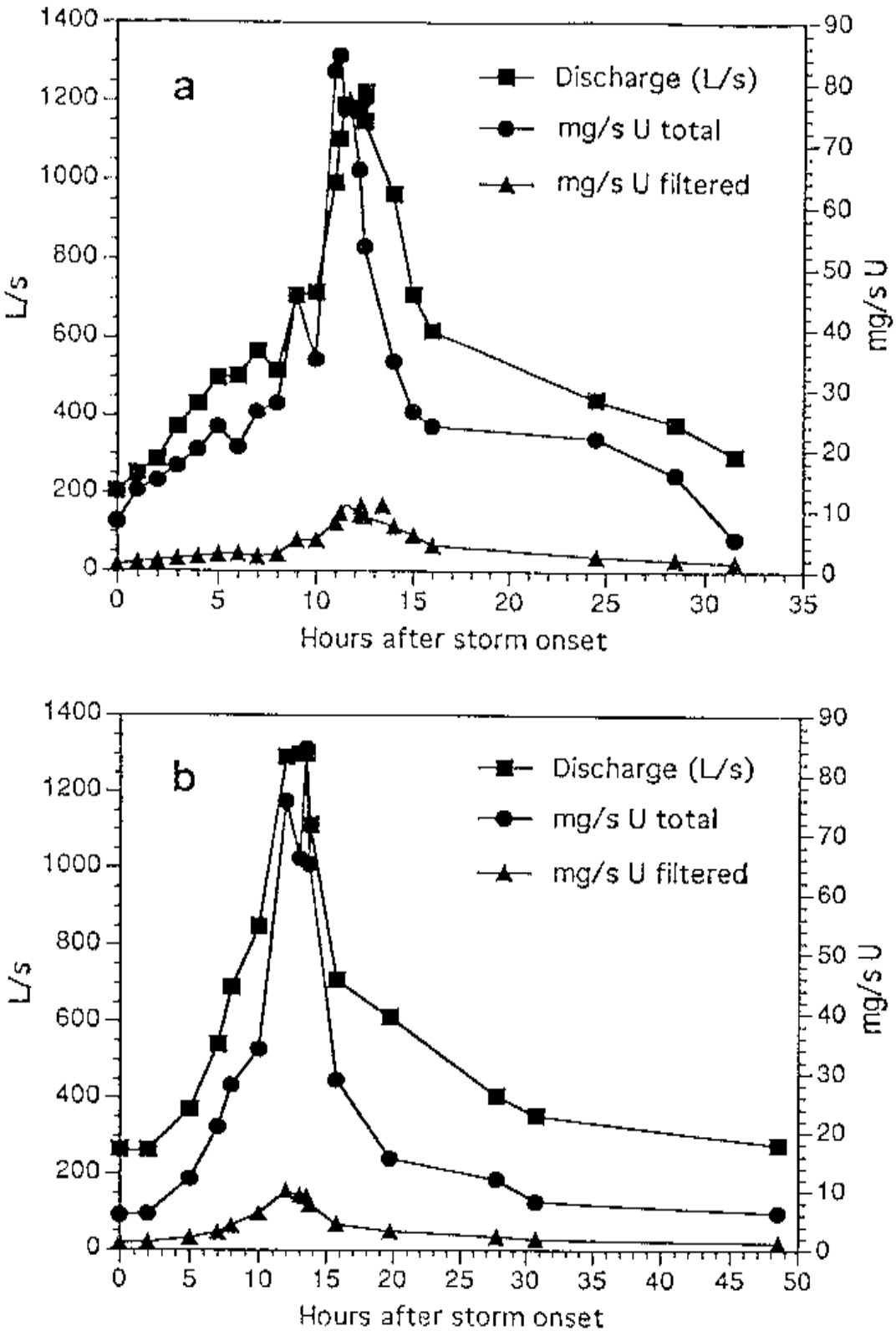

Figure 2.5: Hydrograph of U mass flux vs. discharge for March 23, 1993 (a), and March 26, 1993 (b) (Redrawn from (Batson et al., 1996)).

CHAPTER 3

ANOXIA-INDUCED RELEASE AND SOIL AMENDMENT (IM)MOBLIZATION OF COLLOID-BOUND URANIUM IN FLOODPLAIN SOILS NEAR A NUCLEAR MATERIALS PROCESSING FACILITY SAVANNAH RIVER SITE, SOUTH CAROLINA, USA[1]

---

[1]Buettner, S.W., J.C. Seaman, A. Thompson, T.C. Rasmussen, L. Wicker.

To be submitted to the Journal of Environmental Quality.

Abstract

High rainfall and seasonal soil saturation in the Southeastern Coastal Plain generate conditions where colloid-sized aggregates and nanoparticles can be mobilized by changes in soil solution chemistry. Mobilized particles may pose additional environmental threats in uranium (U) contaminated soils. The use of in situ chemical stabilization for the immobilization of uranium and other metals in contaminated soils/sediments has potential to mitigate contaminant migration. We do not know how these soil amendments impact colloid dispersion under oxic and anoxic conditions, therefore understanding the conditions governing particle mobilization is an essential component in reducing U loss from these soils. We assessed dispersion and desorption of colloid (100 – 1000 nm) and nanoparticle/dissolved U (< 100 nm) from contaminated soils from the Tims Branch riparian corridor. In laboratory incubations, the soils were equilibrated at pH 5.3 and subjected to 7 d or 14 d of anoxic conditions and compared to conditions of elevated pH in the presence of oxygen. Furthermore, additional sediments were spiked with either 2% or 5% hydroxyapatite [$3Ca_3(PO_4)Ca(OH)_2$], phytic acid [$C_6H_8Na_{12}O_{25}P_6$], or humic acid sodium salt [$C_9H_8Na_2O_4$]. These spiked batch samples were also subjected to 14 d of anoxic or oxic conditions. Samples were size fractionated by differential centrifugation and ultrafiltration and analyzed for total U, Ni, Al, Fe, and non-purgable organic carbon. Within the soil incubation slurries, we found that longer anoxic incubations released more U, Ni, Al, Fe, and C –bearing colloids with similar increases in colloid dispersion accompanying increase in soil pH. However, dispersion of Ni-bearing colloids also occurred under oxic incubations and appears to be affected by time-dependent mechanisms. Addition of hydroxyapatite slightly decreased < 100 nm U, but dispersion

of U and Ni-bearing colloids (100-1000 nm) was enhanced with the addition of hydroxyapatite. In contrast, phytate and humic amendments dispersed mostly nanoparticle/dissolved U and Ni. XRF element mapping of U in hydroxyapatite soil shows association with Fe surfaces, while Na-phytate and humic salt released substantial amounts of nanoparticle and aqueous (< 100 nm) U and Ni that is associated with humic ligands and few colloids (100-1000 nm). Our experiments suggest colloidal dispersion during Fe-reducing conditions as well as organic matter has the potential to mobilize colloidal U and Ni. Moreover, U and Ni immobilization with phosphate amendments, though may lower aqueous concentrations, has the potential to disperse colloidal U and Ni in solution.

Introduction

Chemical availability and mobility of uranium, nickel, and other metals is an important concern at the Savannah River Site (SRS) in Aiken, South Carolina, and at several other Department of Energy (DOE) sites. Metals that contaminate water or sediments cannot be destroyed, but the toxicity of these inorganic contaminants can be diminished through alteration of their chemical speciation. Preferably, such chemical changes (i.e., precipitation or reduction) convert mobile and toxic species to immobile and nontoxic species.

From 1954 through 1982, Tims Branch, a second-order stream which drains nearly 16 km^2 within the Savannah River drainage basin, was contaminated with over 44 Mg of depleted U, a similar amount of Ni, along with other metals (e.g., Al, Cr, Cu, Cd, Zn, Pb). These metal contaminants were discharged from contaminated nuclear fuel and target assembly manufacturing wastewater (Bertsch et al., 1994; Evans et al., 1992;

Looney et al., 2003; Pickett, 1990). The majority of the contaminants (~70%) and suspended sediments settled due to longer residence times and reduced stream flow in a former farm pond, Steed Pond. Steed Pond exists today as a wetland following the failure of the spillway in 1984 (Batson et al., 1996; Pickett, 1990; Sowder et al., 2003). The Tims Branch-Steed Pond system (TBSP) currently experiences sporadic beaver activity that can cause periodic flooding along with sediment anoxia.

Furthermore, when similar soils are subject to periods of anoxia, reductive dissolution of Mn^{IV} and Fe^{III}-oxides (principally Fe^{III}) promotes colloid dispersion by dissolving the connective Fe linkages holding U occluded aggregates together (Goldberg and Glaubig, 1987; Scala et al., 2006). Indeed, Batson et al. (1996), through sequential extraction techniques, determined Steed Pond sediment U was largely associated with organically bound and metal oxide phases that we postulate are labile and become dispersed when anoxic Fe-reduction consumes protons causing an increase in solution pH (Gillespie, 1920; Ponnamperuma et al., 1966; Vesparaskas and Faulkner, 2001). It can indirectly influence colloid dispersion through development of negative charges on colloid surfaces causing repulsion (Bunn et al., 2002; Ryan and Gschwend, 1994). Therefore, Fe reduction can influence colloidal mobilization physically via dissolution of particles or chemically through changes in pH and corresponding particle surface charges (Thompson et al., 2006a).

Applying phosphate sequestering agents and humics for the transformation and immobilization of metals in low concentrations in contaminated sediments offers significant potential for long-term environmental remediation. Phosphates (e.g. hydroxyapatite, $[3Ca_3(PO_4)Ca(OH)_2]$) are common surface and subsurface amendments

(Arey et al., 1999; Ma et al., 1994) that effectively immobilize U and other metals (e.g., Cd, Ni, Zn, Pb) in contaminated soils/sediments (Knox et al., 2000; Seaman et al., 2001a), therefore presenting an alternative to treat contaminated natural systems. Contrastingly, Na-phytate (unlike Ca phytate, which sorbs contaminants in the same manner as apatite minerals) disperses particles and therefore is not a suitable sorbent for U (Knox and Brigmon, 2008). Humic substances are present in soils, sediments, and natural waters throughout the southeastern USA (Giesy et al., 1986). Humic acid (HA) is a complex mixture of organic compounds, and affects physical, chemical, and biological reactions in the subsurface (Gu et al., 2005; Jackson et al., 2005; Trenfield et al., 2011). HA contain large numbers of attached hydroxyl and carboxyl groups (Jansen et al., 1997) that function as organic ligands and are known to complex to metal ions (MacCarthy, 1989).

The objectives of this study were to (1) to show the relative influence of Fe-redox and pH increases on the dispersion of particulate U and other toxic metals, and (2) investigate the effects of varied phosphate minerals and organic carbon content on toxic metal complexation as influenced by redox conditions. We expect colloid-bound U and Ni will increase following Fe-(oxyhydr)oxide reduction partly due to the associated pH increase. We also expect anoxia to disperse colloid-bound U and Ni in amended soils. In addition, we hypothesize different size partitioning between amendments with hydroxyapatite amendments reducing soluble (< 100 nm) U and Ni, and phytate and humic acid dispersing U and Ni- bound colloids and aqueous phases (< 1000 nm).

To test these hypotheses we measured U and Ni concentrations in two particle size classes following 7 d or 14 d anoxic conditions compared to conditions of elevated

pH in ~21% oxygen atmosphere. Furthermore, additional sediments were spiked with either 2% or 5% hydroxyapatite [$3Ca_3(PO_4)Ca(OH)_2$], phytic acid [$C_6H_8Na_{12}O_{25}P_6$], or humic acid sodium salt [$C_9H_8Na_2O_4$] and also subjected to 14 d of anoxia or oxic conditions.

Materials and Methods

Exposed sediments of TBSP are characterized by low pH (4.0-5.5), weathered clays (kaolinite), abundant Fe (e.g., ferrihydrite, goethite), and Al (oxyhydro)oxides, and organic carbon (Batson, 1994; Seaman et al., 2001a). Field-moist sediments collected on the banks of Tims Branch under the Road 2 Bridge, (Figure 3.1), were sieved (2 mm) to remove stones and large organic matter (i.e., stems, roots, and leaves). Soil aggregates were lightly crushed by hand to pass through the 2-mm sieve. The bulk material was then air-dried and subsequently stored at ~25°C for further use. Particle size distribution (64% sand, 24% silt, 12% clay) of the collected soil is consistent with a sandy loam. Soil samples from Tims Branch's floodplain were prepared in triplicate for each of the twenty-three incubations, operationally defined in Appendix B1.

Anoxic experiment

All solutions were prepared with ultrapure DI water and reagent-grade chemicals. Triplicate incubations of air-dried soils were suspended in 2.0 mM KCl at a soil : solution ratio of 1:10 (2.73 g of soil (dry mass equivalent): 27.3 mL of 2.0 mM KCl) in 30-mL polypropylene Oak Ridge centrifuge tubes. The suspensions were shaken for 2 h on a horizontal shaker (~100 rpm). Centrifugal fractionation was achieved assuming spherical particle geometry and a nominal particle density of 2.65 g cm^{-3} for particles; the RCF and time required to achieve separation of particles < 1000 nm (5.4 min at 478 RCF or 2,000

rpm for 5.4 min), < 100 nm (10 min at 17,211 RCF or 12,000 rpm for 10 min) was calculated from Stokes' law (Appendix A). The reaction set was then centrifuged using a Sorvall RC 5B plus centrifuge with a Sorvall SS-34 rotor targeting the < 1000 nm fraction (5.4 min at 478 RCF or 2 000 rpm for 5.4 minutes). For each replication, a 5-mL aliquot of supernatant was transferred to 15-mL Falcon tubes and acidified to pH 1 with concentrated HNO_3 (1% of sample volume). The remaining suspension was centrifuged to target the < 100 nm fraction (10 minutes at 17,211 RCF or 12 000 rpm for 10 minutes. Once more, a 5-mL aliquot was transferred to 15-mL Falcon tubes and acidified to pH 1 with concentrated HNO_3 (1% of sample volume). The < 10 kDa fraction was obtained by passing 1 mL of the remaining supernatant through a 10 kDa molecular weight cutoff Millipore Amicon-Microcon filter (at 10 000 rpm for 10 min) using an Eppendorf 5424 centrifuge and acidified to pH 1. These aliquots provided a pre-reaction sample set. Prior to use, glycerol impregnating the 10 kDa filters was successfully removed by a series of three washes using 0.1M NaOH followed by three rinses with 18.2MΩ water.

Anoxic incubations were prepared identical to the oxic triplicate incubations. The anoxic incubations were opened inside of a 95% N_2 : 5% H_2 glovebox (Coy Vinyl Anaerobic Chambers, Grass Lake, MI) and allowed to equilibrate for 16 h before resealing. Suspensions were then secured on a horizontal shaker (Lab-Line Instruments, Inc.) at 100 rpm inside the glovebox and reacted for 7 d or 14 d at ~25°C. Following incubation, size-fractionated samples were isolated by differential centrifugation identical to the methods used for the oxic incubations. Samples were returned to the glovebox where the supernatant solutions were removed and acidified to pH 1 with concentrated HNO_3 (1% of sample volume). The < 10 kDa fraction was obtained by centrifuging

inside the glovebox, passing the supernatant through a 10 kDa molecular weight cutoff Millipore Amicon-Microcon filter (at 10 000 rpm for 10 min) using an Eppendorf Minispin Plus centrifuge.

Oxic pH shifted experiment

A parallel experiment was conducted under oxic conditions to isolate the effects of pH on colloidal dispersion/mobilization. The suspensions were equilibrated ~3 mM ionic strength to a pH near the 14 d anoxic samples of 5.66 through measured additions of 2 mM KCl and 0.1M KOH, respectively. The suspensions were then shaken on a horizontal shaker for 2 h and sampled identical to that described above for the oxic samples (e.g., differential centrifugation and ultrafiltration).

Amendment batch experiments

Triplicate spiked slurries of either hydroxyapatite [$3Ca_3(PO_4)Ca(OH)_2$], sodium phytate [$C_6H_8Na_{12}O_{25}P_6$], or humic acid sodium salt [$C_9H_8Na_2O_4$] were constructed at both 2% and 5% w/w. Spiked anoxic/oxic incubations were prepared identical to the anoxic triplicate incubations and were allowed to run for 14 d. Following incubation, size fractionated samples were isolated by differential centrifugation identical to the methods used for the anoxic incubations to obtain < 1000 nm and < 100 nm fractions. Likewise, the spiked oxic incubations were prepared identical to the 14 d oxic incubations.

Sample analysis

We measured pre- and post-experimental pH, specific conductance or electrical conductivity (E.C.), and redox potential (Eh) data on both the anoxic and pH shifted oxic treatments. Non-purgable organic carbon (NPOC) in each size fraction was analyzed by high temperature combustion following sparging of acidified samples using a Shimadzu

TOC-5050A with Shimadzu ASI-500 sampler. Concentrations of U and other metals were determined using an acid–based microwave assisted digestion method (USEPA, 2008) followed by inductively coupled plasma-mass spectrometry (ICP-MS) (NexIon 300X; PerkinElmer, Norwalk, CT) based on the quality assurance-quality control protocols outlined in USEPA Method 6020a (USEPA, 2007a). We utilized Excel Stat (a Microsoft Excel plug-in) for statistical analysis. Incubation U and Ni levels were subjected to a Tukey's HSD test for post-ANOVA pair-wise comparisons in a one-way ANOVA.

Synchrotron radiation μXRF, μXANES, and Bulk-XAS Analyses

Synchrotron-based measurements were conducted on the VESPERS (Very Sensitive Elemental and Structural Probe Employing Radiation from a Synchrotron) beamline at the Canadian Light Source, Saskatoon, SK, Canada (Feng et al., 2007). Micro X-ray fluorescence spectroscopy (μXRF) technique was employed to generate elemental distribution map in two dimensions. Sample was mounted on a motorized XYZ stage. A raster scan was performed using an incident energy of 18 keV with 1.6% bandpass for 2 s per pixel position in a step size of 2 μm. The fluorescence spectra were recorded with a 50 mm^2 active area single-element Vortex Silicon Drift Detector with a 400-μm thick Si crystal and a 12.5-μm Be entrance window (SII NanoTechnology, California, USA) which was placed 35 mm away from the sample. The detector was positioned 45° relative to the sample and to the incoming X-ray beam within the horizontal plane.

X-ray-absorption-near-edge-structure (μXANES) measurements were performed at the U L3 edge (17166 eV) to investigate the uranium speciation in different samples. Monochromatic X-ray beam from Si(111) monochromator with 0.01% bandpass was

used for the measurements. The experiment was conducted using fluorescence mode with the same setup for μXRF mapping. The intensity of U Lα lines was measured while scanning incident photon energy. The entire XRF spectrum was also saved into a file at each energy.

Results

The sampled Tims Branch floodplain sediments show elevated levels of U, Ni, and Cr that are several orders of magnitude higher than natural soils on SRS (Table 3.1).

Anoxic experiment

The initial pH of the soil slurries (Appendix B2) was consistent with prior pH measurements of these surface soils (Batson, 1994; Sowder et al., 2003). Following the 7 d anoxic incubation, the soil slurries exhibited increases in pH and E.C. (electrical conductivity) of ~0.2 pH units and ~50 μS cm^{-1}, respectively (Appendix B2). The pH increases were greater in the 14 d anoxic incubation, with a recorded pH increase of nearly 0.5 units (Appendix B2).

Prior to anoxic treatment, total C and Fe < 1000 nm from the soils was 66 ± 40 mg kg^{-1} and 28 ± 7 mg kg^{-1}, respectively, with C distributed predominantly between 2.3-100 nm and Fe in the larger 100-1000 nm size fraction (Appendix D1). Furthermore, total colloidal Al, U, and Ni was 36 ± 6 mg kg^{-1}, 0.2 ± 0.1 mg kg^{-1}, 6.1 ± 0.3 mg kg^{-1}, respectively, with Al and U dispersed primarily between 100-1000 nm and Ni in the < 100 nm size fractions (Appendix D1 and Figure 3.2). Following the 7 d anoxic incubation total colloidal C and Fe < 1000 nm increased to 195 ± 37 mg kg^{-1} and 374 ± 53 mg kg^{-1}, respectively, with C and Fe increases rising mostly from the colloidal 100-1000 nm fraction (Appendix D1). Moreover, total colloidal Al, U, and Ni was 480 ± 71 mg kg^{-1},

3.6 ± 0.6 mg kg^{-1}, 8.2 ± 0.4 mg kg^{-1}, respectively, with Al and U dispersed primarily between 100-1000 nm and Ni in the < 100 nm size fractions (Appendix D1 and Figure 3.2) ($p < 0.01$). However, the 7 d anoxic incubation began to show a shift towards more Ni concentrated in the 100-1000 nm fraction (Appendix D1).

Likewise, following the 14 d anoxic incubation total colloidal C and Fe < 1000 nm increased to 367 ± 45 mg kg^{-1} and 833 ± 119 mg kg^{-1}, respectively, with C and Fe increases rising mostly from the colloidal 100-1000 nm fraction (Appendix D1). In addition, total colloidal Al, U, and Ni was 645 ± 161 mg kg^{-1}, 9.3 ± 1.0 mg kg^{-1}, 9.4 ± 0.7 mg kg^{-1}, respectively, with Al and U distributed primarily between 100-1000 nm and Ni in the < 100 nm particle size fractions (Appendix D1 and Figure 3.2). However, U < 100 nm exhibited an increase (Appendix D1 and Figure 3.2) and, similar to the 7 d anoxic incubations, Ni began to show a shift towards more concentrated in the 100-1000 nm fraction (Appendix D1 and Figure 3.2). Some of the dispersion found in the 14 d anoxic slurries was due to kinetic activity, as shown in the 14 d oxic slurries. In theses slurries, total colloidal C and Fe < 1000 nm from the soils was 201 ± 71 mg kg^{-1} and 326 ± 53 mg kg^{-1}, respectively, with C and Fe distributed predominantly between 100-1000 nm size fraction (Appendix D1). Furthermore, total colloidal Al, U, and Ni was 154 ± 19 mg kg^{-1}, 3.4 ± 0.5 mg kg^{-1}, 10 ± 0.5 mg kg^{-1}, respectively, with Al and U dispersed primarily between 100-1000 nm and Ni in the < 100 nm size fractions (Appendix D1 and Figure 3.2). Mean U and Ni increases were statistically significant at the 0.01 level according to Tukey's HSD test.

Anoxia versus pH increase dispersion

The objective of the oxic pH shifted experiments was to quantify colloidal dispersion in the 14 d anoxic incubations resulting exclusively from the development of negative particle-surface charges associated with the higher slurry pH following Fe reduction. Thus, we adjusted the slurry E.C. and pH to correspond to the conditions of our 14 d anoxic experiment and confirmed statistically similar E.C. values where the extrapolated oxic pH intersected with that of the anoxic experiment (Appendix D2) ($p < 0.01$). Total colloidal C was unaffected by pH increases, while Fe < 1000 nm increased in the oxic experiment, resulting in an interpolated 65 mg kg^{-1} and 127 mg kg^{-1} for C and Fe, respectively at the final pH of the 14 d anoxic experiments (Appendix D1). In contrast with the anoxic incubation, increasing pH additions of KOH under oxic conditions only dispersed C with diameter less than 100 nm, while Fe reduction resulted in elevated dispersion of 100-1000 nm C-bearing particles.

Furthermore, total colloidal Al, U, and Ni was 36 ± 6 mg kg^{-1}, 0.2 ± 0.1 mg kg^{-1}, 6.1 ± 0.3 mg kg^{-1}, respectively, with Al and U dispersed primarily between 100-1000 nm and Ni in the < 100 nm size fractions (Appendix D1 and Figure 3.2). Using the Tukey's HSD test, mean U and Ni increases were statistically significant at the 0.01 level. In contrast with the anoxic incubations, increasing pH by addition of KOH under oxic conditions only dispersed C < 100 nm, which was distributed primarily in the < 2.3 nm particle size fraction.

Amendment batch experiments

The initial pH of the amended soil slurries (Appendix B3) were generally higher than non-amended soils depending on the treatment implemented (phytate ≈ 10.27 ± 0.04

pH; apatite ≈ 6.46 ± 0.23 pH; humic ≈ 8.70 ± 0.19 pH). Batch slurries with a higher percentage of the amendment also had a slightly higher pH and E.C. compared with the lower percentage slurries ($p < 0.01$). Following the 14 d anoxic incubation, the phytate soil slurries exhibited decreases in pH of ~0.35 pH units and increases in E.C. of ~2.2 mS cm^{-1}, while oxic incubation decreased ($p < 0.01$) pH by ~0.9 and resulted in similar E.C. to anoxic results ($p < 0.01$) (Appendix B3). Similarly, after 14 d anoxic, humic soil slurries decreased in pH by ~0.5 and ~0.7 units for the 2% and 5% slurries, while E.C. increased for the 2% and 5% slurries by 0.39 and 1.03 mS cm^{-1}, respectively ($p < 0.01$). Similarly, after 14 d oxic, humic soil slurries decreased in pH by ~0.9 and ~0.7 units for the 2% and 5% slurries, while E.C. increased for the 2% and 5% slurries by 0.18 and 0.27 mS cm^{-1}, respectively ($p < 0.01$). In contrast, apatite slurries responded after 14 d anoxia with higher pH, an increase of ~0.3 pH units, and a stable E.C. ($p < 0.01$). However, pH decreased by ~0.4 pH units, and E.C remained stable after 14 d oxic ($p < 0.01$).

After 14 d anoxia, apatite increased < 1000 nm U by more than a factor of 4, with ~10% more U in the 5% apatite than the 2%. Most of this U was between 100 and 1000 nm with less than 15% U below 100 nm. The addition of 2% and 5% humic salt increased total colloidal U < 1000 nm by a factor of ~ 20 and 25, respectively. Most of this U increase was < 100 nm. Correspondingly, the Na-phytate samples resulted in nearly all colloidal U < 100 nm. The 2% phytate resulted in a factor 15 fold increase in total colloidal U and similarly the 5% phytate had roughly 28 times more U < 1000 nm (Appendix D6 and Figure 3.3). According to Tukey's HSD test, mean U and Ni increases were statistically significant at the 0.01 level.

Under oxic conditions, apatite increased < 1000 nm U by more than a factor of 8, with ~25% more U in the 5% apatite than the 2%. Most of this U was between 100 and 1000 nm with less than 1% U below 100 nm. The addition of 2% and 5% humic salt increased total colloidal U < 1000 nm by a factor of ~ 57 and 70, respectively. Most of this U increase was < 100 nm. Correspondingly, the Na-phytate samples resulted in nearly all colloidal U < 100 nm. The 2% phytate resulted in a factor of 57 increase in total colloidal U and similarly the 5% phytate had roughly 100 times more U < 1000 nm (Appendix D6 and Figure 3.3).

Under anoxia nearly all total colloidal Ni < 1000 nm in the apatite samples were larger than 100 nm. Compared to non-amended 14 d anoxic samples, the apatite addition tripled total colloidal Ni < 1000 nm. The addition of 2% and 5% humic salt increased total colloidal Ni < 1000 nm by a factor of ~ 10 and ~12, respectively. Most of this Ni increase was < 100 nm. Moreover, the Na-phytate samples resulted in roughly equal amounts of colloidal 100-1000 nm Ni and < 100 nm Ni. The 2% phytate resulted in a factor of 15 increase in total colloidal Ni and similarly the 5% phytate had roughly 18 times more Ni < 1000 nm (Appendix D7 and Figure 3.3).

In oxic conditions, total colloidal Ni < 1000 nm in the apatite samples was mostly larger than 100 nm. Compared to non-amended 14 d oxic samples, the apatite addition doubled total colloidal Ni < 1000 nm. The addition of 2% and 5% humic salt increased total colloidal Ni < 1000 nm by a factor of ~7. Most of this Ni increase was < 100 nm. Moreover, the Na-phytate samples resulted in roughly equal amounts of colloidal 100-1000 nm Ni and < 100 nm Ni. The 2% phytate resulted in a factor of 11 increase in total

colloidal Ni and similarly the 5% phytate had roughly 12 times more Ni < 1000 nm (Appendix D7 and Figure 3.3).

With the addition of apatite under anoxia, total colloidal C < 1000 nm more than doubled compared with non-amended 14 d anoxic samples, with C distributed predominately below < 100 nm. Furthermore, the 5% apatite samples exhibited about 25% more C than the 2% apatite. Humic additions of 2% and 5% increased total colloidal C < 1000 nm to slightly more than 2.5% and 9%, respectively, with the majority of C < 100 nm. Similarly, Na-phytate increased total colloidal C < 1000 nm to ~ 1.5% and ~ 4.2% for 2 and 5% Na-phytate, respectively, with nearly all C < 100 nm (Appendix D3).

After 14 d in oxic conditions and apatite addition, total colloidal C < 1000 nm more than tripled compared with non-amended 14 d oxic samples, with C distributed evenly between 100-1000 nm and < 100 nm. Furthermore, the 5% apatite samples exhibited about 15% more C than the 2% apatite. Humic additions of 2% and 5% increased total colloidal C < 1000 nm in only the 5% to 15%, with the majority of C < 100 nm. Similarly, Na-phytate dispersed total colloidal C < 1000 nm to ~ 2.1% and ~ 4.2% for 2 and 5% Na-phytate, respectively, with nearly all C < 100 nm (Appendix D3).

After 14 d of anoxia nearly all total colloidal Fe < 1000 nm in the apatite samples were larger than 100 nm. Compared to non-amended 14 d anoxic samples, the apatite addition quadrupled total colloidal Fe < 1000 nm. The addition of 2% and 5% humic salt increased total colloidal Fe < 1000 nm by a factor of ~ 8 and 13, respectively. Most of this Fe increase was < 100 nm. Correspondingly, the Na-phytate samples resulted in nearly all colloidal Fe < 100 nm. The 2% phytate resulted in a factor of 4 increase in total

colloidal Fe and similarly the 5% phytate had roughly 7 times more Fe < 1000 nm (Appendix D4).

In oxic conditions, total colloidal Fe < 1000 nm in the apatite samples was mostly larger than 100 nm. Compared to non-amended 14 d oxic samples, the apatite addition increased total colloidal Fe < 1000 nm more than a factor of 40. The addition of 2% and 5% humic salt increased total colloidal Fe < 1000 nm by a factor of ~60 and ~100, respectively. Most of this Fe increase was < 100 nm. Correspondingly, the Na-phytate samples resulted in nearly all colloidal Fe < 100 nm. The 2% phytate resulted in an increase by a factor of 30 in total colloidal Fe and similarly the 5% phytate had roughly 60 times more Fe < 1000 nm (Appendix D4).

Data for Al under anoxia was similar to Fe data in the three amended soils. Practically all total colloidal Al < 1000 nm in the apatite samples were larger than 100 nm. Compared to non-amended 14 d anoxic samples, the 2% and 5% apatite additions increased total colloidal Al < 1000 nm by a factor of ~1.4 and ~1.7, respectively. The addition of 2% and 5% humic salt increased total colloidal Al < 1000 nm by a factor of ~2.7 and ~4.2, respectively. This Al increase was similarly divided between < 100 nm and 100-1000 nm. Likewise, the Na-phytate samples resulted in the same equal division of colloidal 100-1000 nm Al and < 100 nm Al. The 2% phytate resulted in a factor of 5 increase in total colloidal Al and similarly the 5% phytate had roughly 5.6 times more Al < 1000 nm (Appendix D5).

Likewise, under oxic conditions Al behavior was similar to Fe data in the three amended soils. Practically all total colloidal Al < 1000 nm in the apatite samples were larger than 100 nm. Compared to non-amended 14 d oxic samples, the 2% and 5% apatite

additions increased total colloidal Al < 1000 nm by a factor of ~5.3 and ~7.3, respectively. The addition of 2% and 5% humic salt increased total colloidal Al < 1000 nm by a factor of ~8.3 and ~11, respectively. This Al increase was similarly divided between < 100 nm and 100-1000 nm. Likewise, the Na-phytate samples resulted in the same equal division of colloidal 100-1000 nm Al and < 100 nm Al. The 2% phytate resulted in a factor of 26 increase in total colloidal Al and similarly the 5% phytate had roughly 26.7 times more Al < 1000 nm (Appendix D5).

Synchrotron Element Mapping and X-Ray Micro-Diffraction

Distribution of U, Fe, and Ca in Tims Branch floodplain sediments after 5% hydroxyapatite treatment under 14 d reducing conditions using μ-XRF mapping is shown in Figure 3.4 with concentrations shown as a color scale. The XRF mapping indicates regions where U and Fe are associated and Ca from unreacted hydroxyapatite. Uranium $L_{(III)}$-edge X-ray absorption spectra from samples were too noisy to be presented even after 8 hour data collection. However, presented in Appendix C1 are spectra for model compounds containing U(IV), U(VI), and a mixed valence mineral (i.e., U_3O_8).

Discussion

Nickel and Uranium dispersion after anoxia and pH increases

The TBSP system is still subject to periodic flooding and drying from beaver activity and ongoing drought conditions. Therefore, investigating the effects of sediment anoxia on U and Ni mobilization assists in determining the fate of the contaminants. Generally, periods of inundation provide low oxygen levels and obligate anaerobe populations grow. These obligate anaerobes include sulfate-reducing microbes as well as redox metal-reducing bacteria such as *Shawanella alga*, *Geobacter metallireducens*, and

Geobacteraceae that use humics as the terminal electron acceptor and then donate electrons to redox-sensitive metals (Gu et al., 2005). U commonly binds to Fe surface sites (Figure 3.3) and during Fe-(oxyhydr)oxide reduction, concomitant dissolution of the Fe-U aggregates disperses large colloids into smaller nanoparticles (Ames et al., 1983; Arduino et al., 1989; Bonneville et al., 2004; Ryan and Gschwend, 1994). Figure 3.2 demonstrates a modest increase in dispersible < 1000 nm U and Ni after reduction periods of 7 and 14 days. However, for Ni this dispersion seems to be mostly time dependent since the 14 d oxic resulted in similar amounts of Ni dispersed. Compared to U, Ni is expected to associate preferentially with aluminosilicates, which are more stable in redox environments than Fe-(oxyhydr)oxides (Bartlett and James, 1993; Sowder et al., 2003). Additionally, aluminosilicates tend to be more soluble at lower pH (Goldberg and Glaubig, 1987), which could account for the elevated release of Ni at lower pH in the 14 d oxic treatment (Figure 3.2).

Following 7 and 14 d of anoxic incubation the pH of the soil increased only marginally (~0.2 and 0.5 units, respectively) likely due to a lack of microbial activity ionizing surface functional groups. However, one outlier showed larger microbial activity, with Δ pH > 1. Small pH increases, shown in the oxic-pH increased soil (Figure 3.2), showed a modest increase in colloidal U (p not significant), and a slight decrease in colloidal Ni ($p < 0.01$). This decrease in Ni in the oxic-pH increased soils indicates that Ni is not associated with easily dispersible colloids but primarily in the free-cation form (Jackson et al., 2005). Evidently, U and Ni are present on very different types of particles and thus respond differently to changes in redox and pH. Hence, U appears much more influenced by metal reduction and pH than does Ni.

Uranium dispersion in phosphate and humic amended sediment

All three amendments (e.g., hydroxyapatite, humic sodium salt, and sodium phytate) resulted in higher colloidal U and Ni concentrations than without amendment. Though studies conducted on Tims Branch sediments using hydroxyapatite amendments show a decrease of soluble U and Ni (Arey et al., 1999; Seaman et al., 2001a; Seaman et al., 2001b), our results suggest a mechanism for mobilization of hydroxyapatite immobilized U and Ni can occur by formation of suspended colloids (100 – 1000 nm). U increase in our studies could be due to a difference in the size fractions measured in the former studies or the incubation period. Arey et al., (1999) and Seaman et al., (2001b) measured U < 220 nm after 6 d incubations while our study analyzed larger < 1000 nm colloids after 14 d. The increase we observe in U concentration in this size range may be attributed to small PO_4-U aggregates that have not fully precipitated and settled. However, there was little change in < 100 nm U after hydroxyapatite addition that could be due to 1) increased solution dispersion from slight pH increase of solution (Appendix D6) and 2) the failed re-precipitation of U-apatite species (i.e., autunite). Indeed, XRF mapping (Figure 3.4) in anoxic soil with 5% hydroxyapatite addition indicates regions of U associated with Fe and not Ca from the hydroxyapatite, which indicates little precipitation of autunite species in this soil.

Colloidal P in the hydroxyapatite and Na-phytate soils corresponded with the concentration of added amendments (Figure 3.5). Na-phytate was ~7X more dispersive in P than hydroxyapatite with nearly all dispersion in the < 100 nm fraction. Na-phytate acts as a ‘detergent’ raising pH significantly into alkaline conditions (> pH 9) and fully dispersing colloids in solution. This high concentration of phosphate still in solution and

colloidal form leaves little phosphate to react with U and Ni; consequently, there was substantial colloidal U and Ni dispersion. The colloidal P dispersion increases in the 14 d anoxic treatments compared to 14 d oxic treatments agrees with the general paradigm for the generation of dispersion during reductive dissolution.

We attribute the increased colloidal U concentration (Figure 3.3) in the humic salt or Na-phytate amended treatments increases in dissolved and colloidal C due to the strong positive relationship between DOC and U concentrations shown in Tims Branch soils (Jackson et al., 2005; Sowder et al., 2003). Solubility of U generally increases with organic matter due to humic and fulvic acid ligands complexion to UO_2^{2+} in solution (Davis, 1984; Looney et al., 1990; Trenfield et al., 2011). Jackson et al., (2005) detected U by flow field flow fractionation-inductively coupled plasma-mass spectrometry (FL FFF-ICP-MS) associated with carbon < 2 nm in diameter. Furthermore, they found more than 20% of the U in the Tims Branch sediment in the <2 nm diameter associated with the humic fraction, while up to 50% of the U was in larger aggregate colloidal sizes (~35 nm) (Jackson et al., 2005). This tendency with U agrees with the present additions of humics in both Na-phytate and humic salt where we saw most of the U and Ni increases in the < 100 nm size that should be associated with humic fractions.

Conclusion

Our data suggests sediment anoxia in Tims Branch initiates U mobilization. Anoxic conditions intended to disperse U and Ni showed increases in colloidal (100-1000 nm) sizes as well as slight increases of pH (~0.2 and ~0.5, respectively) after 7 and 14 d incubations. However, Ni had roughly the same amount of dispersion in anoxic and oxic soils with slightly more colloidal (100-1000 nm) concentrations in the 14 d oxic

treatments, which suggests Ni is not dispersed primarily from reductive dissolution but is present in free-cation form. Unexpectedly, pH increases in oxic conditions only increased colloidal (100-1000 nm) U and Ni, and actually lowered nanoparticle and dissolved (< 100 nm) Ni. Overall, pH increases only accounted for ~10% of U and 40% of Ni dispersed < 1000 nm colloids.

Goals of immobilizing U and Ni in contaminated floodplain soils should not only study dissolved, but also easily mobilized nanoparticle colloids seen in organo-metallic flocs of suspended sediments in surface and ground waters (McCarthy and Zachara, 1989). Many phosphate amendments (e.g., apatites, Ca-phyate) show potential of precipitating out U and other toxic metals from aqueous size fractions (< 220 nm) (Arey et al., 1999; Knox et al., 2000; Seaman et al., 2001a; Seaman et al., 2001b). However, our study shows that a significant amount of colloidal (100-1000 nm) U and Ni forms after phosphate additions, that may be very mobile in hydrologic systems. Furthermore, anoxic conditions complicate aqueous and colloidal U and Ni partitioning with more dispersion in apatite soils, but unclear effects in organic and organophosphate amended soils. Humic materials and Na-phytate amendments cause dispersion of nanoparticle organic matter and colloidal soil aggregates and therefore are not appropriate for metal immobilization.

Table 3.1 Total concentrations of selected metals in Tims Branch samples via X-ray fluoresce spectrometry (XRF) (USEPA, 2007b) compared with the average for Savannah River Site (SRS) sediments (Looney et al., 1990; Pickett, 1990).

Metals	Tims Branch Sample	Avg. for SRS soils/sediments
	----------mg kg^{-1}----------	
U	533 (±54)	2
Ni	347 (±61)	10
Al	14 000 (±2 500)	~6 000
Cr	120 (±35)	38
Fe	43 400 (±8 071)	~6 000
Mn	408 (±116)	~190

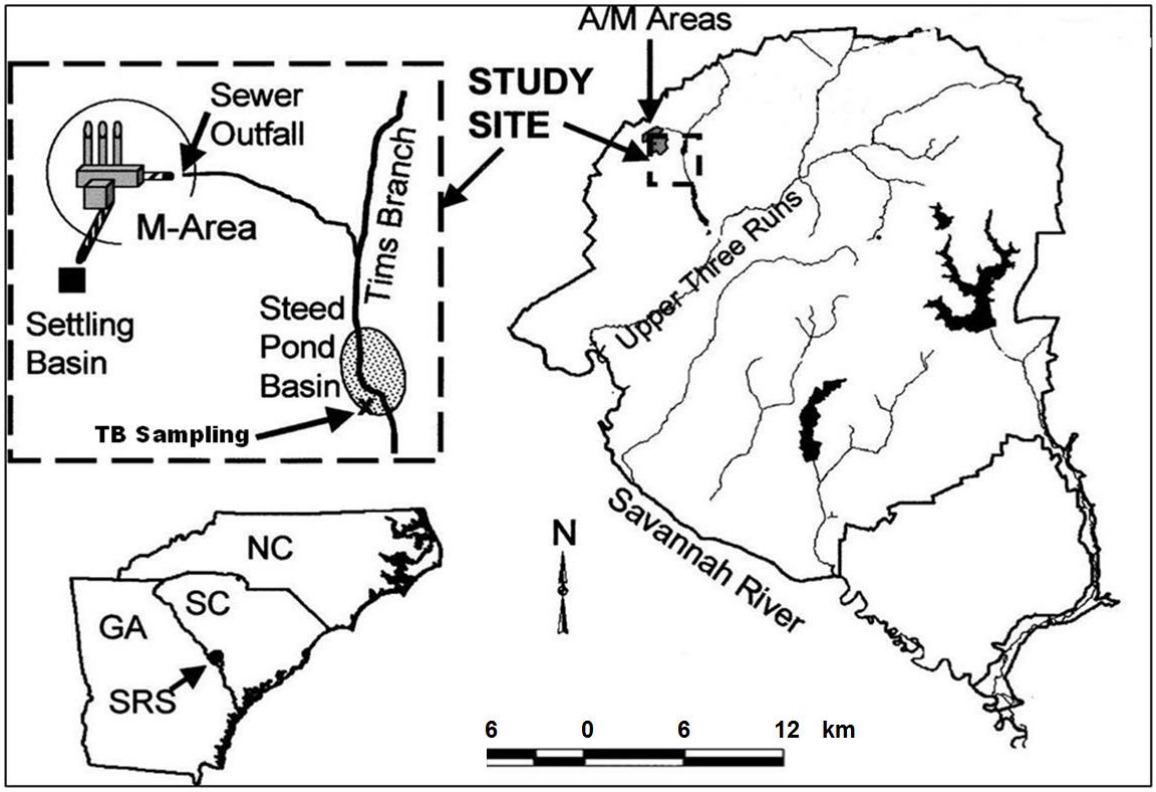

Figure 3.1: Regional location of the Savannah River Site, Manufacturing Area, and Tims Branch/Steed Pond (adapted from Sowder et al., 2003).

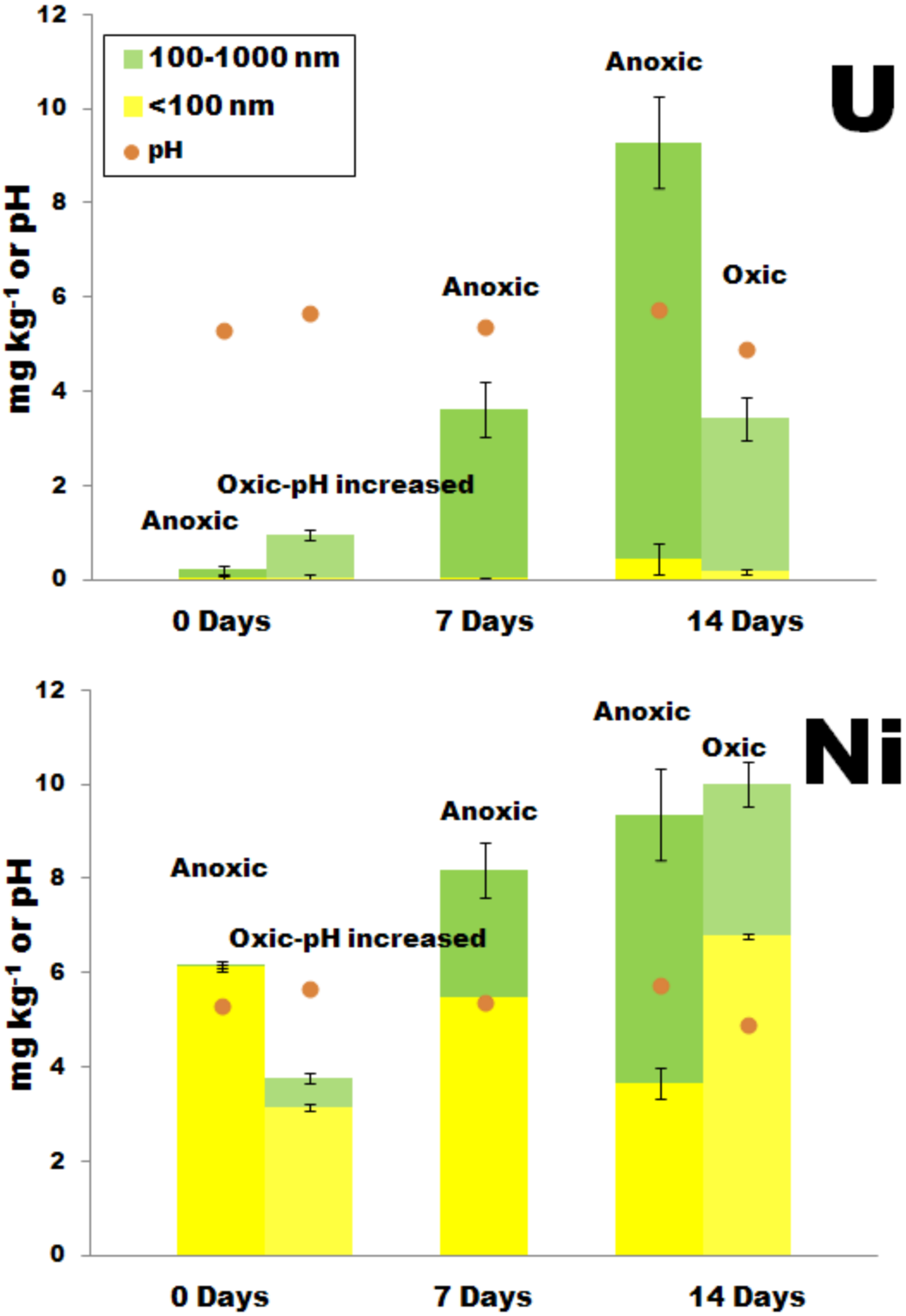

Figure 3.2: U and Ni concentrations (mg kg^{-1} soil) and pH after oxic and anoxic incubations of 0, 7, and 14 d and KOH pH-increased incubation in 2 mM KCl solution. Statistical differences exist between all incubations except [U] 0 d anoxic and oxic-pH-increased and [Ni] 14 d oxic/anoxic ($p < 0.01$).

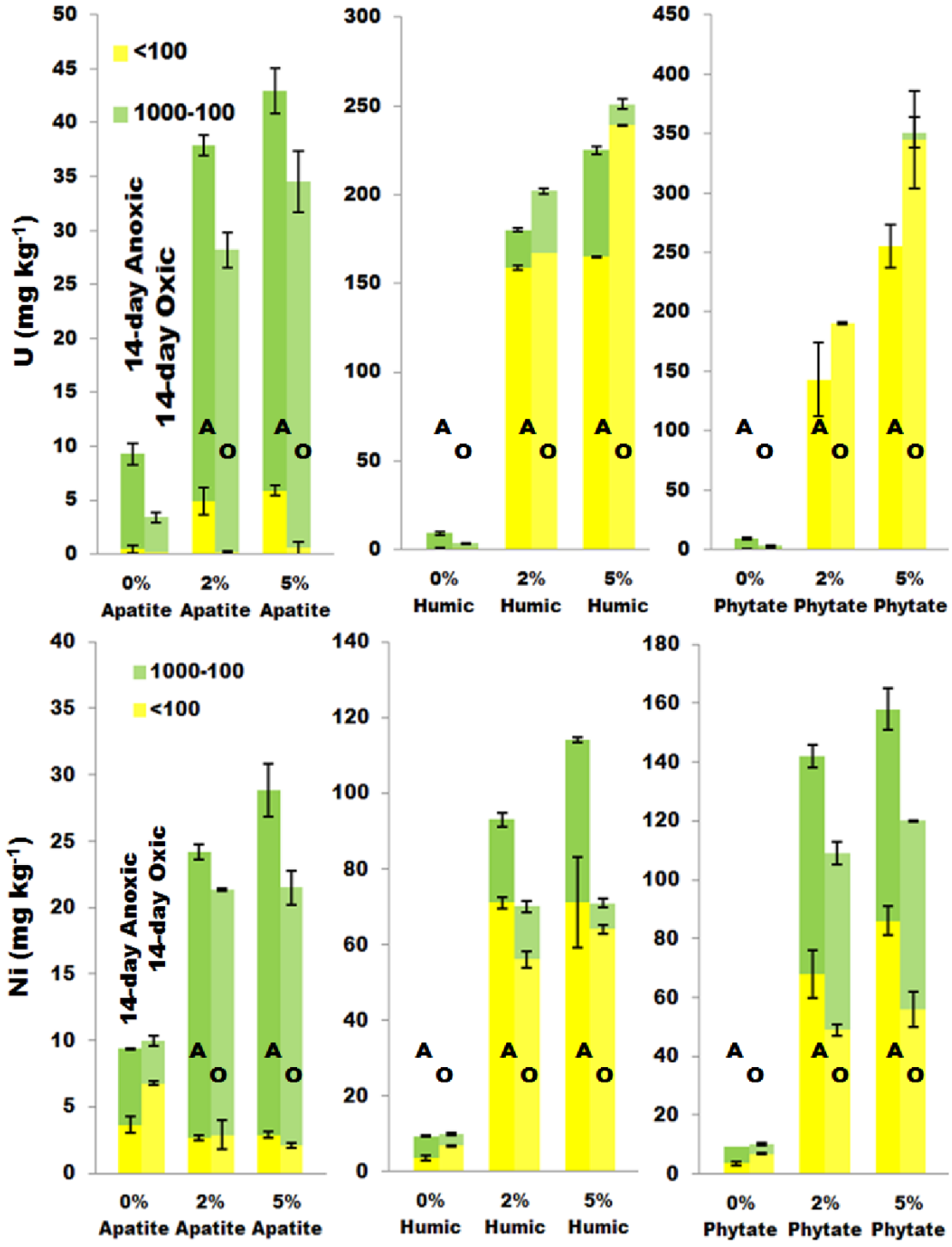

Figure 3.3: 2 mM KCl extracted soil U and Ni size fraction concentrations (mg kg^{-1} soil) as related to pH in 2% and 5% hydroxyapatite, humic salt, or Na-phytate and 14 d oxic and anoxic conditions in stacked bars. Yellow bars represents < 100 nm in diameter, and green bars represent between 100 and 1000 nm in diameter. Brackets indicate one standard deviation (n=3). Statistical differences exist between all incubations except [Ni] 14 d, 0% amendment ($p < 0.01$).

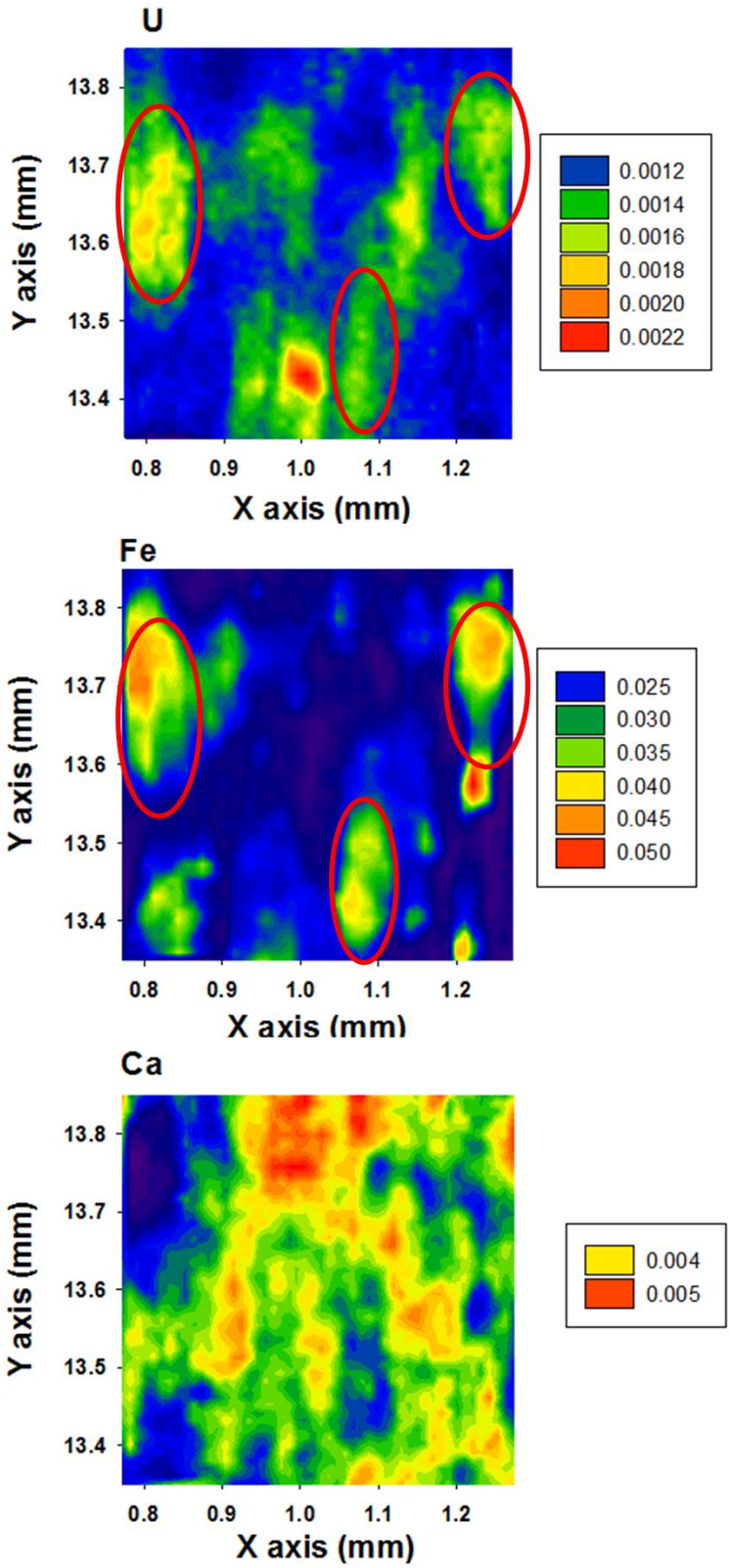

Figure 3.4: XRF mapping of Tims Branch soil after hydroxyapatite treatment after 14 d anoxia. Size 0.5 × 0.5 mm. Red circles show Fe-U associations (relative concentration).

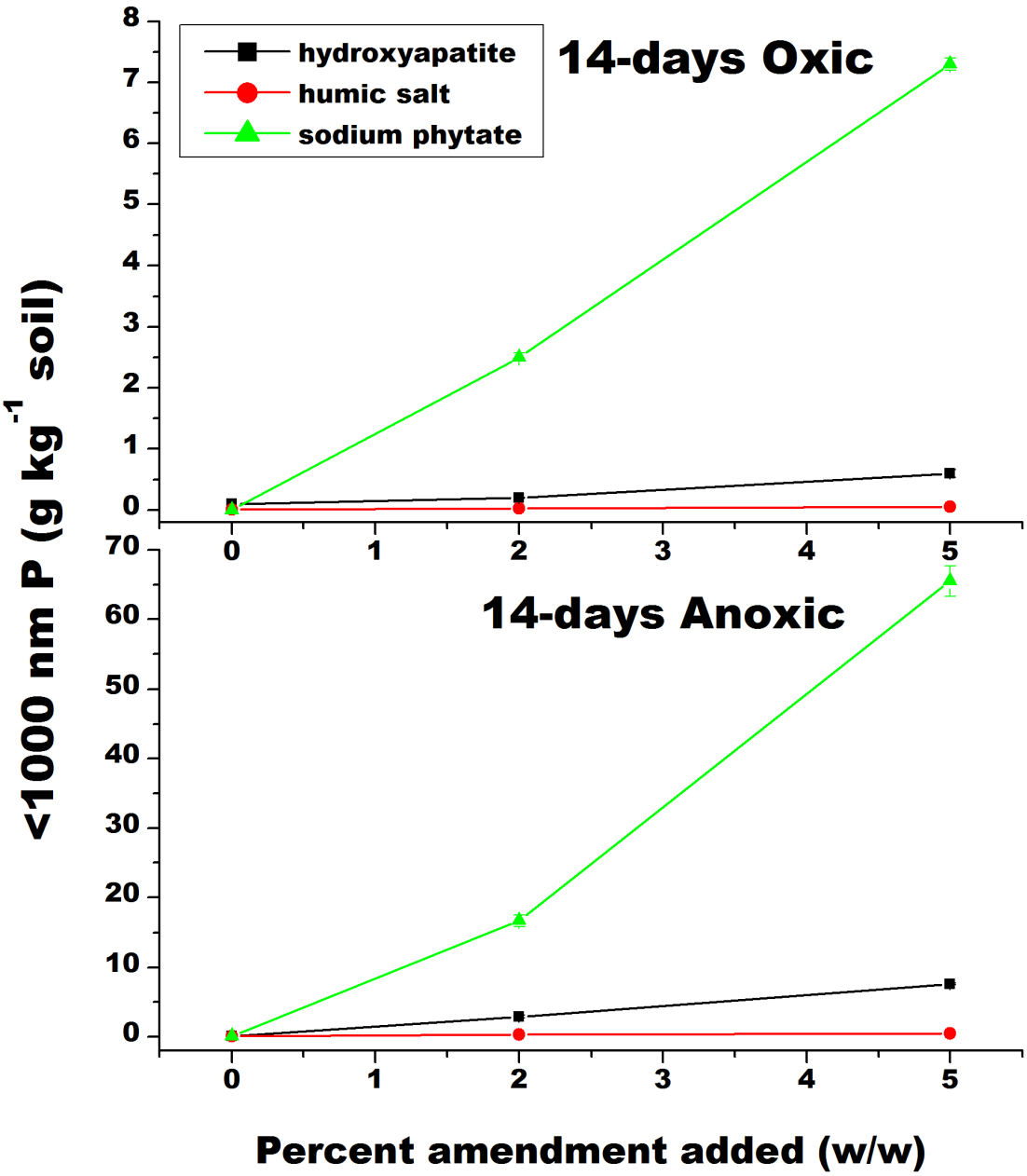

Figure 3.5: Effect of addition of sodium phytate, hydroxyapatite, and humic salt to the Tims Branch sediment on < 1000 nm phosphorus (g P / kg soil) after 14 d oxic/anoxic in 2 mM KCl. Brackets indicate one standard deviation (n=3).

CHAPTER 4

MOBILIZATION OF ANTHROPOGENIC URANIUM AND NICKEL FROM SEDIMENTS TO SURFACE WATERS DURING EPISODIC STORM EVENTS[1]

---

[1]Buettner, S.W., J.C. Seaman, A. Thompson, T.C. Rasmussen, L. Wicker.

To be submitted to the Journal of Environmental Quality

Abstract

Following construction of the Department of Energy's Savannah River Site (SRS) near Aiken, SC in 1954, over 44,000 kg of depleted uranium (U), a similar amount of nickel (Ni), and other metal contaminants were released into the Tims Branch-Steed Pond (TBSP) system. Failure of the Steed Pond dam in the 1980s facilitated substantial transfer of U to downstream ecosystems largely in association with particulates suspended during rainfall events. Since that time Steed Pond has become much more densely vegetated and the effect of this landcover shift on U and Ni mobilization is investigated in this study. Monitoring of Tims Branch below Steed Pond suggests during baseflow, mobilized Ni predominately occurs in soluble or nanoparticulate (< 220 nm) form, while large portions of U are mobilized as filterable particulates (> 220 nm). Similar U and Ni partitioning occurs when stream discharge is elevated during storm events, however automated stream sampling indicates U and Ni mass flux increase by ~200-300% due to higher discharge rates. Present day drought conditions and changes in fluvial geomorphology have reduced discharge rates as well as suspended sediment concentrations in Tims Branch leading to a 1000% reduction in U mass flux over the last twenty years. Our study suggests Fe and dissolved organic C are potential vectors in colloidal and aqueous U and Ni transport.

Introduction

Suspended sediment is the portion of the total sediment load that is transported in the water column, consisting of colloids (100 – 1000 nm), suspended clays (1 – 2 μm), and silts (2 – 75 μm). These sediments originate from erosive runoff from watershed areas as well as unstable stream channels (Robinson, 1979). Contaminants adsorb to the surfaces of colloidal particles such as Fe and Al (oxyhydro)oxides, silicas, and

phosphates, as well as smaller sized (< 220 nm) dissolved organic carbon (DOC) and are mobilized in streams (Bunn et al., 2002; Itami and Fujitani, 2005; Kretzschmar et al., 1999; McCarthy and Zachara, 1989; Pokrovsky and Schott, 2002).

Past releases of untreated wastewaters into the environment from Department of Energy (DOE) nuclear weapons materials production and processing has led to long-term contamination of areas on the Savannah River Site (SRS) in Aiken, South Carolina (Looney et al., 2003; Reed et al., 2002). In 1954, uranium discharge began just north of Tims Branch and Steed Pond (TBSP) shortly after construction of the nuclear fabrication facility in the M-Area (manufacturing area). During the etching and washing of fuel and target assemblies, metals such as uranium (U), nickel (Ni), aluminum (Al), and chromium (Cr) were released into the facility sewer system with some eventually reaching Tims Branch (TB), a second-order stream system flowing into a 16 km^2 drainage basin of Upper Three Runs Creek (UTRC), a tributary of the Savannah River (Evans et al., 1992). Diversion of the primary U discharge to the M-Area settling basin in 1982, finally ended the over 25 years of contaminant release to TBSP waters. In total nearly 44,000 kg of depleted U and a similar amount of Ni were released to the TBSP (Evans et al., 1992; Pickett, 1990). As evidenced by aerial alpha activity surveys, Steed Pond's (SP) residence time of around 3 days was sufficient to settle the majority of particulate bound U (Evans et al., 1992; Hayes, 1986). SP originally had an area of about 5.7 ha, which decreased to 4.5 ha when the wooden dam gave way in the early 1960's (Evans et al., 1992). In 1984, there was complete failure of the dam leaving SP U-contaminated sediments exposed in a wetland environment.

An 8-month study of erosive sediment transport in TBSP began immediately following the dam rupture in September 1984. Hayes et al, (1986) concluded that erosion in SP was less than predicted and reestablishment of vegetation in SP should reduce U associated suspended solid transport to UTRC even further. However, 10 years later Batson et. al, (1996) found erosion during episodic storm events mobilized a 2800% increase in U, mostly in particulate form, relative to baseflow. As little as 16 mm of rainfall was necessary to cause significant increase in stream turbidity and associated U, that was mostly attributed to particles > 450 nm (Batson et al., 1996).

Since the 1990's, vegetation cover in the TBSP has increased and flooding is more common due to beaver activity. Despite seasonal variations in redox conditions within SP, Bertsch et al. (1994) found that U in the SP sediments was present primarily in the oxidized and more soluble uranyl (U(VI)) species instead of insoluble U(IV). Reactive surfaces of Al/Fe-(oxyhydr)oxides act as effective adsorbents for oxidized uranium ions and both Ni and U are correlated with Al/Fe-(oxyhydr)oxide surfaces in the TBSP (Amonette et al., 1994; Gambrell, 1994; Sowder et al., 2003). Wetland systems often undergo reprecipitation of iron (oxyhydr)oxides with significant substitution by other metals such as Al that form amorphous (non-crystalline) iron that is even more sorbent due to increased surface area (Ames et al., 1983; Axt and Walbridge, 1999; Waite et al., 1994). Indeed Sowder et al. (2003) found SP contained nearly 60% non-crystalline iron in contaminated sediments suggesting seasonal variations in redox conditions within SP has lead to iron mineral isomorphic substitution associated with U and Ni sorption.

Our goal in this study was to directly compare episodic rain event induced contaminated sediment transport from the early 1990's (Batson, 1994; 1996) to current

conditions after nearly 20 years of monitored natural attenuation. In this comparison, it is important to include factors that have recently affected TBSP geomorphology including re-vegetation, drought, and periodic flooding from beaver activity. Restoration of native plants within SP has transformed exposed sediments into an unconfined wetland system. However, unvegetated "hot spots" of contaminated sediments continue to exist and are prone to selective erosion (Looney et al., 2003). According to climate data from the National Oceanic and Atmospheric Administration (NOAA), the SRS region suffered moderate to severe drought conditions for the past two years preceding this study. During this period of drought, precipitation was less than 75% of normal amounts. Furthermore, in the 6 months immediately preceding the studied storm event, only one month reached normal precipitation amounts while other months were at less than 50% normal. Presently, Tims Branch above SP is dry with virtually all baseflow into SP discharged from anthropogenic process waters and treated groundwater from a pump and treat system (Looney et al., 2003). Contrastingly, precipitation during the Batson et al., (1994; 1996) study was within average monthly normals for the SRS, resulting in measured average baseflow (127 L s^{-1}) during that study that was roughly 320% higher than current drought condition baseflow (~40 L s^{-1}) (Hayes, 1986). Indeed, steep incised banks along TB indicated that present stream levels are nearly a meter below past peak stage.

Our research objective was to quantify changes since TBSP re-vegetation in stream U contaminated suspended sediments. We expected conditions in TBSP to have stabilized erosive sediments and U and Ni mass flux during storm events and reduced relative to re-vegetation. We expected mobilized U is associated preferentially with colloidal aggregates (> 220 nm), while Ni is in aqueous and nanoparticle (< 220 nm) phases. To

test these hypotheses, we measured U and Ni concentrations in Tims Branch during storm events, and analyzed the current process of mobilized suspended sediments by employing stream discharge, turbidity, and rainfall.

Materials and Methods

The transport study consisted of installing an automatic sampling device at one location in TB to collect stream samples during storm events. We chose this location because it lies downstream of a culvert and effectively captures the mass flux of U transported out of SP and into UTRC. The site is approximately 129 m downstream of SP dam and is in a riparian zone with large tree canopies covering the stream (Figure 4.1).

An ISCO model 6712 automatic pump sampler, with attached flow meter, equipped with acid washed 1000-mL polyethylene bottles was used to sample the stream from the center of the stream flow using Teflon tubing hung over a rope. An ultrasonic flow meter (750 Area Velocity Module, Isco, Inc.) positioned in the center of the stream bed was programmed to engage the sampler when stream flow increased 56 L s^{-1} above base flow.

It was determined that rain intensity in the Tims Branch watershed must exceed 1.2 cm in 24 hours (Hayes, 1986) for a detectable increase in runoff and sediment load to be distinguished. A rain gauge was installed at the site to monitor storm intensity and initiate sampling with rainfall detection. A single storm on August 11th 2012 was monitored during this study. During the rain event water samples were collected bi-hourly until the rate of change in flow decreased significantly; the stream was then sampled at 4 hour intervals until base flow was achieved. Sample bottles were collected and transported to the laboratory for processing.

After through mixing, one 30-mL aliquot of each stream sample was transferred to acid washed polyethylene bottle and, acidified to 1% v/v with ultra-pure concentrated HNO_3 (Baker) acid. Total dissolved U was measured using an independent 30-mL aliquot that was filtered through a 0.22-µm nylon filter (VWR International) and acidified. This fraction was acidified using the same criteria as the total fraction. Total and dissolved U and Ni were analyzed by inductively coupled plasma mass spectrometry (ICP-MS) using a modified microwave acid digestion method (USEPA, 2007a; USEPA, 2008). Acid digestion was accomplished using ultra-pure concentrated HNO_3 (Baker) acid and heating with microwave energy. Blanks and non-impacted SRS stream controls were included in all digestion batches. Samples collected prior to storm events were used to establish background U and Ni levels. Base flow U mass flux was calculated using the same duration as the collection of storm samples (46 h), and from presently observed average stream discharge and U concentrations of 30 L s^{-1} and 6 µg L^{-1}, respectively. Similarly, base flow Ni mass flux was calculated using the same duration as the collection of storm samples (46 h), and from presently observed average stream discharge and Ni concentrations of 30 L s^{-1} and 10 µg L^{-1}, respectively.

Routine measurements of the stream sample included pH (YSI Inc.), temperature (YSI Inc.), conductivity (YSI Inc.), dissolved organic carbon, and turbidity (FTS Ltd.). Samples for dissolved organic carbon were filtered through 0.22-µm nylon filters prior to analysis utilizing a combustion non-dispersive infrared gas method with a Shimadzu TOC-5050A carbon analyzer with Shimadzu ASI-500 sampler.

Results

The studied storm event on August 11th 2012 was marked by heavy rain intensity, which was strongest during the first 3 hours of storm duration, with over 58 mm of rainfall (Table 4.1). The total ~61 mm storm rainfall exceeded Hayes (1986) determined 12.7 mm of rain needed in a day for detectable suspended sediments in TBSP. Using historical rainfall data, Batson et al., (1996) showed that rainfall will exceed this limit an average of 29 times per year. The stream rain transit response for the storm shows that peak flow occurred 6 to 9 h after the greatest amount of rainfall was received (Figure 4.2). The largest amount of turbidity occurred during rainfall and diminished once rain ceased (Figure 4.2). Once flow began to descend there was again a slight increase of turbidity above baseflow (Figure 4.2). Routine measurements of pH, temperature, conductivity are shown in Appendix E1.

Total U transported during the storm correlated less with stream flow than did filtered U (< 220 nm) (Figure 4.3). U concentration was correlated with rainfall with the highest concentrations coinciding with periods of higher turbidity and decreasing once turbidity fell and rain stopped (Figures 4.2 and 4.3). Total U concentration (~13 µg L^{-1}) during peak rainfall and turbidity was slightly more than double baseflow concentrations (2-6 µg L^{-1}). Once turbidity fell and flow increased, stream flow dilution decreased U concentrations to within baseflow concentrations (< 5 µg L^{-1}). However, the mass flux of U transported during increased discharge is significantly higher (~237%) than baseflow conditions due to a higher volume of transported suspended sediments during equal time periods (Table 4.2).

Ni mass flux was slightly higher than U and increased similarly with stream discharge (Figure 4.4) to 320% of baseflow (Table 4.2). The higher flux of Ni than U is not surprising since baseflow concentrations of Ni are ~4 µg L^{-1} higher than U. Most of the Ni suspended in the storm flow waters was < 220 nm in size and appeared less influenced by turbidity and suspended sediments than U (Figure 4.4).

Likewise, Fe mass flux generally increased with rising flow rate (Figure 4.5). However, colloidal Fe behaved similar to U and occurred with turbidity, while filtered Fe increased more with discharge rate. Streamflow Fe was primarily in particulate form during peak-flow and ~500% above baseflow mass flux levels (Figure 4.5). DOC mass flux acted similar to suspended Ni and increased with stream discharge. Peak DOC concentrations were ~3.5 mg L^{-1} at maximum turbidity, representing ~170% of baseflow concentrations (Figure 4.6).

Additionally, the migration of beavers from UTRC towards TBSP has altered stream morphology through series of small dam formation, which can also cause dynamic redox to sediments. The vegetated riparian zone of TB has the potential to form sediment traps from fallen limbs and leaf litter that hinder sediment mobilization during low flow. Also during low flow conditions flocculation of aggregate organo-metallic colloids (Appendix E2) typically occurs in TB, enabling the suspension and transport of contaminated sediments (Furrer et al., 2002; Goldberg and Glaubig, 1987; Itami and Fujitani, 2005; McCarthy and Zachara, 1989; Stone and Krishnappan, 2003). These flocs are heavily influenced by Derjaguin-Landau-Verwey-Overbeek. (DLVO) theory, which describes colloid behavior through balancing attractive van der Walls forces with repulsive forces from the overlap of diffuse electric double layers (Derjaguin and Landau,

1941; Lyklema, 1977; Matijevic, 1973; McDowell-Boyer et al., 1986; Ryan and Elimelech, 1996; Verwey, 1947). Indeed, factors that affect surface charge of colloids, such as redox potential and pH, also influence colloid dispersion and flocculation (Grolimund and Borkovec, 1999; Healy et al., 1973; Itami and Fujitani, 2005). Due to high concentrations of reactive Fe and Al metals surfaces in TBSP sediments as well as a dynamic redox and pH environment, potential for dramatic shifts in colloidal behavior is evident, making it difficult to predict contaminated sediment fate (Looney et al., 2003).

Discussion

Contaminant transport

In the early 1990's, Batson et al., (1994; 1996) determined that baseflow U mass flux greatly underestimated mobilization of contaminated sediments in TBSP fluvial systems during episodic rain events. Their study determined that during rain events 1500-2800% more U exported to UTRC relative to base flow measurements. The main driver of this drastic increase of U mobilization was the vast increase of stream discharge from baseflow (~1000% higher) during storms. For comparison, in the present storm studied measured discharge increase above baseflow was around 500% higher. Overall, both total and filtered U mass flux levels have decreased significantly from the levels shown in the 1993 storms. Much of this decrease is due to the ~300-500% decrease in TB discharge, however, analyzing U concentrations per equal volume still indicates a ~1000% decrease in U mobilization compared to storm events in 1993. Current U partitioning corresponds with past observations, linking suspended sediment U to larger colloidal sizes > 220 nm indicative of Fe oxides (Amonette et al., 1994; Batson, 1994; Bertsch et al., 1994; Evans et al., 1992; Sowder et al., 2003). Total Fe concentrations in Tims Branch were

surprisingly >13,000% times higher compared to a non-impacted creek (Boggy Gut Creek) at SRS, showing a huge potential for U-Fe interaction. However, in stream samples with low turbidity there appears to be a relative increase in < 220 nm U indicative of humic bound U (Jackson et al., 2005; Trenfield et al., 2011).

Total suspended Ni concentrations exhibited similar increases during peak discharge with little Ni associated with particles > 220 nm. This is consistent with past evidence showing Ni present as labile complexes and free-metal cations in the TBSP system (Jackson et al., 2005; Sowder et al., 2003). Fe mass flux pattern was similar to Ni, however with more Fe partitioning to particles > 220 nm (Appendix E3). In TBSP, coatings of ferrihydrite and goethite on sediment surfaces are an important sorbent for U and Ni (Bertsch and Seaman, 1999; Bertsch et al., 1994). During the storm event, total Ni and Fe mass flux exhibited similar patterns during storm flow and may be associated in aggregates (Appendix E3). DOC is also recognized as an important complexation agent with U, Ni, and many other metals (Bertsch and Seaman, 1999; Bertsch et al., 1994; Evans et al., 1992; Gu et al., 2005; Jackson et al., 2005; Jansen et al., 1997; MacCarthy, 1989; Sowder et al., 2003; Trenfield et al., 2011). DOC regulates the solubility of metals by acting as a highly reactive substrate for sorption and forming soluble organic ligands with metals. U associated with humic and fulvic acids is characterized as small size nanoparticle and aqueous phases, while DOC solubilization of Ni is much less (Jackson et al., 2005; Looney et al., 2003). However, in the studied storm event the pattern of DOC and U mass flux do not correlate ($r^2 < 0.54$) suggesting U sorption to organic carbon molecules may not occur in TBSP during storm flow.

Storm analysis

The observed high precipitation amount does not occur normally at SRS, with storm intensities of this magnitude occurring less than a few times a year (summer being the most probable time of occurrence) (Batson, 1994; 1996). However, these sporadic rainstorms have significant potential to mobilize U suspended sediments, and if not considered can vastly underestimate annual U and Ni transport (Batson, 1994; 1996). The storm event monitored by Batson et al, (1994; 1996) in June 1993 showed similar rain intensity, with over 47 mm of rain collected in the storms first 3 hours. However, the stream rain transit response for the 1993 storm shows that peak flow occurred 3 to 6 h after rainfall (Batson, 1994; 1996), a decrease of ~3 h compared to the studied storm event in August 2012. The longer TBSP response time in our study likely reflects higher infiltration in the present, drought stricken soils, which can be expected to reduce runoff quantities (Penna et al., 2011), as well as changes in stream morphology by beaver activity (Pollock et al., 2003).

Unlike the storms in 1993, maximum amount of turbidity and associated suspended sediment release occurred at the onset of rainfall and not at peak discharge rate indicating erosion of unstable stream banks during runoff (Hooke, 1979; Kinnell, 2005). In fact, pH and conductivity dropped with increasing discharge and turbidity levels decreased once peak discharge was reached, implying dilution of the soil runoff waters (Meybeck et al., 1992). The lack of continued turbidity throughout the hydrograph suggests beaver dams and other sediment traps within SP may effectively immobilize suspended sediments at high discharges.

Conclusion

Natural attenuation within TBSP has shown to be effective for reducing U and Ni contaminated sediment transport by stabilizing stream channel sediments and reducing streamflow turbidity. The recent buildup of organic material in TBSP may be burying contaminated sediments or conceivably these sediments are slowly leaving the TBSP watershed at low concentrations. Our monitoring efforts below SP suggest that during baseflow, mobilized Ni predominately occurs in soluble or nanoparticulate (< 220 nm) form, while ~55% of U is mobilized as filterable particulates (> 220 nm). During episodic storm event, Batson et al., (1996) found filterable (> 450 nm) U to comprise nearly 90% of total U at peak flow conditions. Compared to storms in 1993, U mass flux as a percent above baseflow, has decreased by an order of magnitude (e.g., U decreased from ~2800% to 237%). Similarly, Ni mass flux during current stormflow was estimated 320% higher than baseflow conditions. Unlike the episodic storms in 1993, turbidity and related suspended sediments in the studied storm event increased during rainfall rather than stream discharge rate. Either this suggests a change in stream geomorphology that has reduced erosive conditions in TBSP stream banks or dilution of runoff waters due to much lower baseflow levels than 20 years ago. U in turbid samples suggest colloidal aggregates (> 220 nm) bound to Fe(oxyhydro)oxides or high molecular weight organic carbon molecules. We found suspended Ni mostly associated with nanoparticle (< 220 nm) and aqueous forms with some correlation with Fe and DOC. In order to clarify U and Ni colloid mobilization in this system, sample analysis from additional storm events is necessary.

Table 4.1: Storm rainfall totals for episodic rain event on Aug. 11th 2012.

Hours after storm onset	mm Rain
1	8.8
2	32.9
3	16.8
4	0.3
5	0
6	0.7
7	0.9
8	0.7
31	0.1
50	0
Total	**61.2**

Table 4.2: Comparison of mass flux U and Ni during storm and baseflow conditions.

	Mass transported during storm	Mass during baseflow	Increase above baseflow during storm
	——————kg——————		——%——
U	~0.071	~0.030	237
Ni	~0.128	~0.040	320

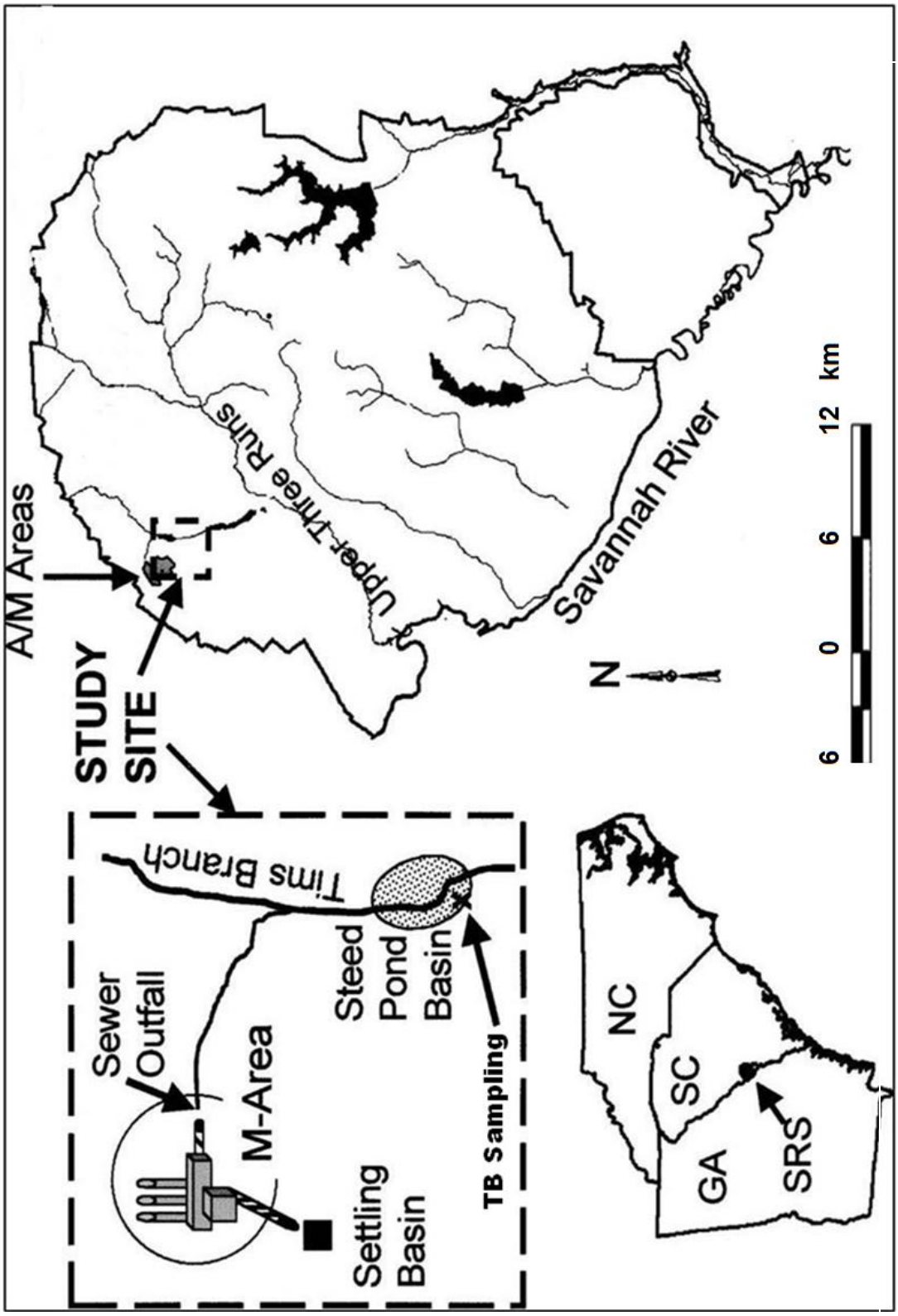

Figure 4.1: Regional location of the SRS, M Area, and Tims Branch/Steed Pond. Adapted from (Sowder et al., 2003).

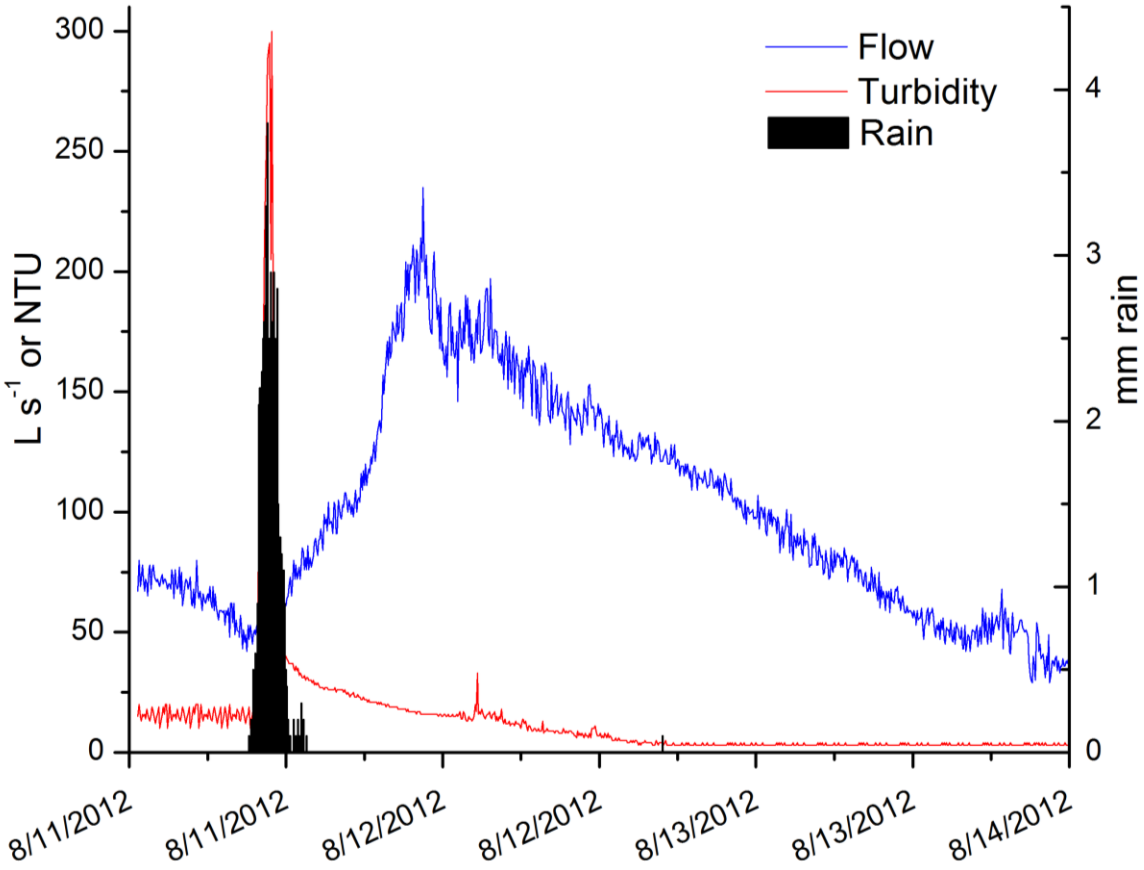

Figure 4.2: Storm hydrograph versus rainfall (mm) and turbidity (NTU, nephelometric units) on August 11th 2012 showing Tims Branch rain transit response time.

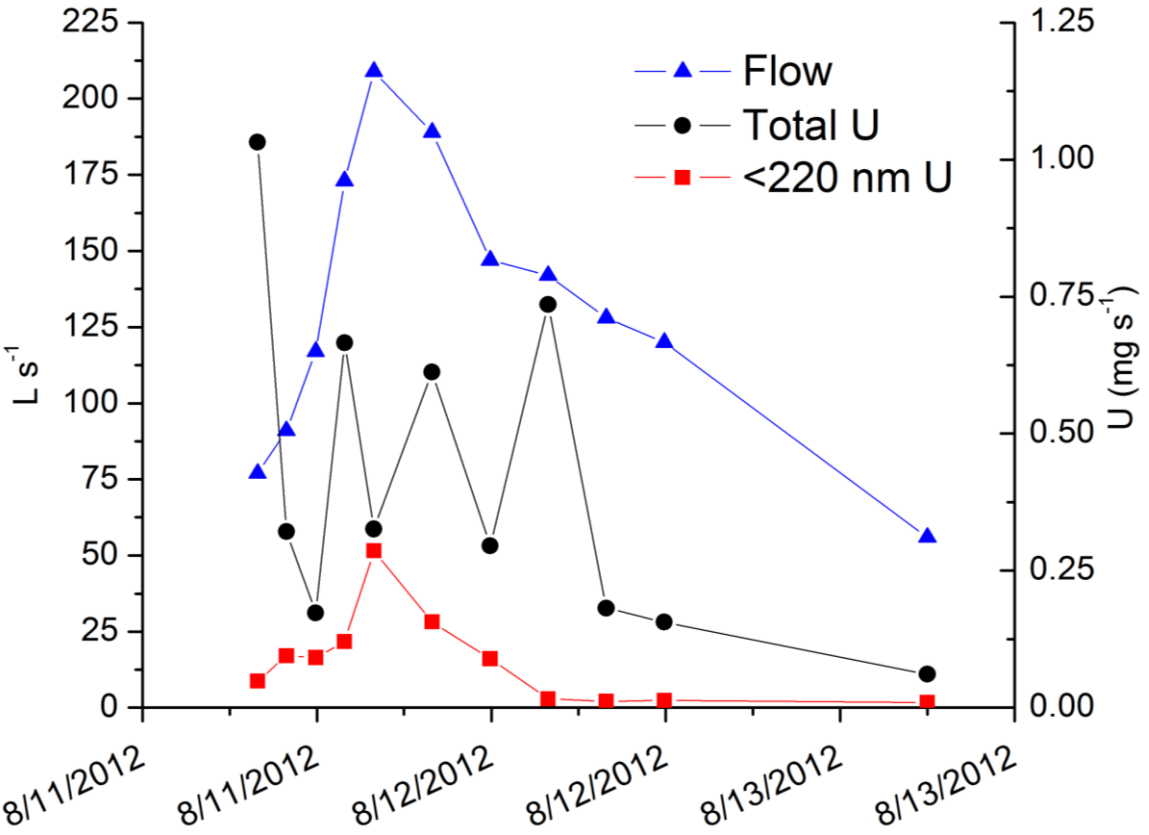

Figure 4.3: August 11th 2012 storm hydrograph at Tims Branch showing mass flux of both total and filtered (< 220 nm) U versus flowrate.

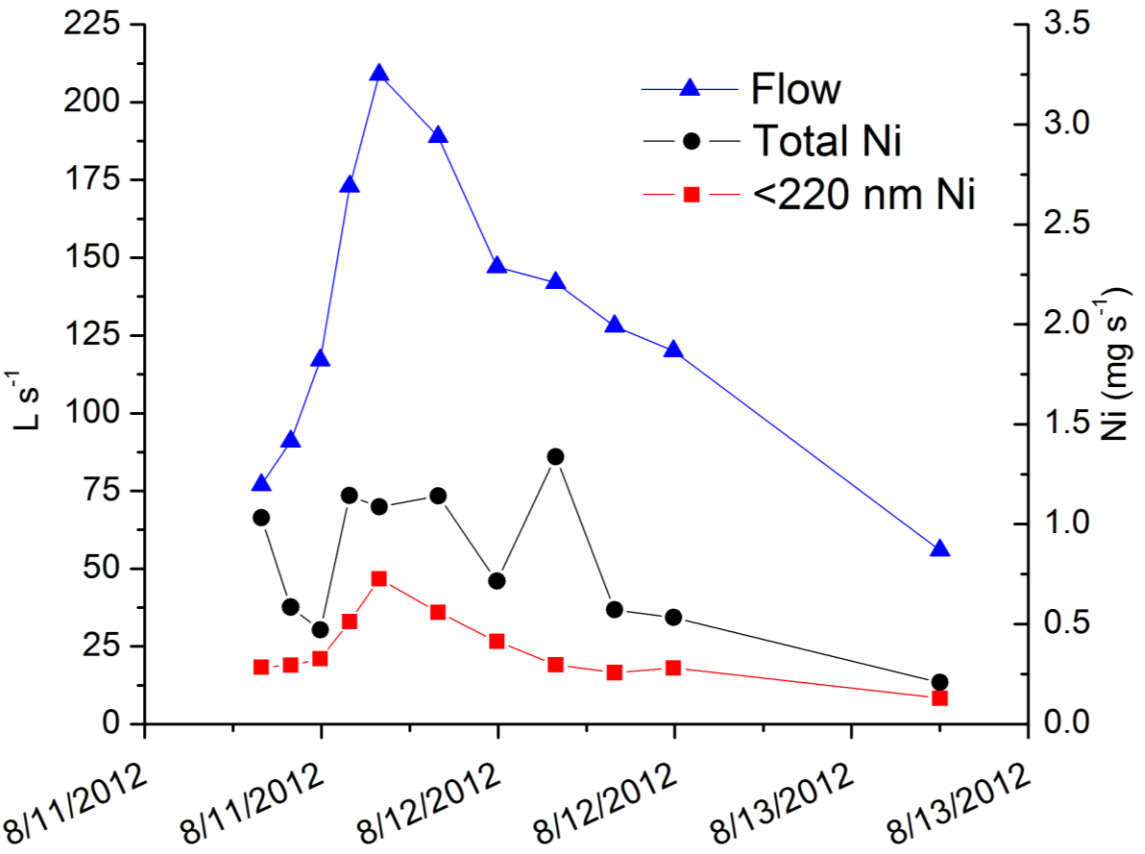

Figure 4.4: August 11th 2012 storm hydrograph at Tims Branch showing mass flux of both total and filtered (< 220 nm) Ni versus flowrate.

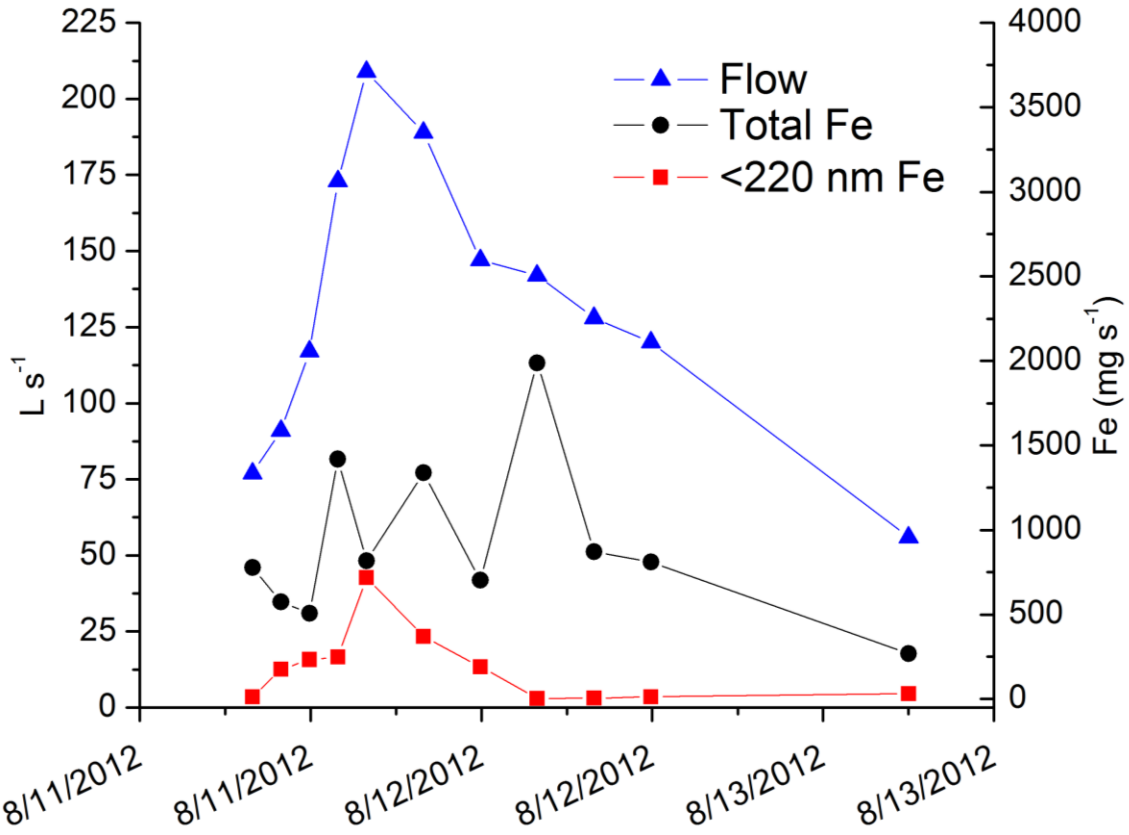

Figure 4.5: August 11th 2012 storm hydrograph at Tims Branch showing mass flux of both total and filtered (< 220 nm) Fe versus flowrate.

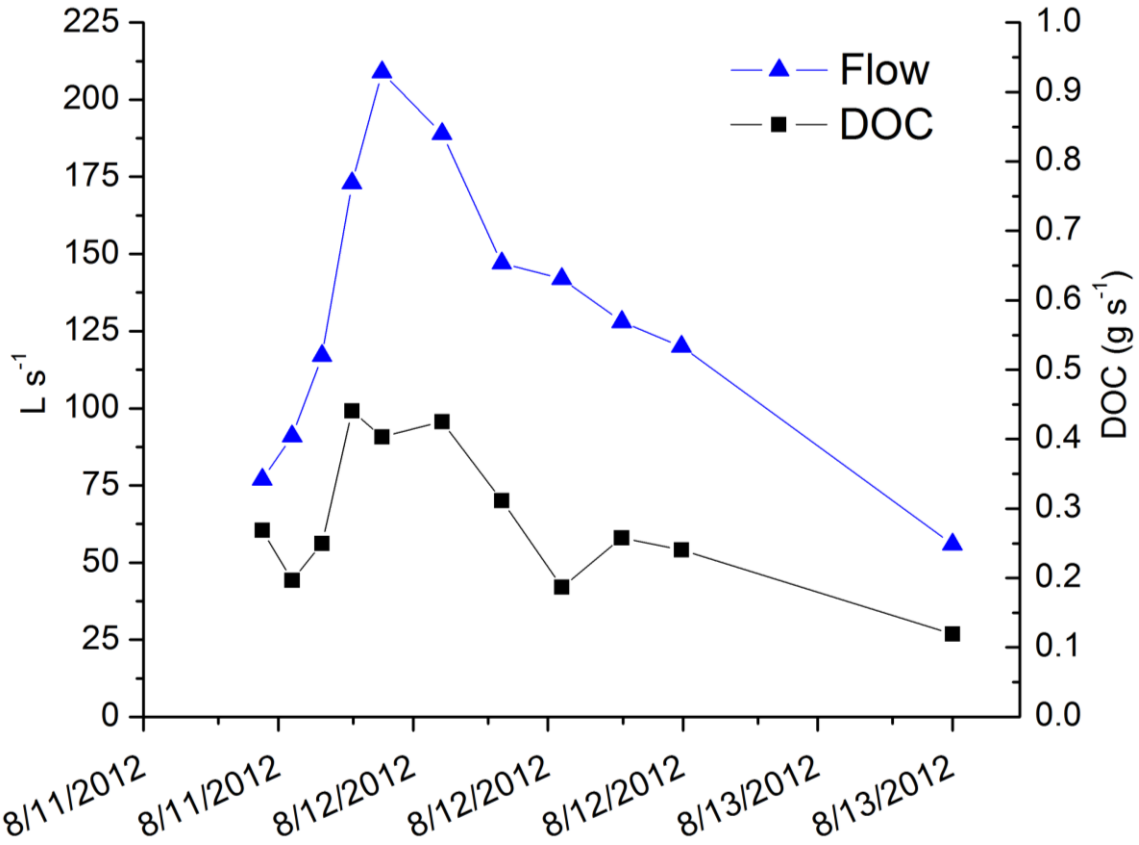

Figure 4.6: August 11th 2012 storm hydrograph at Tims Branch showing mass flux of DOC versus flowrate.

CHAPTER 5

MOBILIZATION OF COLLOIDAL CARBON IN HAWAIIAN SOILS[1]

[1]Buettner, S.W., Kramer, M., Chadwick, O.A., Thompson, T.C.

To be submitted to Geoderma.

Abstract

The transport of organic carbon to deep mineral horizons in soils can lead to long-term carbon stabilization. In basaltic soils, carbon associations with nano-crystalline minerals often lead to colloid-sized aggregates that can be dispersed and mobilized by changes in soil solution chemistry. In the montane forest region of Hawaii, basaltic soils are exposed to high rainfall and anoxic redox conditions that facilitate ferric (Fe^{III}) oxide reduction. We explored the potential of Fe-reducing conditions to mobilize carbon by exposing the A horizon of three soils, aged 0.3, 150, and 350 ka from the Island of Hawai'i, to 21 days of anoxic incubation in 1:10 soil slurries. Mobilized carbon was quantified by fractionating slurries into three particle-size classes (< 260 nm, < 35 nm, < 2.3 nm ≈ 10 kDa). Across all studied soils, we found Fe reduction (maximum Fe^{2+} (aq) ≈ 17.7 ± 1.9 mmol kg^{-1}) resulted in ~500% and ~700% increase of carbon in the 2.3 - 260 nm, and < 2.3 nm size fractions, respectively. In addition, Fe reduction increased solution ionic strength by 127 µS/cm and generated hydroxyl ions sufficient to increase the slurry pH by one unit. We compared this to carbon mobilized from the slurries during a 2-hr oxic incubation across a similar range of pH and ionic strength and found similar amounts of dissolved (< 2.3 nm) and nanoparticulate (2.3 – 35 nm) carbon were mobilized as pH was increased. However carbon associated with the largest particles (35 – 260 nm) was only dispersed during the Fe reduction experiments, suggesting binding to Fe-oxide phases. Our experiments suggest colloidal dispersion during Fe-reducing conditions has the potential to mobilize high concentrations of carbon and offers a potential mechanism for migration of C into deep mineral horizons in redox dynamic soils.

Introduction

The Earth's carbon (C) cycle is influenced strongly by the distribution and behavior of C in soils. Considerable effort is now directed at understanding the mechanisms regulating soil carbon stabilization and turnover rates (Schmidt et al., 2011), with climate (Giardina and Ryan, 2000; Townsend et al., 1997; Trumbore, 1997) including the duration of rainfall inundation and temperature major factors (Schuur et al., 2001). Many studies observe carbon deep in the soil profile has longer turnover times (Harrison et al., 2011; Torn et al., 1997) and suggest lower microbial activity and increased association with mineral surfaces, particularly short-range-ordered (SRO) minerals (Chorover et al., 2004; Lalonde et al., 2012; Mikutta et al., 2009), contribute to its persistence at depth. Carbon generated at the surface of the soil can be delivered to deep soil horizons by root death, burrowing animals or the soil solution (Strahm et al., 2009). The later route is greatly facilitated by preferential flow channels, which reduce the travel time and potential for degradation during transport as well as allow movement of carbon associated with soil colloids.

The recent work by Marin-Spiotta et al. (2011) illustrates the importance of preferential flow channels for the movement of carbon from the surface horizons to deep mineral horizons in tropical rainforest soils from intermediate-aged sites in Hawaii. These sites are of particular interest because the carbon at depth has a very low turnonver time and is strongly associated with SRO minerals (Harrison et al., 2011; Torn et al., 1997)]. Marin-Spiotta et al. (2011) suggest both dissolved and particulate carbon are important vehicles for carbon transport in these soils, but they reported only soluble carbon and did not offer a mechanism for the generation of mobilized organic carbon (MOC) in these

soils. The soils studied by Marin-Spiotta et al. (2011) are subject to periods of reducing conditions that promote Fe reduction and lead to a net loss of Fe in the upper horizons. Reductive dissolution of Fe^{III}-oxides can promote colloid dispersion by dissolving the connective Fe cement holding aggregates together (Goldberg and Glaubig, 1987). Also, because Fe reduction consumes protons and causes an increase in solution pH (Gillespie, 1920; Ponnamperuma et al., 1966; Vesparaskas and Faulkner, 2001), it can indirectly influence colloid dispersion through development of negative charge on colloid surfaces (Bunn et al., 2002; Ryan and Gschwend, 1994). Therefore, Fe reduction can influence colloidal mobilization physically via dissolution of particles or chemically through changes in pH and corresponding particle surface charges (Thompson et al., 2006a). Fimmen et al. (2008) and Grybos et al. (2009) have suggested that organic matter is likely subject to dispersion during Fe-C redox cycles, although they do not provide direct evidence.

Our research objective is to quantify changes in dissolved, nanoparticulate, and colloidal organic matter following Fe reduction events and induced pH increases. We suspect that these conditions are prevalent in organic-rich Hawaiian soils during high water periods, which would enable leaching of "new" carbon to depths where the organic matter is expected to degrade very slowly (Marin-Spiotta et al., 2011; Torn et al., 1997).

We hypothesize that anoxic conditions destabilizes carbon in organic-rich basaltic soils and generate mobile organic colloids. Thompson et al. (2006b) have shown Fe reduction in similar-age Hawaiian soils promoted colloid dispersion primarily through the indirect effects of hydroxide production. We hypothesize dispersion of colloid carbon can be similarly explained by pH changes. To test these hypotheses, we measured the carbon

content across three particle size classes following laboratory incubations of Hawaiian surface soils exposed to either a 21-day period of anoxia or short-term pH adjustments.

Materials and Methods

Site description

Soil was collected from three different sites on the Island of Hawai'i; Pu'u Eke (ca. 350 ka) from the lava flow of the now-extinct volcano Kohala; Laupāhoehoe (ca. 20 ka) from the dormant volcano Mauna Kea; and Thurston (ca. 0.3 ka) from the active volcano Mauna Loa (Figure 5.1).

Anoxic experiment

Triplicate incubations of field-moist soil were suspended in 2.0 mM KCl at a soil:solution ratio of 1:10 (dry mass equivalent) in 12-mL polypropylene tubes. Soil-dry mass was determined after drying a separate subsample for 24 h at 110°C. The suspensions were shaken in 12-mL polypropylene vials for 2 h on a horizontal shaker (~120 strokes per minute (spm)). Three, 1.5-mL aliquots were removed and subjected to differential centrifugation targeting < 260 nm, < 35 nm, and < ~2.3 nm (10 kDa) particle-size fractions as described below. These aliquots provided a pre-reaction sample set. The remaining suspension was opened in an anoxic chamber (95% N_2, 5% H_2) and allowed to equilibrate for 16 h before resealing. Suspensions were then secured on an end-over-end shaker (8 rpm) inside the glovebox and reacted for 21 days at room temperature (~25°C).

Following incubation, size-fractionated samples were isolated by differential centrifugation in an Eppendorf 5430 centrifuge with a F45-30-11 rotor for < 260 nm and < 35 nm hydrodynamic diameters. Centrifugal fractionation was achieved assuming spherical particle geometry and a nominal particle density of 2.65 g cm^{-3} for particles; the

RCF and time required to achieve separation of particles < 260 nm (3 min at 3,195 RCF or 5,400 rpm for 3 min), < 35 nm (24 min at 21,169 RCF or 13,900 rpm for 24 min) was calculated from Stokes' law (Henderson et al., 2012). Samples were returned to the glovebox where the supernatant solutions were removed and acidified to pH 1 with trace metal grade 6 M HCl (0.8% of sample volume). The < 10 kDa fraction was obtained by centrifuging identically to the < 35 nm fraction and then supernatant was passed through a 10 kDa molecular weight cutoff Millipore Amicon-Microcon filter (at 14,000 rpm for 10 min) using an Eppendorf Minispin Plus centrifuge inside the glovebox. Prior to use, we removed glycerin contamination of the < 10 kDa filters by running a solution of 0.1M NaOH through the filters three times, followed by three 18.2MΩ water washes. Filters were then immediately used for ultrafiltration of the soil solutions.

Oxic pH shifted experiment

A separate experiment was conducted under oxic conditions to isolate the effects of pH on colloidal carbon mobilization. The intent of the oxic pH shifted experiments was to quantify colloidal dispersion in the anoxic incubations resulting solely from the development of negative particle surface charge associated with the higher slurry pH following Fe reduction. Thus, we adjusted the slurry E.C. and pH to span the conditions of our anoxic experiments and confirm statistically similar E.C. values. The suspensions were equilibrated between 3 and 5 mM ionic strength across a pH range of 4 to 6 through measured additions of 0.1M KOH. The suspensions were then shaken on a horizontal shaker for 2 h and sampled identical to that described above for the anoxic samples (e.g., differential centrifugation and ultrafiltration).

Sample analysis

We measured pre and post experimental pH, electrical conductivity (EC), and redox potential (Eh) data on both the anoxic and pH shifted oxic treatments. Organic carbon (TOC) in the aqueous and solid phases was analyzed by high-temperature combustion following sparging of acidified samples on a Shimadzu TOC-5050A with Shimadzu ASI-500 sampler. To access the presence of reducing conditions in the anoxic experiment, we measured ferrous iron using a revised ferrozine spectrophotometric method (Stookey, 1970; Thompson et al., 2006c) on a Shimadzu UV-1700 Spectrophotometer.

Multi-angle light scattering and AF4 analysis

Particle size was validated on an Eclipse 2 (Wyatt Technology) asymmetrical-flow Field Flow Fractionation (AF4) channel (19.7 cm × 5.6 cm) coupled to a DAWN Heleos® multi-angle laser light scattering (MALS) device (Wyatt Technology). The AF4 separates fractionates particles on the basis of their diffusion coefficients in a flow channel. The AF4 was operated with a 490 μm thick separation spacer and a 10 kDa cellulose membrane. Our carrier solution was a sodium azide-SDS buffer (pH 7.5) prepared from 18.2MΩ H_2O with 3 x 10^{-4} mol L^{-1} sodium dodecyl sulfate and 200 mg L^{-1} sodium azide. For the control, 30 μL of the solution was loaded into the AF4 injection loop, and the separation was conducted with a 1.0 mL min^{-1} channel flow. The crossflow was continuously varied from 0.8 mL min^{-1} to zero over 20 minutes with an initial 8 minutes of sample focusing. For the Pu'u Eke sample, the same conditions were used, except with a 60 minutes elution time. Light-scattering data were collected

simultaneously at 10 scattering angles θ on each eluting sample and were analyzed for hydrodynamic radius using the Astra® instrument software (Dubascoux et al., 2008).

TEM analysis

The size and composition of the dispersed colloids was further characterized via transmission electron microscopy (TEM). Supernatants from the 2.3 nm – 260 nm particle size separations of our 21-d anoxic treatments were dialyzed against de-oxygenated 18.2MΩ water inside our anoxic chamber to remove dissolved salts and Fe^{2+}(aq). The colloids were then freeze dried, re-suspended briefly in 18.2MΩ water while shaking for 20 min. and then applied to a formvar-coated TEM grid. Samples were visualized on a 200 kV TEM (Philips/FEI Technai 20, FEI Co., Eindhoven, Netherlands).

Results

Anoxic experiment

The initial pH of the soil slurries (Table 1) was consistent with prior pH measurements of these surface soils (Chorover et al., 2004; Mikutta et al., 2009). Following the 21-day anoxic incubation, all soil slurries exhibited increases in pH, EC (electrical conductivity), aqueous [Fe^{+2}], and a decrease in Eh (Table 1). The pH increase was similar between the Laupāhoehoe (20 ka) and Pu'u Eke (350 ka) soils (~ 0.7 pH units), while significantly greater (~1.6 units) for the Thurston (0.3 ka) soil, likely reflecting differences in the pH range of the Thurston soil, as the calculated soil buffering capacity assuming a 2 mol H^+ are consumed per mole of Fe^{III} reduced to Fe^{2+} (see Table S-2 in Thompson et al., 2006b) was between 33 and 38 mmol C kg^{-1} for all soils. Likewise the lower Eh for the Thurston soil following the anoxic incubation is partially due to the higher pH of this soil with final Eh values adjusted to pH 7 (Bartlett and

James, 1993) of -348, -319 mV, and -254 mV for the 0.3 ky, 20 ky, and 350 ky soils, respectively.

At the beginning of the experiment, total desorbed carbon < 260 nm from the soils was 0.93 ± 0.03 g kg^{-1}, 1.01 ± 0.05 g kg^{-1}, 0.61 ± 0.03 g kg^{-1} for the 0.3 ky, 20 ky, and 350 ky soils, respectively, with C distributed similarly across the three particle size fractions (Figure 5.2). Following the anoxic incubation total desorbed C < 260 nm increased to 7.1 ± 0.3 g kg^{-1}, 7.1 ± 0.5 g kg^{-1}, 5.2 ± 0.3 g kg^{-1} for the 0.3 ky, 20 ky, and 350 ky soils, respectively. The distribution of C across the three particle size fractions (< 2 nm, 2 – 35 nm, and 35 – 260 nm) was similar before and after incubation across all soils and relatively consistent between the 0.3 ky and 20 ky. However, the 350 ky soil contained less carbon in the 35 – 260 nm particle size class than the other two soils and this accounted for the majority of its lower total carbon desorption (Figure 5.2).

Oxic pH shifted experiment

Total desorbed C < 260 nm increased with increasing pH in the oxic experiments (Figure 5.2), resulting in an interpolated 3.8 g kg^{-1}, 3.7 g kg^{-1}, 2.7 g kg^{-1} (Table 2) for the 0.3 ky, 20 ky, and 350 ky soils, respectively at the final pH of the anoxic experiments (Tables 5.1 and 5.2). In contrast with the anoxic incubations, increasing pH by addition of KOH under oxic conditions only dispersed C < 35 nm, which was distributed similarly between the < 2.3 nm and the 2.3 nm – 35 nm particle size fractions.

Nanoparticle characterization

The hydrodynamic radius of the oxic pH shifted Hawaiian soil particles (< 260 nm diameter) were validated by asymmetrical flow field-flow fractionation, AF4 (Figure 5.4). It is apparent from the chromatogram that particle aggregation has occurred to some

degree in the instrument as the particle distribution does not match that of the 100 nm standard. Instead, it appears that the humic substances did not elute from the channel until nearly zero cross flow rate was achieved, resulting in a sharp-narrow band of 180-280 nm sized particles. The absence of smaller sized particle might be attributed to immobilization or loss into the membrane of the accumulation wall (Wahlund and Giddings, 1987) or aggregation during the "focus" phase of the AF4 (Benincasa et al., 2002; Lead et al., 1997). Additionally, the lack of particle separation into bins of identical sizes "hides" the smaller particles among the larger particles during MALS analysis (Wyatt, 1998). TEM analysis on Pu'u Eke (Figure 5.5) indicates aciniform (grape-like clusters) morphology, typical of black soil carbon. However, due to the poor resolution of the image, our conclusions are uncertain.

Discussion

Carbon mobilization during Fe reduction (dissolved and particulate)

Downward mobilization of carbon to deep soil profiles as colloidal carbon-iron-oxide complexes is an important process driving elevated SOM in volcanic subsoils (Osher et al., 2003). Inundation of organic-rich soil horizons triggers the release of carbon to the soil solution once anoxic conditions are established (Fiedler and Kalbitz, 2003; Grybos et al., 2009; Hagedorn et al., 2000; Jacinthe et al., 2003; Kogel-Knabner et al., 2010; MacDonald et al., 2011). Most studies ascribe this to a decrease in the availability of sorbent Fe-(oxyhydr)oxide surface area associated with reductive iron dissolution. Lower carbon mineralization rates in the absence of oxygen may also contribute to higher carbon concentrations during anoxic conditions (Kalbitz et al., 2000), but this is not generally supported by experimental data (Fiedler and Kalbitz, 2003;

Moore and Dalva, 2001). The large carbon release we observe when our soils are exposed to anoxic conditions (Figure 5.2) is consistent with this general paradigm, although the magnitude of carbon mobilization is more pronounced than for most other soils studied.

Indeed, 21-day anoxic reduction of ferric oxides released concomitant dissolved (< 2.3 nm) and particulate (2.3-260 nm) C in all the studied soils. Unexpectedly, more C dispersion occurred in the younger (~0.2 ka) Thurston and (~20 ka) Laupāhoehoe soils after anoxia than in the older (~350 ka) Pu'u Eke soil. This relative decrease of C in the Pu'u Eke soil could be attributed to a comparative lack of Fe-oxide and hydroxide dissolution in the reduced conditions, shown as reduced Fe^{+2} production in Table 5.1, and prevented releasing associated C (Hagedorn et al., 2000).

Role of metal reduction in particle mobilization

Reducing conditions may break Fe-oxide linkages between particles and facilitate their dispersion (Ryan and Gschwend, 1992). Fe minerals are commonly cited as important binding agents for larger soil aggregates (Arduino et al., 1989), especially the high surface area, nanoparticulate and SRO Fe phases that are most susceptible to reductive dissolution (Bonneville et al., 2004). Indeed, experiments confirm that anoxic incubation and associated Fe reduction decreased soil aggregate stability to a greater extent than changes in solution pH alone (De-Campos et al., 2009). Thus, both mechanisms appear to be feasible in these soils. Dispersion of soil colloids ultimately reflects changes in the repulsive or lack of attraction between particles.

In our present study of Hawaiian soils, reducing conditions evidently disperse different sized colloids than those dispersed through manipulation of pH conditions alone. For instance, carbon of the 2.3 - 35 nm size fraction are uniformly higher

following anoxic incubation than in the oxic samples of similar ionic strengths and pH (Figure 5.2). This is even more evident when we examine the carbon content of the 35 - 260 nm particles, which are substantially more enriched in carbon following anoxic incubation than after pH increases under oxic conditions (Figure 5.2). The older soils, Pu'u Eke (~350 ka) and Laupāhoehoe (~20 ka) showed more relative dispersion of the smaller (< 35 nm) particles sizes compared to the younger Thurston soil. This suggests during the experiment larger particles are breaking apart and dispersing into smaller sizes that are more mobile.

Electrostatic induced dispersion

DLVO theory characterizes the stability of colloidal suspension of like charge particles by the balance of van der Waals attractive forces that promote aggregation and by electrostatic repulsive forces that drive particles apart (Derjaguin and Landau, 1941; McDowell-Boyer et al., 1986; Ryan and Elimelech, 1996; Verwey, 1947). When electrostatic repulsive forces are dominant, the particles are stabilized and remain in a dispersed state. Colloid stabilization therefore is influenced by particle mineralogy and surface chemistry, by other chemical factors controlling surface charge, and by the extent of the electrical double layer (Lyklema, 1977; Matijevic, 1973). Physiochemical conditions that promote collapse of particle double layer, such as elevated solution ionic strength or when the solution pH approaches the point of zero charge of the particle (pzc), will induce particle coagulation (Grolimund and Borkovec, 1999).

Fe reduction reactions consume protons associated with the following general reaction (Ponnamperuma et al., 1966): $Fe(OH)_3 + e^- + 3H^+ \longleftrightarrow Fe^{2+}(aq) + 3H_2O$

Hence, the development of Fe reducing conditions in acidic to neutral soils is nearly always accompanied by an increase in pH unless the soil buffering capacity in high, the Fe atom reduced is not released from the solid phase (Stucki, 2011), or other secondary precipitation reactions ensue. This has prompted several recent studies to examine the role of pH increases on the mobilization of organic nanoparticles and associated bound-constituents (Grybos et al., 2007; Grybos et al., 2009; Pédrot et al., 2008).

In many highly weathered tropical forest soils, soil organic matter (SOM) coatings on colloids often dominate surface charge characteristics, leading to negative surface charge repulsion and dispersion (Thompson et al., 2006a). Moreover, soils across the Hawaiian archipelago are replete with nanoscale organo-mineral phases with a high density of ionizable surface functional groups that readily undergo deprotonation reactions as a function of solution pH (Krishnaswamy and Richter, 2002; Osher et al., 2003). Therefore, biogeochemical processes that induce shifts in solution pH can strongly alter the surface charge characteristics of these phases as well as contribute to particle dispersion. In the studied soils, increasing the pH through addition of KOH caused dispersion of nanoparticle (2.3 – 35 nm) and dissolved carbon across all soils, while the amount of colloid-bound (35 – 260 nm) carbon was affected sparingly (Figure 5.2). Furthermore, compared to the anoxic experiment, less than 40% of total colloidal (non-dissolved) carbon was released from the pH increases alone (Figure 5.3). These observations point toward a pH induced dispersion of SOM coated soil particles, and suggests that release of larger colloidal carbon is associated with Fe-(oxyhydr)oxides rather than strictly resulting from electrostatic dispersion due to pH increases.

Broader implications of anoxia on carbon mobilization

Carbon mobilization to depth in these Hawaiian rain forest volcanic soils is linked to the movement of carbon through preferential-flow pathways(Marin-Spiotta et al., 2011). The recent forest litter horizon (Oie) is the zone of greatest MOC production with MOC, Fe, and Al all decreasing with depth from organic to the mineral horizons at the Pu'u Eke site and high rainfall (2800 to 3500 mm) ensures a constant supply of fresh SOM to the deeper horizons (Marin-Spiotta et al., 2011). The presence of cracks and macropores were also reported for 22 soil pits in a highly weathered forest soil receiving 2500 mm mean annual precipitation in Hawai'i (Lohse and Dietrich, 2005). Spectroscopic and chemical data of SOM accumulating along the surfaces of cracks and in black pockets at depth matched material in the surface humic mineral horizons (Bh), where the network of cracks and channels are first observable. Additionally, an abundance of many open channels and cracks that were filled with loose, particulate SOM were reported (Marin-Spiotta et al., 2011).

The release of soil colloids, nanoparticles, and dissolved species may result from changes in pH, Eh, and decreases in ionic strength (Chorover and Sposito, 1995; Itami and Fujitani, 2005; Pokrovsky and Schott, 2002; Ryan and Gschwend, 1994; Thompson et al., 2006a). The organic carbon concentration of the colloidal (35 – 260 nm) and nanoparticle (2.3 – 35 nm) fractions (Figure 5.2 and 5.3) indicates that both oxic and anoxic treatments facilitate nanoparticle dispersion.

Conclusion

Our data suggest mineralogy and rainfall variability interact to establish conditions favorable for mobilization of carbon from the surface organic horizons to deep

mineral horizons (Giambelluca et al., 1986). Hawaiian soils are rich in hydrated-SRO minerals that shrink in response to periodic droughts and generate cracks in subsurface B horizons (Marin-Spiotta et al., 2011). These macropores become preferential conduits for the mobilization of carbon during the ensuing wet periods (in both dissolved and colloidal form) by gravitational flow (Marin-Spiotta et al., 2011).

We have demonstrated that colloidal carbon disperses during anoxic conditions in 0.3 – 350 ka Hawaiian soils. More carbon is found in the smaller fractions after anoxic treatment. Moreover, the pH-increased soils in oxic conditions showed this same relationship. By matching the pH changes between anoxic and oxic soils, we suggest that pH increases alone cause colloidal releases of carbon in the smallest fractions (< 10 kDa – 35 nm). We suggest the increase in pH causes a net negative surface charge on soil particles, which separate due to electrical repulsion. In addition, it can be concluded that this increase of pH alone by Fe-oxide reduction can account for nearly half of colloidal carbon released. We suggest the observed mobilization of carbon to subsoil depths may be driven in part through Fe-redox induced particle dispersion of carbon-rich colloids.

Table 5.1: 21-day anoxic experiment ion data

	Thurston	Laupāhoehoe	Pu'u Eke
Pre pH	4.79 ± 0.02	4.03 ± 0.3	3.92 ± 0.01
Pre E.C. (µS cm^{-1})	324 ± 10	310 ± 29	434 ± 12
Pre Eh (mV)	349 ± 9	428 ± 26	418 ± 18
Post Fe^{+2} (mmol kg^{-1})	19 ± 3	17 ± 2	17 ± 1
Post pH	6.43 ± 0.03	4.64 ± 0.04	4.73 ± 0.04
Post E.C. (µS cm^{-1})	557 ± 54	483 ± 54	510 ±18
Post Eh (mV)	-314 ± 21	-180 ± 48	-120 ± 32
Total C (g kg^{-1})	7.1 ± 1.1	7.1 ± 0.9	5.2 ± 0.6

Table 5.2: 2-hr oxic experiment ion data. (BD - below detection limit, ≈2µmol kg^{-1})

Soil (age)	pH	E.C. (µS cm^{-1})	Eh (mV)	Fe^{+2} (mmol kg^{-1})	Interpolated Total C (g kg^{-1})
Thurston	4.79 ± 0.02	324 ± 29	349 ± 9	BD	3.8 @ pH 6.43
(0.3 ka)	6.12 ± 0.24	461 ± 25	457	BD	
	6.68 ± 0.30	471 ± 24	592	BD	
Laupāhoehoe	4.03 ± 0.30	310 ± 29	428 ± 26	BD	3.7 @ pH 4.64
(20 ka)	5.22 ± 0.05	514 ± 25	515	BD	
	5.90 ± 0.06	551 ± 12	576	BD	
Pu'u Eke	3.92 ± 0.01	434 ± 29	418 ± 18	BD	2.7 @ pH 4.73
(350 ka)	4.75 ± 0.09	453 ± 36	489	BD	
	5.90 ± 0.16	495 ± 9	584	BD	

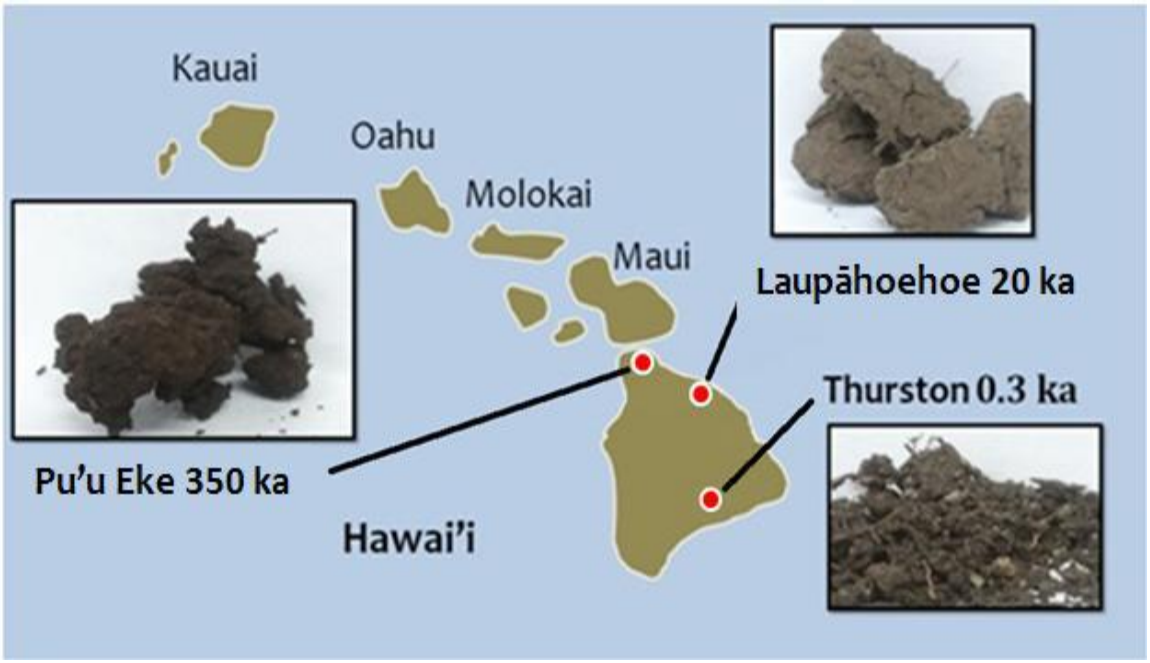

Figure 5.1: Location of the experimental soils along with their approximate age and photo.

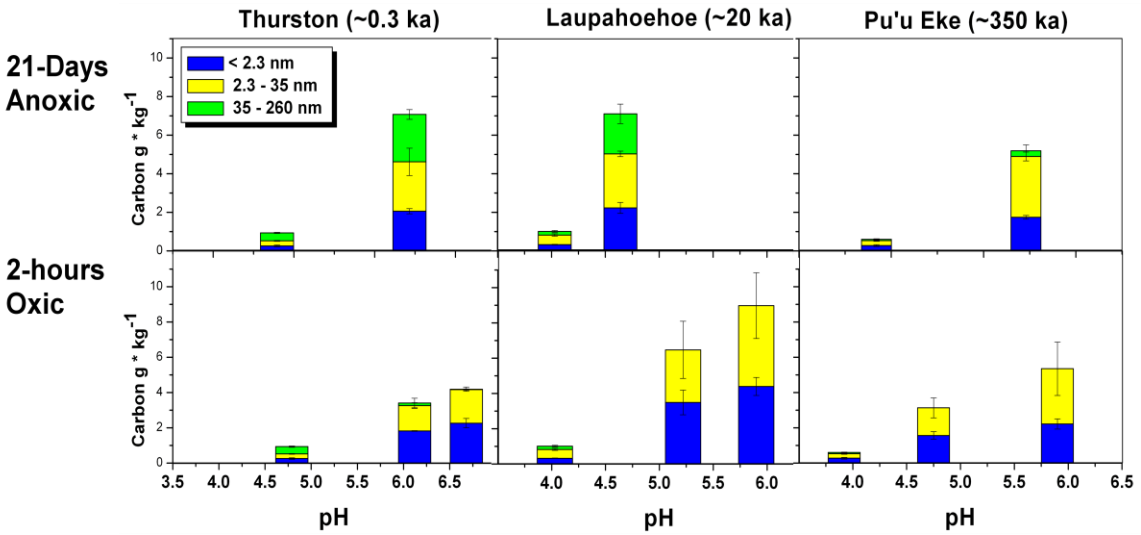

Figure 5.2: Hawaiian soil (Pu'u Eke, Laupāhoehoe, Thurston) carbon size fraction concentrations (g C kg^{-1} soil) as related to pH in 21-day anoxic and 2-h oxic conditions in stacked bars. Blue bars represents carbon less than 2.3 nm in diameter, yellow bars represents carbon between 2.3 and 35 nm in diameter, and green bars represent carbon between 35 and 260 nm in diameter. Brackets indicate 1 standard deviation (n=3).

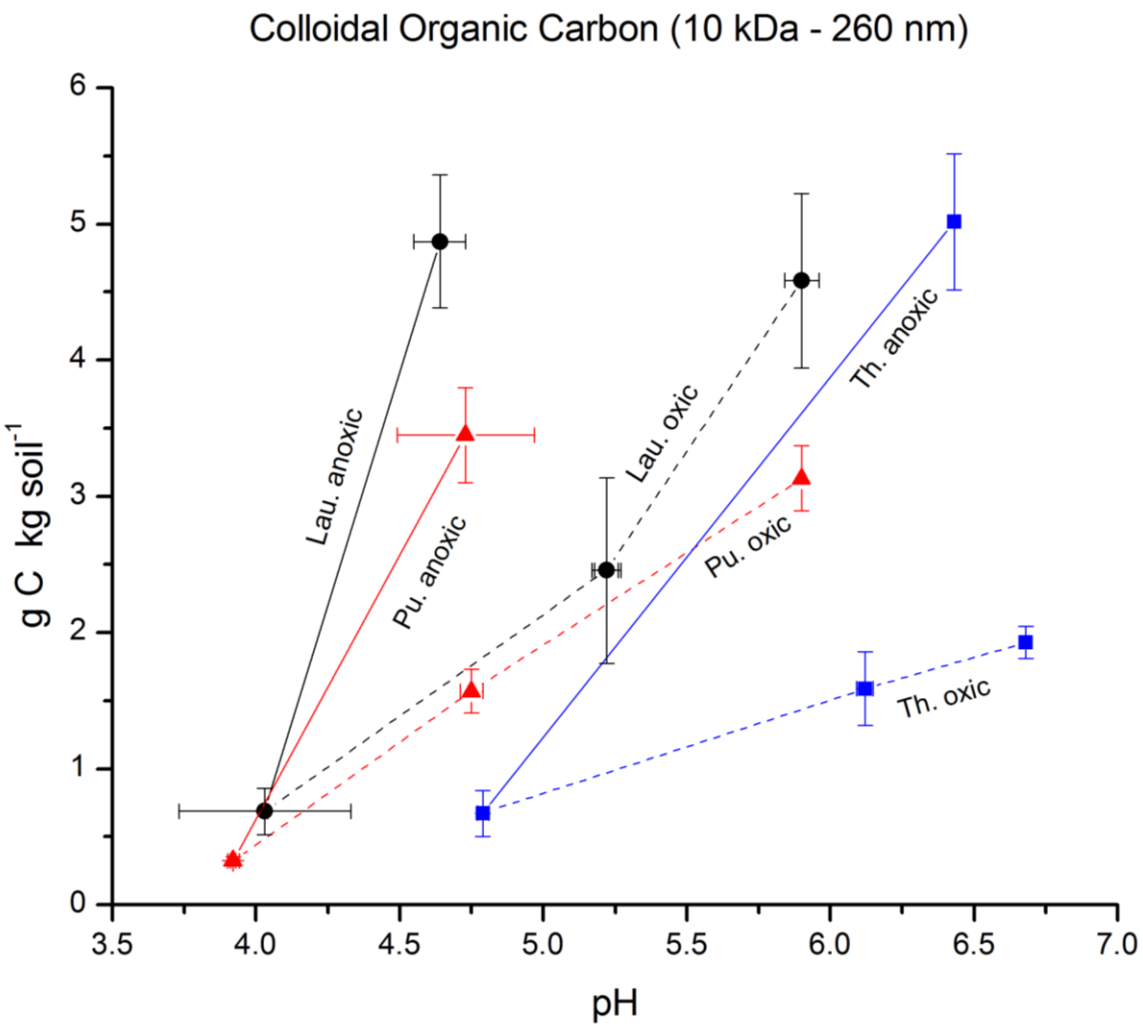

Figure 5.3: Hawaiian soil (Pu'u Eke, Laupāhoehoe, Thurston) colloidal (260 nm – 2.3 nm) carbon concentrations (g C kg^{-1} soil) as related to pH in 21-day anoxic and 2-h oxic conditions. Solid lines represent anoxic experiements, while dashed lines are the oxic runs. Black lines represent Laupāhoehoe soil, red lines represent Pu'u Eke soil, and blue lines represent Thurston soil.

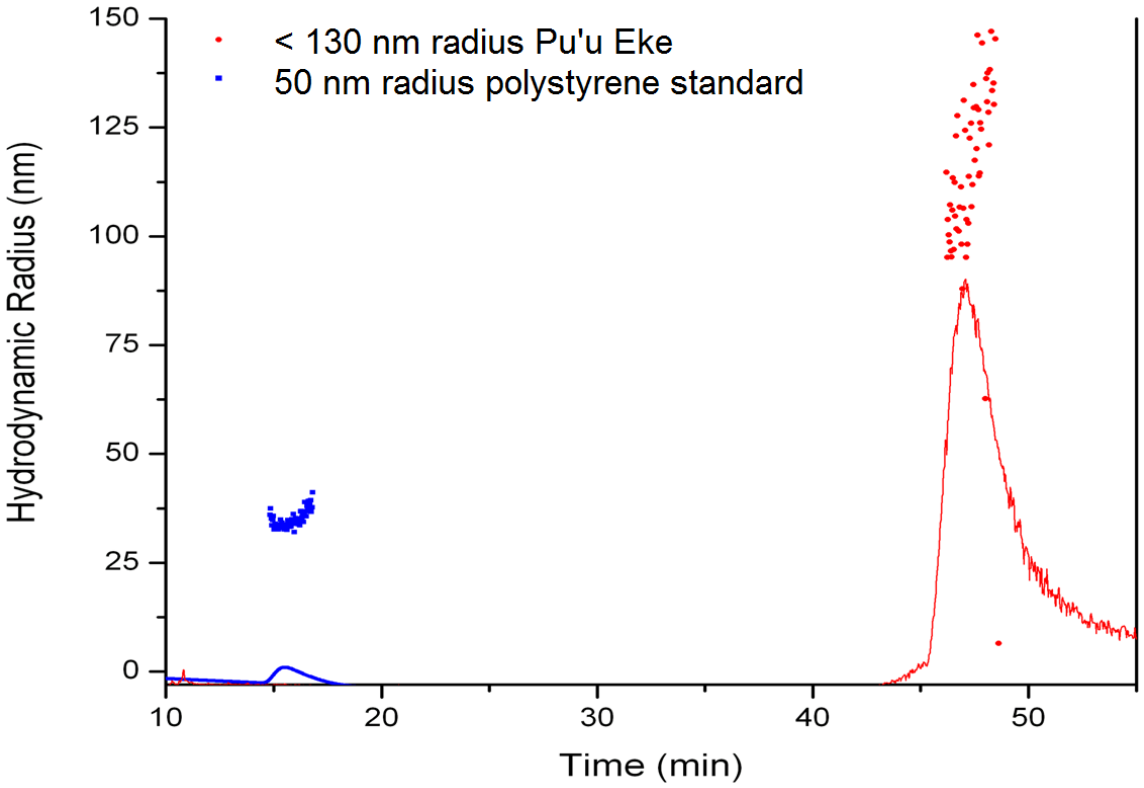

Figure 5.4: Asymmetrical flow field-flow fractionation (AF4) data of < 260 nm Pu'u Eke and a 100 nm diameter standard. Solid lines represent relative intensity, while up triangles represent particle hydrodynamic radius. Pu'u Eke (red up triangles) was below 140 nm in radius, therefore a less than 280 nm diameter can be assumed.

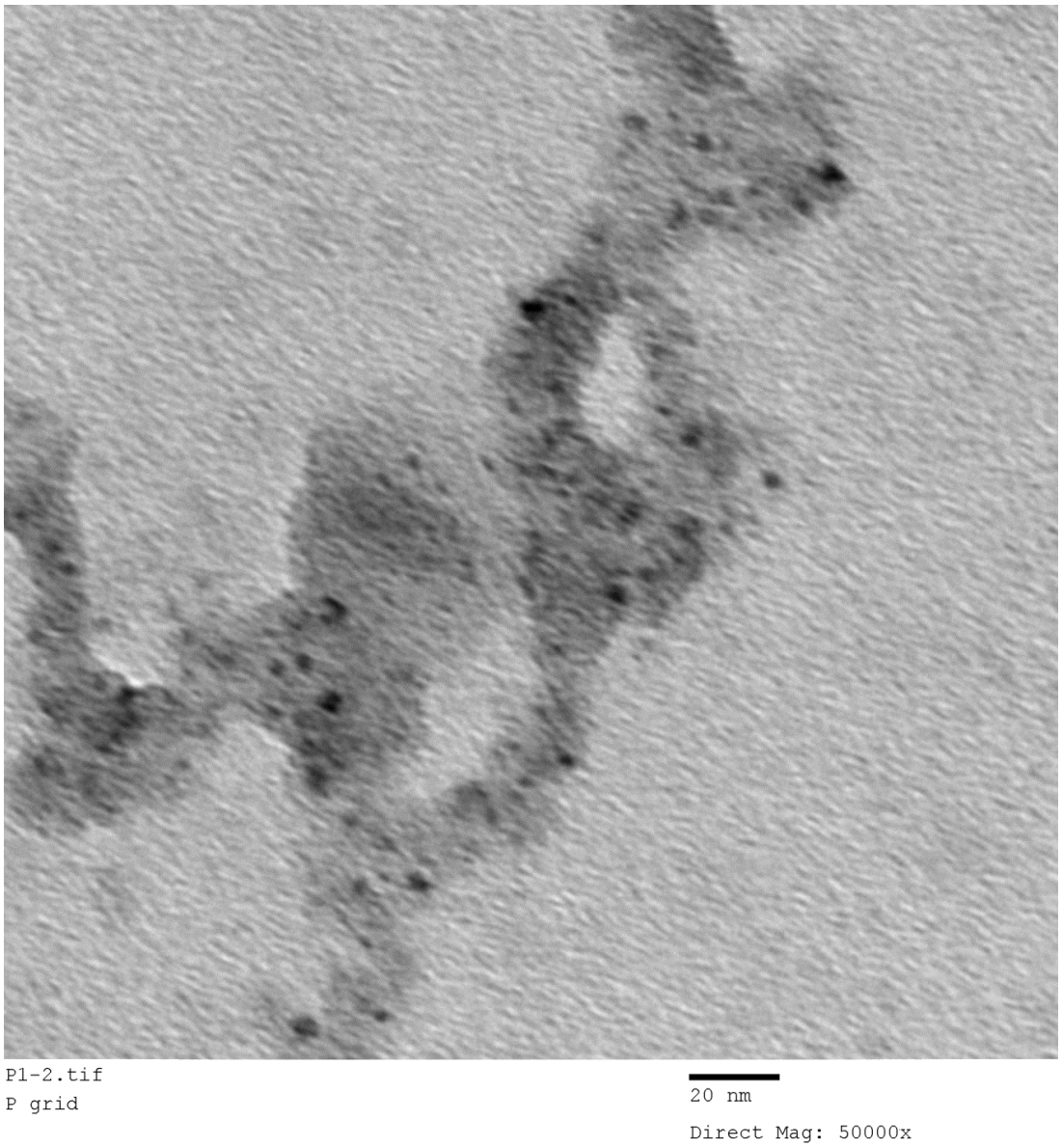

Figure 5.5: Transmission electron microscopy image of < 260 nm Pu'u Eke.

CHAPTER 6

SUMMARY AND CONCLUSION

Broadening our understanding of contaminant metal and carbon mobilization in sediment sub-surface and surface flow is vital in remediation efforts. Past studies have shown reductions in soluble (< 220 nm) U and Ni using phosphate amendments. We conducted experiments to test different processes that may disperse U and other metals. We showed that hydroxyapatite amendments can reduce soluble (< 100 nm) U and Ni, while increasing suspended colloids (100 – 1000 nm). In addition, we demonstrated that prolonged periods of inundation under anoxic conditions can disperse additional colloidal (100 – 1000 nm), nanoparticle and aqueous (< 100 nm) U by concomitant Fe/Mn-(oxyhydr)oxide dissolution, while Ni dispersion is controlled by time dependent mechanisms. Increasing soil pH dispersed colloidal (100 – 1000 nm) U and Ni while decreasing the concentration of these elements present below < 100 nm. This may be due to aggregation of U and Ni –containing nanoparticles in response to the development of negative surface charge or changes in U and Ni solubility. Additions of Na-phytate and humic acid Na salt to soils slurries resulted in substantial release of U and Ni < 100 nm which is likely associated with humic ligands. Our study recognized that immobilizing amendments under oxic conditions reduce small nanoparticle and aqueous phases and increase larger and less mobile colloidal sizes, but under anoxic conditions may cause particle dispersion further complicating amendment U and Ni immobilization.

For the past twenty years the former Steed Pond area has been heavily vegetated and beavers have constructed dams, which collectively have altered the TBSP geomorphology and hydrology. The rainstorm we studied had lower turbidity and suspended U and Ni compared with storms 20 years ago. This may be due to the lower flow conditions associated with the present day drought or beaver dam developments. However, unlike the episodic storms in 1993, turbidity and related suspended sediments in the studied storm event increased during rainfall rather than stormflow rate. This may result from a change in stream morphology that reduced erosive conditions in TBSP stream banks relative to 20 years ago or less initial dilution of runoff waters due to much lower stream discharge levels. U was present primarily in the > 220 nm fraction and Ni was < 220 nm. Past synchrotron X-ray fluorescence, scanning electron microscopy, and sequential extraction data on Steed Pond sediments suggest colloid-bound U aggregates bound to Fe(oxyhydro)oxides or high molecular weight organic carbon molecules, while suspended Ni is found mostly in nanoparticle (< 220 nm) and aqueous forms with some correlation with Fe.

Using a set of Hawaiian soils that represents a range of ages, we found that colloidal carbon primarily disperses to smaller size fractions during anoxic conditions. These shrinking and swelling soils generate cracks in subsurface B horizons that become conduits for the gravitational flow of carbon during inundation, both in dissolved and colloidal form. In our experiments these carbon-bearing colloids disperse considerably to changes in surface charge (i.e., pH shifts) as well as concomitant mineral reductive dissolution. Our data suggest mineralogy (e.g., hydrated short-range-ordered minerals) and climate (e.g., high rainfall variability) act together to create circumstances that

mobilize carbon from the surface organic horizons to deep mineral horizons. By matching the pH changes between anoxic and oxic soils we suggest that pH increases alone release significant colloidal carbon in the smallest size fractions (< 10 kDa – 35 nm). The increase in pH generates net negative surface charge on soil particles, which then repel each other accounting for nearly half of colloidal carbon released during Fe-oxide reduction. We suggest Fe-reduction induced dispersion of carbon-rich colloids may drive the observed mobilization of carbon to deep subsoil.

REFERENCES

Albarran N., Alonso Ú., Missana T., Garcia-Gutierrez M., Mingarro M. (2008) Evaluation of geochemical conditions favourable for the colloid-mediated uranium migration in a granite fracture. e-Terra 5.

Ames L.L., McGarrah J.E., Walker B.A., Salter P.F. (1983) Uranium and radium sorption on amorphous ferric oxyhydroxide. Chem. Geol. 40:135-148. DOI: 10.1016/0009-2541(83)90095-5.

Amonette J.E., Holdren G.R. Jr., Krupa K.M., Lindenmeier C.W. (1994) Assessing the environmental availability of uranium in soils and sediments, Pacific Northwest Lab, Richland, WA

Arduino E., Barberis E., Boero V. (1989) Iron oxides and particle aggregation in B horizons of some Italian soils. Geoderma 45:319-329. DOI: 10.1016/0016-7061(89)90014-1.

Arey J.S., Seaman J.C., Bertsch P.M. (1999) Immobilization of uranium in contaminated sediments by hydroxyapatite addition. Environ. Sci. Technol. 33:337-342. DOI: 10.1021/es980425+.

Axt J.R., Walbridge M.R. (1999) Phosphate removal capacity of palustrine forested wetlands and adjacent uplands in Virginia. Soil Sci. Soc. of Am. J. 63:1019-1031.

Bartlett R.J., James B.R. (1993) Redox Chemistry of Soils. Advances in Agronomy 50:151-208.

Batson V. (1994) Surface water transport and distribution of uranium in contaminated sediments near a nuclear weapons processing facility, Texas A&M University, College Station, TX.

Batson V.L., Bertsch P.M., Herbert B.E. (1996) Transport of anthropogenic uranium from sediments to surface waters during episodic storm events. J. Environ. Qual. 25:1129-1137.

Benincasa M.-A., Cartoni G., Imperia N. (2002) Effects of ionic strength and electrolyte composition on the aggregation of fractionated humic substances studied by flow field-flow fractionation. Journal of Separation Science 25:405-415. DOI: 10.1002/1615-9314(20020501)25:7<405::aid-jssc405>3.0.co;2-f.

Bertsch P.M., Seaman J.C. (1999) Characterization of complex mineral assemblages: Implications for contaminant transport and environmental remediation. Proceedings of the National Academy of Sciences 96:3350-3357. DOI: 10.1073/pnas.96.7.3350.

Bertsch P.M., Hunter D.B., Sutton S.R., Bajt S., Rivers M.L. (1994) In Situ chemical speciation of uranium in soils and sediments by micro x-ray absorption spectroscopy. Environ. Sci. Technol. 28:980-984.

Bonneville S., Van Cappellen P., Behrend T. (2004) Microbial reduction of iron(III) oxyhydroxides: Effects of mineral solubility and availability. Chem. Geol. 212:255-268.

Bunn R.A., Magelky R.D., Ryan J.N., Elimelech M. (2002) Mobilization of natural colloids from an iron oxide-coated sand aquifer: Effect of pH and ionic strength. Environ. Sci. Technol. 36:314-322. DOI: 10.1021/es0109141.

Chorover J., Sposito G. (1995) Colloid chemistry of kaolinitic tropical soils. Soil Sci. Soc. Am. J. 59:1558-1564.

Chorover J., Amistadi M.K., Chadwick O.A. (2004) Surface charge evolution of mineral-organic complexes during pedogenesis in Hawaiian basalt. Geochim Cosmochim Acta 68:4859-4876.

Cline R., Cole G., Meganhan W., Patten R., Potyondy J. (1981) Guide for Predicting Sediment Yields from Forested Watersheds., in: U. S. F. S. N. R. I. Region (Ed.).

Davis J.A. (1984) Complexation of trace metals by adsorbed natural organic matter. Geomchim. Cosmochim. Acta 48:679-691.

De-Campos A.B., Mamedov A.I., Huang C.H. (2009) Short-term reducing conditions decrease soil aggregation. Soil Sci. Soc. Am. J. 73:550-559.

Derjaguin B.V., Landau L. (1941) Theory of the stability of strongly charged lyophobic sols and of the adhesion of strongly charged particles in solutions of electrolytes. Acta. Physicochim. 14:633-662.

Dubascoux S., Von Der Krammer F., Le Hécho I., Gautier M.P., Lespes G. (2008) Optimisation of asymmetrical flow field flow fractionation for environmental nanoparticles separation. J. Chromatogr. A 1206:160-165.

Evans A.G., Bauer L.R., Haselow J.S., Hayes D.W., Martin H.L., McDowell W.L., Pickett J.B. (1992) Uranium in the Savannah River Site Environment WSRC-RP-92-315, WSRC.

Feng R., Gerson A., Ice G., Reininger R., Yates B., McIntyre S. (2007) VESPERS: A Beamline for Combined XRF and XRD Measurements. AIP Conference Proceedings 879:872-874.

Fiedler S., Kalbitz K. (2003) Concentrations and properties of dissolved organic matter in forest soils as affected by the redox regime. Soil Sci. 168:793-801.

Fimmen R., Richter D., Vasudevan D., Williams M., West L. (2008) Rhizogenic Fe–C redox cycling: A hypothetical biogeochemical mechanism that drives crustal weathering in upland soils. Biogeochemistry 87:127.

Furrer G., Phillips B.L., Ulrich K.-U., Pöthig R., Casey W.H. (2002) The Origin of Aluminum Flocs in Polluted Streams. Science 297:2245-2247. DOI: 10.1126/science.1076505.

Gambrell R.P. (1994) Trace and Toxic Metals in Wetlands—A Review. J. Environ. Qual. 23:883-891. DOI: 10.2134/jeq1994.00472425002300050005x.

Giambelluca T.W., Nullet M.A., Schroeder T.A. (1986) Rainfall Atlas of Hawaii, in: D. o. L. a. N. Resources (Ed.), Honolulu, Hawaii. pp. 267.

Giardina C.P., Ryan M.G. (2000) Evidence that decomposition rates of organic carbon in mineral soil do not vary with temperature. Nature 404:858-861. DOI: http://www.nature.com/nature/journal/v404/n6780/suppinfo/404858a0_S1.html.

Giesy J.P., Geiger R.A., Kevern N.R., Alberts J.J. (1986) UO_2^{2+}-humate interactions in soft, acid, humate-rich waters. J. Environ. Rad. 4:39-64. DOI: 10.1016/0265-931x(86)90020-2.

Gillespie L.J. (1920) Reduction potentials of bacterial cultures and water- logged soils. Soil Sci. 9:199-216.

Goldberg S., Glaubig R.A. (1987) Effect of saturating cation, pH, and aluminum and iron oxides on the flocculation of kaolinite and montmorillonite. Clays. Clay Miner. 35:220-227.

Grolimund D., Borkovec M. (1999) Long-term release kinetics of colloidal particles from natural porous media. Environ. Sci. Technol. 33:4054-4060. DOI: 10.1021/es990194m.

Grybos M., Davranche M., Gruau G., Petitjean P. (2007) Is trace metal release in wetland soils controlled by organic matter mobility or Fe-oxyhydroxides reduction? J. Colloid Interf. Sci. 314:490-501.

Grybos M., Davranche M., Gruau G., Petitjean P., Pédrot M. (2009) Increasing pH drives organic matter solubilization from wetland soils under reducing conditions. Geoderma 154:13-19. DOI: 10.1016/j.geoderma.2009.09.001.

Gu B., Yan H., Zhou P., Watson D.B. (2005) Natural humics impact uranium bioreduction and oxidation. Environ. Sci. Technol. 39:5268-5275.

Hagedorn F., Kaiser K., Feyen H., Schleppi P. (2000) Effects of redox conditions and flow processes on the mobility of dissolved organic carbon and nitrogen in a forest soil. J. Environ. Qual. 29:288-297.

Harmsen K., Haan F.A.M.d. (1980) Occurrence and behaviour of uranium and thorium in soil and water. Neth. J. Agric. Sci. 28 (1980) 40-62.

Harrison R.B., Footen P.W., Strahm B.D. (2011) Deep soil horizons: Contribution and importance to soil carbon pools and in assessing whole-ecosystem response to Management and Global Change. Forest Sci. 57:67-76.

Hayes D.W. (1986) Sediment transport studies in Tims Branch. DPST-86-468, Westinghouse Savannah River Company, Aiken, SC.

Healy T.W., Wiese G.R., Yates D.E., Kavanagh B.V. (1973) Heterocoagulation in mixed oxide colloidal dispersions. J. Colloid Interface Sci. 42 647.

Henderson R., Kabengi N., Mantripragada N., Cabrera M., Hassan S., Thompson A. (2012) Anoxia-induced release of colloid and nanoparticle-bound phosphorus in grassland soils. Environ. Sci. Technol. 46:11727-11734.

Hochella M.F., Lower S.K., Maurice P.A., Penn R.L., Sahai N., Sparks D.L., Twining B.S. (2008) Nanominerals, mineral nanoparticles, and Earth systems. Geochim. Cosmochim. Acta 72:A382-A382.

Hoekstra H.R., Katz J.J. (1954) The chemistry of uranium, in: G. T. Seaborg and J. J. Katz (Eds.), The actinide elements, Mcgraw-Hill Book Company, New York, NY. pp. 130-180.

Hooke J.M. (1979) An analysis of the processes of river bank erosion. Journal of Hydrology 42:39-62. DOI: 10.1016/0022-1694(79)90005-2.

Hudson E.A., Terminello L.J., Viani B.E., Denecke M., Reich T., Allen P.G., Bucher J.J., Shuh D.K., Edelstein N.M. (1999) The structure of U^{6+} sorption complexes on vermiculite and hydrobiotite. Clays. Clay Miner. 47:439-457.

Itami K., Fujitani H. (2005) Charge characteristics and related dispersion/flocculation behavior of soil colloids as the cause of turbidity. Colloid. Surface. A 265:55-63.

Jacinthe P.A., Groffman P.M., Gold A.J. (2003) Dissolved organic carbon dynamics in a riparian aquifer: Effects of hydrology and nitrate enrichment. J. Environ. Qual. 32:1365-1374.

Jackson B.P., Ranville J., Bertsch P.M., Sowder A.G. (2005) Characterization of colloidal and humic-bound Ni and U in the "dissolved" fraction of contaminated sediment extracts Environ. Sci. Technol. 39:2478-2485.

Jansen S.A., Varnum J.M., Kolla S., Paciolla M.D., Sein Jr. L.T., Nwabara S., Ghabbour E.A., Fataftah A., Davies G. (1997) Metal uptake by metal free humic acid, in: J. Drozd, et al. (Eds.), The Role of Humic Substances in Ecosystems and in Environmental Protection Polish Society of Humic Substances, Wroclaw. pp. 741.

Kalbitz K., Solinger S., Park J.H., Michalzik B., Matzner E. (2000) Controls on the dynamics of dissolved organic matter in soils: A review. Soil Sci. 165:277-304.

Kinnell P.I.A. (2005) Raindrop-impact-induced erosion processes and prediction: a review. Hydrological Processes 19:2815-2844. DOI: 10.1002/hyp.5788.

Knox A.S., Brigmon R.L. (2008) Interactions among phosphate amendments, microbes and uranium mobility in contaminated sediments. Science of The Total Environment 395:63-71.

Knox A.S., Seaman J., Mench M.J., Vangronsveld J. (2000) Remediation of metal- and radionuclide- contaminated soils by in situ stabilization techniques. CRC Press, Boca Raton, FL.

Kogel-Knabner I., Amelung W., Cao Z.H., Fiedler S., Frenzel P., Jahn R., Kalbitz K., Kolbl A., Schloter M. (2010) Biogeochemistry of paddy soils. Geoderma 157:1-14.

Kretzschmar R., Borkovec M., Grolimund D., Elimelech M. (1999) Mobile subsurface colloids and their role in contaminant transport, in: L. S. Donald (Ed.), Advances in Agronomy, Academic Press. pp. 121-193.

Krishnaswamy J., Richter D.D. (2002) Properties of advanced weathering-stage soils in tropical forests and pastures. Soil Sci. Soc. Am. J. 66:244-253.

Lalonde K., Mucci A., Ouellet A., Gelinas Y. (2012) Preservation of organic matter in sediments promoted by iron. Nature 483:198-200. DOI: 10.1038/Nature10855.

Langmuir D. (1978) Uranium solution-mineral equilibria at low temperatures with applications to sedimentary ore deposits. Geochim. Cosmochim. Acta 42:547-569. DOI: 10.1016/0016-7037(78)90001-7.

Lead J.R., Davison W., Hamilton-Taylor J., Buffle J. (1997) Characterizing colloidal material in natural waters. Aquatic Geochemistry 3:213-232. DOI: 10.1023/a:1009695928585.

Lohse K.A., Dietrich W.E. (2005) Contrasting effects of soil development on hydrological properties and flow paths. Water Resour. Res. 41.

Looney B.B., Bertsch P.B., Geesey G.G. (2003) Research opportunities for studies of contaminant transport in fluvial systems at the Tims Branch - Steed Pond system, Savannah River Site. Technical Report SREL-71-UC-66e, WSRC-TR-2003-00312, Environmental Remediation Sciences Division, Office of Biological and Environmental Research, Office of Science, U.S. Department of Energy, Aiken, SC.

Looney B.B., Eddy C.A., Ramdeen M., Pickett J., Rogers V., Scott M.T., Shirley P.A. (1990) Geochemical and physical properties of soils and shallow sediments at the Savannah River Site. pp. Medium: ED; Size: Pages: (548 p).

Lyklema J. (1977) Surface Chemistry of Colloids in Connection with Stability, in: K. J. Ives (Ed.), The Scientific Basis of Flocculation, Sijthoff & Noordoff International Publishers, Alphen aan den Rijn, The Netherlands. pp. 3-33.

Ma Q., Traina S., Logan T., Ryan J. (1994) Effects of aqueous Al, Cd, Cu, Fe(II), Ni, and Zn on Pb immobilization by hydroxyapatite. Environ Sci Technol 28:1219-1228.

MacCarthy P. (1989) Aquatic humic substances and their infuence in the fate and treatment of pollutants, in: I. H. Suffet and P. MacCarthy (Eds.), American Chemical Society, Washington, DC. pp. 17-30.

MacDonald J.D., Chantigny M.H., Angers D.A., Rochette P., Royer I., Gasser M.O. (2011) Soil soluble carbon dynamics of manured and unmanured grasslands following chemical kill and ploughing. Geoderma 164:64-72.

Marin-Spiotta E., Chadwick O.A., Kramer M., Carbone M.S. (2011) Carbon delivery to deep mineral horizons in Hawaiian rain forest soils. J. Geophys. Res. 116:G03011. DOI: 10.1029/2010jg001587.

Matijevic E. (1973) Colloid stability and complex chemistry. J. Colloid Interface. Sci. 43:217-245.

McCarthy J.F., Zachara J.M. (1989) Subsurface transport of contaminants. Environ. Sci. Technol. 23:496-502. DOI: 10.1021/es00063a001.

McDowell-Boyer L.M. (1992) Chemical mobilization of micron-sized particles in saturated porous media under steady flow conditions. Environ. Sci. Technol. 26:586-593. DOI: 10.1021/es00027a023.

McDowell-Boyer L.M., Hunt J.R., Sitar N. (1986) Particle transport through porous media. Water Resour. Res. 22:1901-1921.

Meybeck M., Friedrich G., Thomas R., Chapman D. (1992) Rivers, in: D. Chapman (Ed.), Water quality assessments: A guide to the use of biota, sediments and water in environmental monitoring, 2nd ed., E&FN Spon, 2-6 Boundary Row, London SE1 8HN, UK.

Mikutta R., Schaumann G.E., Gildemeister D., Bonneville S., Kramer M.G., Chorover J., Chadwick O.A., Guggenberger G. (2009) Biogeochemistry of mineral-organic associations across a long-term mineralogical soil gradient (0.3-4100 kyr), Hawaiian Islands. Geochim Cosmochim Acta 73:2034-2060. DOI: 10.1016/j.gca.2008.12.028.

Moore T.R., Dalva M. (2001) Some controls on the release of dissolved organic carbon by plant tissues and soils. Soil Science 166:38-47.

Osher L.J., Matson P.A., Amundson R. (2003) Effect of land use change on soil carbon in Hawaii. Biogeochem. 65:213-232.

Pédrot M., Dia A., Davranche M., Bouhnik-Lacoz M., Henin O., Gruaua G. (2008) Insights into colloid-mediated trace element release at the soil/water interface. J. Colloid Interface Sci. 325 187-197.

Penna D., Tromp-van Meerveld H.J., Gobbi A., Borga M., Dalla Fontana G. (2011) The influence of soil moisture on threshold runoff generation processes in an alpine headwater catchment. Hydrol. Earth Syst. Sci. 15:689-702.

Pickett J.B. (1990) Heavy metal contamination in Tims Branch sediments. Westinghouse Savannah River Company, Aiken, SC.

Pokrovsky O.S., Schott J. (2002) Iron colloids/organic matter associated transport of major and trace elements in small boreal rivers and their estuaries (NW Russia) Chem. Geol. 190:141-179.

Pollock M., Heim M., Werner D. (2003) Hydrologic and geomorphic effects of beaver dams and their influence on fishes in: S. Gregory, et al. (Eds.), The Ecology and management of wood in world rivers American Fisheries Society, Bethesda, MD. pp. 213-233.

Ponnamperuma F.N., Martinez E., Loy T. (1966) Influence of redox potential and partial pressure of carbon dioxide on pH values and the suspension effect of flooded soils. Soil Sci. 101:421-431.

Poppe L.J., Fredericks J.J., Hathaway J.C. (1998) A computer-program to calculate centrifugation parameters for sedimentation analyses. Comput. Geosci. 14:541-545.

Reed M.B., Swanson M.T., Gaither S., Joseph J.W., Henry W.R. (2002) Savannah River Site at Fifty. U.S. Government Printing Office.

Robinson A.R. (1979) Sediment yield as a function of upstream erosion, in: A. E. Peterson and J. B. Swan (Eds.), Universal soil loss equation: Past present and future, SSSA Special Publication No. 8. pp. 7-16.

Ryan J.N., Gschwend P.M. (1992) Effect of iron diagenesis on the transport of colloidal clay in an unconfined sand aquifer. Geochim. Cosmochim. Acta 56:1507-1521.

Ryan J.N., Gschwend P.M. (1994) Effect of solution chemistry on clay colloid release from an iron oxide-coated aquifer sand. Environ. Sci. Technol. 28:1717-1726. DOI: 10.1021/es00058a025.

Ryan J.N., Elimelech M. (1996) Colloid mobilization and transport clay in groundwater Colloids & Surface. A 107:1-56.

Scala D.J., Hacherl E.L., Cowan R., Young L.Y., Kosson D.S. (2006) Characterization of Fe(III)-reducing enrichment cultures and isolation of Fe(III)-reducing bacteria from the Savannah River site, South Carolina. Res. Microbiol. 157:772-783. DOI: 10.1016/j.resmic.2006.04.001.

Schmidt M.W.I., Torn M.S., Abiven S., Dittmar T., Guggenberger G., Janssens I.A., Kleber M., Kogel-Knabner I., Lehmann J., Manning D.A.C., Nannipieri P., Rasse D.P., Weiner S., Trumbore S.E. (2011) Persistence of soil organic matter as an ecosystem property. Nature 478:49-56.

Schuur E.A.G., Chadwick O.A., Matson P.A. (2001) Carbon cycling and soil carbon storage in mesic to wet hawaiian montnae forests. Ecology 82:3182-3196. DOI: 10.1890/0012-9658(2001)082[3182:ccascs]2.0.co;2.

Seaman J., Meehan T., Bertsch P. (2001a) Immobilization of cesium-137 and uranium in contaminated sediments using sediment amendments. J. Environ. Qual. 30:1206-1213.

Seaman J.C., Arey J.S., Bertsch P.M. (2001b) Immobilization of nickel and other metals in contaminated sediments by hydroxyapatite addition. J. Environ. Qual. 30:460-469.

Seaman J.C., Vulava V.J., Sowder A.G., Jackson B.P., Aburime S.A., Bertsch P.M. (2005) Metal extractability from contaminated SRS sediments: Comparison of column and batch results. Environ. Geosciences 12:235-242.

Sowder A.G., Bertsch P.M., Morris P.J. (2003) Partitioning and availability of Uranium and Nickel in contaminated riparian sediments. J. Environ. Qual. 35:885-898.

Sposito G. (1992) The characterization of particle surface charge. Lewis Publishers, Chelsea, MI.

Sposito G. (2000) Ion exchange phenomena. CRC Press, Washington, DC.

Stone M., Krishnappan B.G. (2003) Floc morphology and size distributions of cohesive sediment in steady-state flow. Water Res. 37:2739-2747. DOI: 10.1016/s0043-1354(03)00082-4.

Stookey L.L. (1970) Ferrozine---a new spectrophotometric reagent for iron. Anal. Chem. 42:779-781. DOI: 10.1021/ac60289a016.

Strahm B.D., Harrison R.B., Terry T.A., Harrington T.B., Adams A.B., Footen P.W. (2009) Changes in dissolved organic matter with depth suggest the potential for postharvest organic matter retention to increase subsurface soil carbon pools. Forest Ecol. Manag. 258:2347-2352.

Stucki J.W. (2011) A review of the effects of iron redox cycles on smectite properties. C.R. Geosci. 343:199-209.

Stumm W. (1977) Chemical interaction in particle separation. Environ. Sci. Technol. 11:1066-1070. DOI: 10.1021/es60135a010.

Thompson A., Chadwick O.A., Chorover J. (2006a) GEOC 110-Mobilization of metal-organic colloids during soil redox oscillations. Abstr. Pap. Am. Chem. S. 232.

Thompson A., Chadwick O.A., Boman S., Chorover J. (2006b) Colloid mobilization during soil iron redox oscillations. Environ. Sci. Technol. 40:5743-5749.

Thompson A., Chadwick O.A., Rancourt D.G., Chorover J. (2006c) Iron-oxide crystallinity increases during soil redox oscillations. Geochim. Cosmochim. Acta. 70:1710-1727. DOI: 10.1016/j.gca.2005.12.005.

Tokunaga T.K., Wan J., Kim Y., Sutton S.R., Newville M., Lanzirotti A., Rao W. (2008) Real-time X-ray absorption spectroscopy of uranium, iron, and manganese in contaminated sediments during bioreduction. Environ. Sci. Technol. 42:2839-2844. DOI: 10.1021/es702364x.

Torn M.S., Trumbore S.E., Chadwick O.A., Vitousek P.M., Hendricks D.M. (1997) Mineral control of soil organic carbon storage and turnover. Nature 389:170-173.

Townsend A.R., Vitousek P.M., Desmarais D.J., Tharpe A. (1997) Soil carbon pool structure and temperature sensitivity inferred using CO_2 and $^{13}CO_2$ incubation fluxes from five Hawaiian soils. Biogeochemistry 38:1-17. DOI: 10.1023/a:1017942918708.

Trenfield M.A., McDonald S., Kovacs K., Lesher E.K., Pringle J.M., Markich S.J., Ng J.C., Noller B., Brown P.L., van Dam R.A. (2011) Dissolved organic carbon reduces uranium bioavailability and toxicity. 1. Characterization of an aquatic fulvic acid and its complexation with uranium[VI]. Environ. Sci. Technol. 45:3075-3081. DOI: 10.1021/es103330w.

Trumbore S.E. (1997) Potential responses of soil organic carbon to global environmental change. Proc. of the Natl. Acad. Sci. 94:8284-8291.

USEPA. (2007a) Inductively coupled plasma-mass spectrometry. Method 6020a, Rev. 1. In SW-846: Test methods for evaluating solid waste, physical/chemical methods, in: O. o. S. Waste (Ed.), Washington, DC.

USEPA. (2007b) Method 6200: Field portable X-ray fluorescence spectrometry for the determination of elemental concentrations in soil and sediment, in: O. o. S. Waste (Ed.), Washington, DC.

USEPA. (2008) Method 3015a: Microwave assisted acid digestion of aqueous samples and extracts (Rev 1), in: O. o. S. Waste (Ed.), Washington, DC.

Verwey E.J.W. (1947) Theory of the Stability of Lyophobic Colloids 51:631-636. DOI: 10.1021/j150453a001.

Vesparaskas M.J., Faulkner S.P. (2001) Redox chemistry of hydric soils, in: J. L. Richardson (Ed.), Wetland soils: Genesis, hydrology, landscapes, and classification, CRC Press: Lewis Publishers, New York. pp. 85-105.

Wahlund K.G., Giddings J.C. (1987) Properties of an asymmetrical flow field-flow fractionation channel having one permeable wall. Analytical Chemistry 59:1332-1339. DOI: 10.1021/ac00136a016.

Waite T.D., Davis J.A., Payne T.E., Waychunas G.A., Xu N. (1994) Uranium(VI) adsorption to ferrihydrite: Application of a surface complexation model. Geochimica Et Cosmochimica Acta 58:5465-5478. DOI: 10.1016/0016-7037(94)90243-7.

Wyatt P.J. (1998) Submicrometer particle sizing by multiangle light scattering following fractionation. J. Colloid Interf. Sci. 197:9-20. DOI: 10.1006/jcis.1997.5215.

APPENDICES

APPENDIX A

STOKES-LAW CALCUALTION

Particle size fractions were achieved by subjecting each sample to differential centrifugation. Time (T) for a given particle regime was calculated assuming ideal spherical geometry according to Equation 6 (Poppe et al., 1998) with the time of acceleration(*ta*), time of deceleration (*td*), fluid viscosity (η), minimum radius from the rotational axis (*R*1), maximum radius from the rotational axis (*R*2), particle radius (*r*), angular velocity (*N*), particle density (ρ), and media density (ρ_o).

$$T = \frac{9\eta \ln(R2/R1)}{8\pi^2 N^2 r^2 (\rho - \rho_o)} + \frac{2(ta+td)}{3} \quad \text{(A1)}$$

Where,

T = time (sec)
ta = time of acceleration (sec)
td = time of deceleration (sec)
η = viscosity (poises)
R1 = minimum radius (cm)
R2 = maximum radius (cm)
r = particle radius (cm)
N = angular velocity (rps)
ρ = particle density (g × cm^{-3})
ρ_o = media density (g × cm^{-3})

We assume a fluid viscosity of 0.00891 poises, that particle density is 2.65 g × cm^{-3} and that the media density is 0.99713 g × cm^{-3}. The maximum radius from the rotational axis is 13.7 cm. The minimum radius from the rotational axis is 3.5 cm for the < 1000 nm size fraction and 4.5 cm for the < 100 nm size fraction.

APPENDIX B

TIMS BRANCH SOIL INCUBATION ROUTINE MEASUREMENTS

B1. Soil slurry batch experiments

	0%	2%	5%
0 d Anoxic/Oxic	No amendment KOH 14	Apatite Phytate Humic	Apatite Phytate Humic
7 d Anoxic	No amendment		
14 d Anoxic	No amendment	Apatite Phytate Humic	Apatite Phytate Humic
14 d Oxic	No amendment	Apatite Phytate Humic	Apatite Phytate Humic

B2. Anoxic and Oxic pH shifted experiment ion data. (E.C. units in µS cm^{-1})

Soil	Pre pH	Pre E.C.	Post pH	Post E.C.
0 d anoxic / 2 h oxic	5.31 ± 0.06	450 ± 40	5.31 ± 0.06	450 ± 40
7 d anoxic	5.17 ± 0.01	431 ± 6	5.38 ± 0.04	480 ± 5
14 d anoxic	5.26 ± 0.15	417 ± 1	5.75 ± 0.11	430 ± 10
14 d oxic	4.92 ± 0.01	434 ± 12	4.90 ± 0.05	480 ± 4
KOH 14	5.66 ± 0.02	440 ± 27	5.66 ± 0.02	440 ± 27

B3. Amendment spiked experiment ion data. (E.C. units in mS cm^{-1})

Soil	Pre pH	Pre E.C.	Post pH	Post E.C.
2% Phytate 14 d oxic	10.24 ± 0.02	5.47 ± 0.70	10.14 ± 0.02	7.31 ± 0.03
5% Phytate 14 d oxic	10.30 ± 0.01	10.65 ± 0.12	10.23 ± 0.04	13.20 ± 0.34
2% Phytate 14 d anoxic	10.24 ± 0.02	5.47 ± 0.70	9.88 ± 0.02	7.19 ± 0.02
5% Phytate 14 d anoxic	10.30 ± 0.01	10.65 ± 0.12	9.96 ± 0.04	13.33 ± 0.64
2% Apatite 14 d oxic	6.25 ± 0.01	0.53 ± 0.01	5.93 ± 0.04	0.692 ± 0.007
5% Apatite 14 d oxic	6.66 ± 0.01	0.659 ± 0.003	6.21 ± 0.03	0.757 ± 0.012
2% Apatite 14 d anoxic	6.25 ± 0.01	0.53 ± 0.01	6.60 ± 0.05	0.522 ± 0.012
5% Apatite 14 d anoxic	6.66 ± 0.01	0.659 ± 0.003	6.88 ± 0.05	0.692 ± 0.004
2% Humic 14 d oxic	8.53 ± 0.02	3.99 ± 0.03	7.54 ± 0.02	4.17 ± 0.02
5% Humic 14 d oxic	8.86 ± 0.01	7.99 ± 0.09	8.13 ± 0.01	8.26 ± 0.04
2% Humic 14 d anoxic	8.53 ± 0.02	3.99 ± 0.03	8.01 ± 0.05	4.38 ± 0.06
5% Humic 14 d anoxic	8.86 ± 0.01	7.99 ± 0.09	8.18 ± 0.03	9.02 ± 0.09

APPENDIX C

SYNCHROTRON-BASED DATA FOR TIMS BRANCH SOIL

C1. XANES of model compounds – UO_2, U_3O_8 and UO_3 (courtesy of Dien Li)

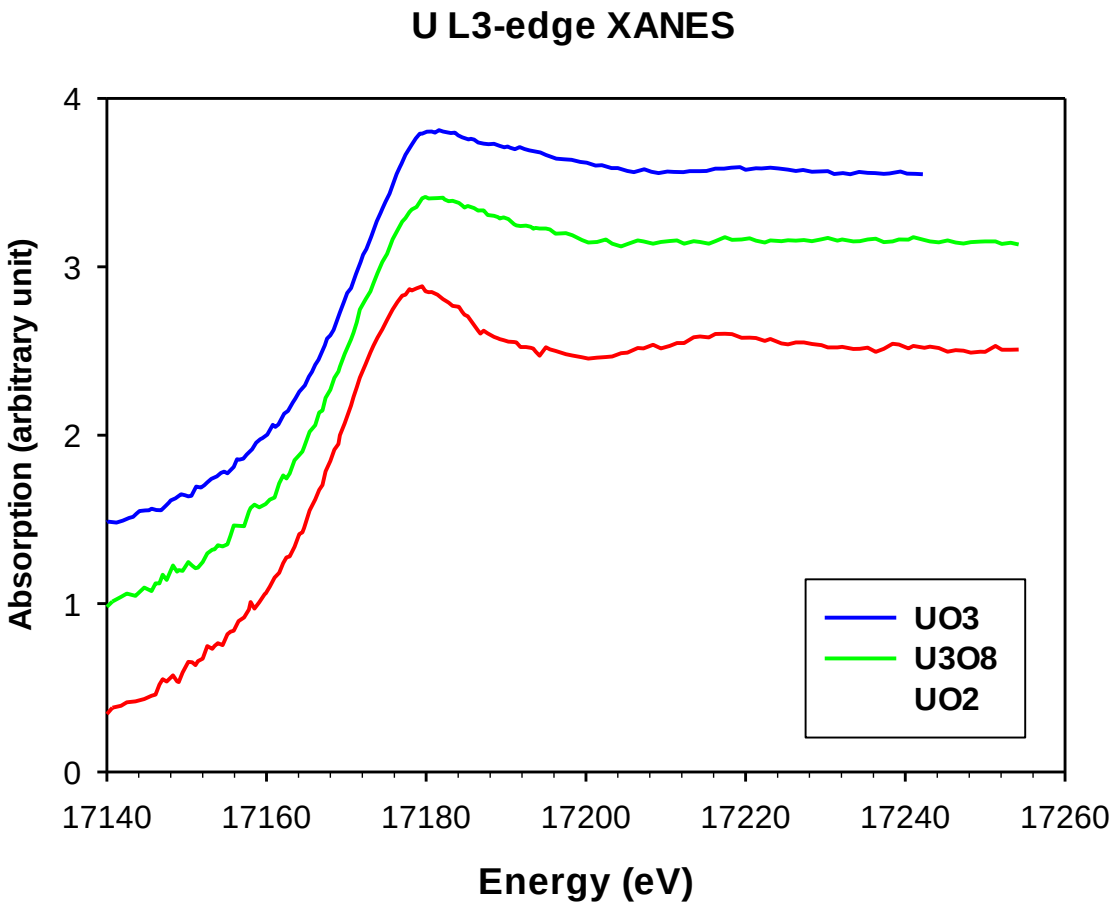

C2. Bulk XRF Results for Tims Branch Floodplain Sediments

	mg · kg^{-1}		mg · kg^{-1}		mg · kg^{-1}
Mo	48 ± 2	**Cu**	24 ± 8	**V**	146 ± 13
Zr	362 ± 3	**Ni**	291 ± 15	**Ti**	3 138 ± 28
Sr	18 ± 1	**Fe**	33 194 ± 131	**Ca**	1 661 ± 64
U	501 ± 7	**Mn**	306 ± 27	**K**	1 700 ± 59
Rb	60 ± 1	**Ba**	97 ± 19	**Al**	14011 ± 2537
Th	13 ± 2	**Sn**	20 ± 12	**P**	5866 ± 890
Pb	10 ± 3	**Pd**	3 ± 2	**Si**	119952 ± 20654
As	10 ± 2	**Nb**	43 ± 1	**Cl**	492 ± 27
Zn	54 ± 4	**Cr**	87 ± 14	**S**	1207 ± 323

APPENDIX D

ELEMENT PARTITIONING IN TIMS BRANCH SOIL INCUBATIONS

D1. 2 mM KCl extracted soil carbon size fraction concentrations (mg / kg soil) as related to pH in 2-h oxic, 2-h oxic pH-increased and 0, 7, and 14-day anoxic conditions in stacked bars. Blue bars represents carbon less than 2.3 nanometers in diameter, yellow bars represents carbon between 2.3 and 100 nanometers in diameter, and green bars represent carbon between 100 and 1000 nanometers in diameter. Brackets indicate 1 standard deviation (n=3).

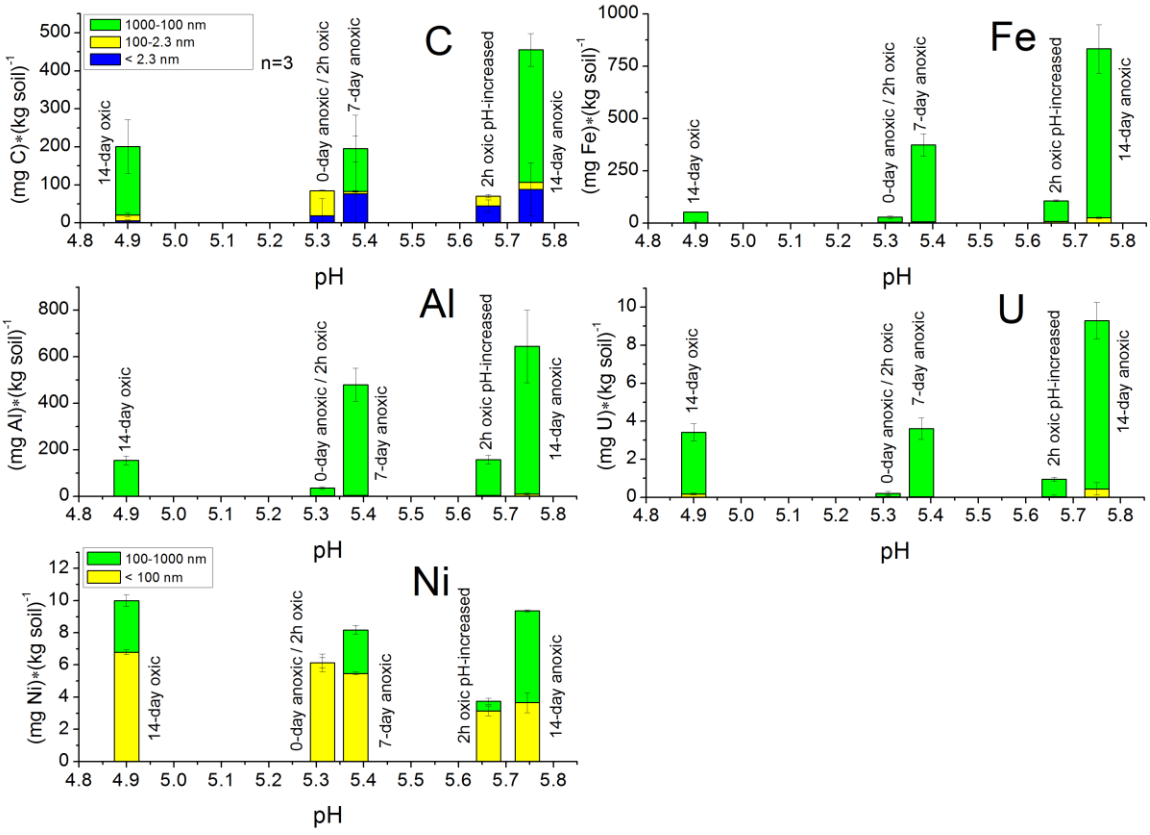

D2. Extrapolated total collidal and dissolved (< 1000 nm) Fe, C, Al, U, and Ni concentrations (mg / kg soil) from 2-h oxic and 2-h oxic pH-increased samples.

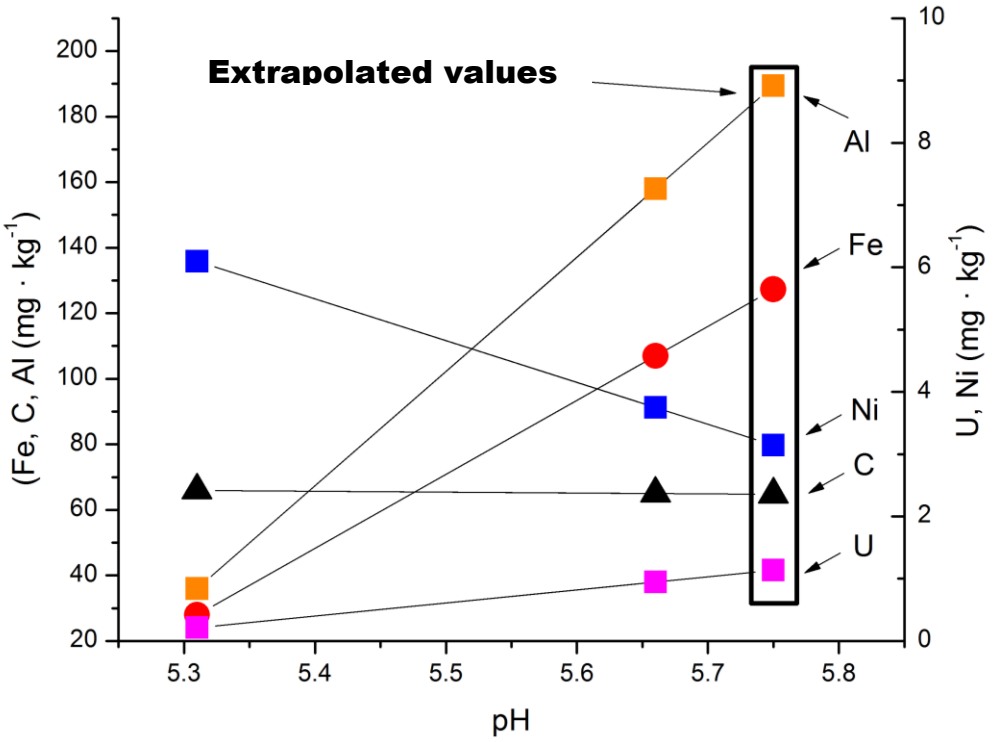

D3. 2 mM KCl extracted soil C size fraction concentrations (mg C / kg soil) as related to pH in 2% and 5% hydroxyapatite, humic salt, or Na-phytate and 14-day oxic and anoxic conditions in stacked bars. Yellow bars represents carbon < 100 nanometers in diameter, and green bars represent carbon between 100 and 1000 nanometers in diameter. Brackets indicate 1 standard deviation (n=3).

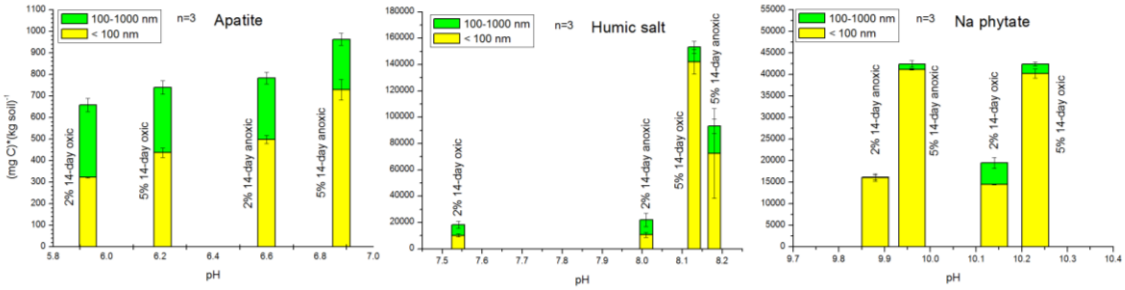

D4. 2 mM KCl extracted soil Fe size fraction concentrations (mg Fe / kg soil) as related to pH in 2% and 5% hydroxyapatite, humic salt, or Na-phytate and 14-day oxic and anoxic conditions in stacked bars. Yellow bars represents carbon < 100 nanometers in diameter, and green bars represent carbon between 100 and 1000 nanometers in diameter. Brackets indicate 1 standard deviation (n=3).

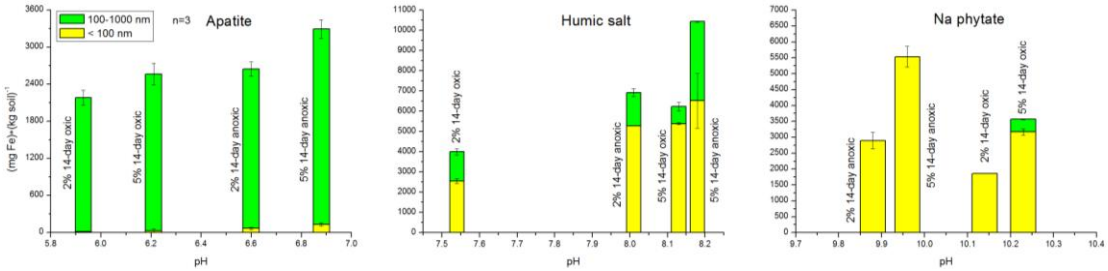

D5. 2 mM KCl extracted soil Al size fraction concentrations (mg Al / kg soil) as related to pH in 2% and 5% hydroxyapatite, humic salt, or Na-phytate and 14-day oxic and anoxic conditions in stacked bars. Yellow bars represents carbon < 100 nanometers in diameter, and green bars represent carbon between 100 and 1000 nanometers in diameter. Brackets indicate 1 standard deviation (n=3).

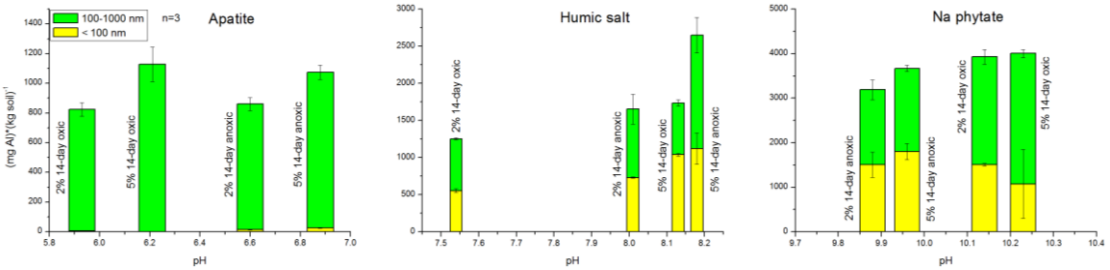

D6. 2 mM KCl extracted soil U size fraction concentrations (mg U / kg soil) as related to pH in 2% and 5% hydroxyapatite, humic salt, or Na-phytate and 14-day oxic and anoxic conditions in stacked bars. Yellow bars represents carbon < 100 nanometers in diameter, and green bars represent carbon between 100 and 1000 nanometers in diameter. Brackets indicate 1 standard deviation (n=3).

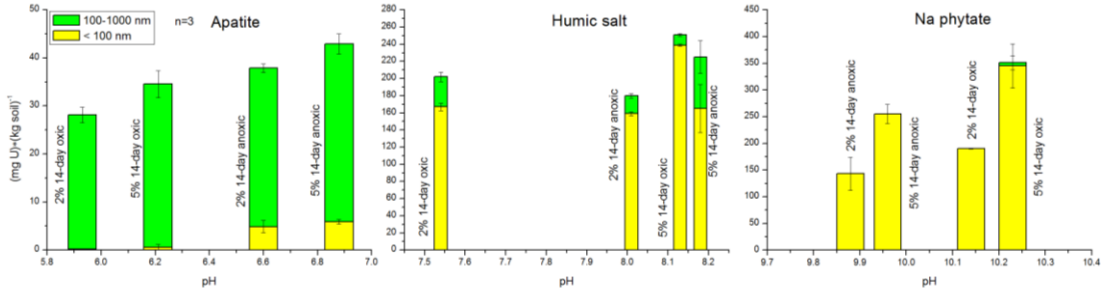

D7. 2 mM KCl extracted soil Ni size fraction concentrations (mg Ni / kg soil) as related to pH in 2% and 5% hydroxyapatite, humic salt, or Na-phytate and 14-day oxic and anoxic conditions in stacked bars. Yellow bars represents carbon < 100 nanometers in diameter, and green bars represent carbon between 100 and 1000 nanometers in diameter. Brackets indicate 1 standard deviation (n=3).

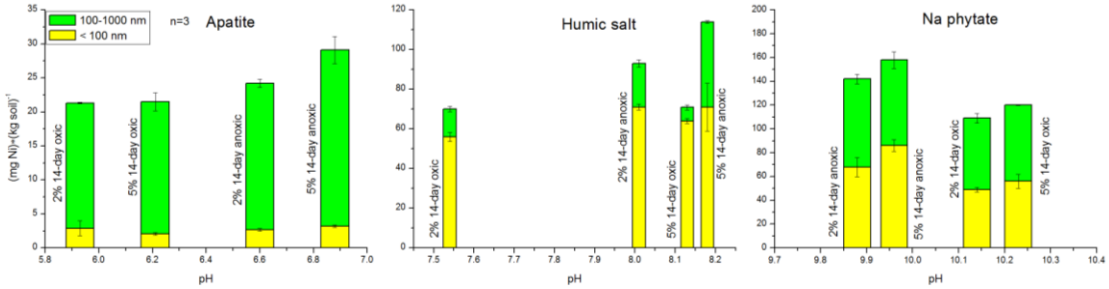

APPENDIX E

SUPPLEMENTAL DATA FOR TIMS BRANCH STORM EVENTS

E1. Routine measurements during storm event on August 11th 2012.

Hours after storm onset	pH	Temp (°C)	Specific Conductivity (mS m^{-1})
1	7.1	23	4.9
2	7.0	22	4.1
3	6.9	22	4.3
4	6.1	23	4.5
5	6.0	23	4.6
6	6.0	23	4.5
7	6.0	23	4.5
8	6.3	23	4.4
31	6.3	24	4.4
50	6.8	25	5.5

E2. Suspended flocs of sediment at low flow during September 2011.

E3. Graphs of metal correlation during Tims Branch stormflow.